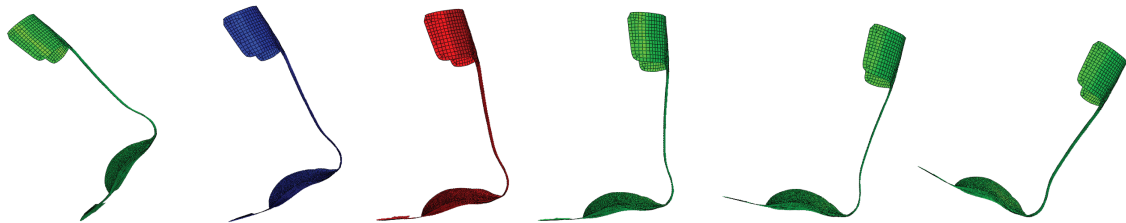


# CHALMERS



## Spring orthosis analysis

Finite element modelling and optimization of a composite material

*Master's Thesis in Solid and Fluid Mechanics*

JOAKIM BERGE

ERIK LERNERYD

Department of Applied Mechanics  
*Division of Material and Computational Mechanics*  
CHALMERS UNIVERSITY OF TECHNOLOGY  
Gothenburg, Sweden 2010  
Master's Thesis 2010:40



# Spring orthosis analysis

Finite element modelling and optimization of a composite material

Master's Thesis in Solid and Fluid Mechanics

JOAKIM BERGE

ERIK LERNERYD

Department of Applied Mechanics

*Division of Material and Computational Mechanics*

CHALMERS UNIVERSITY OF TECHNOLOGY

Gothenburg, Sweden 2010

Spring orthosis analysis  
Finite element modelling and optimization of a composite material  
JOAKIM BERGE  
ERIK LERNERYD

©JOAKIM BERGE, ERIK LERNERYD, 2010

Master's Thesis 2010:40  
ISSN 1652-8557  
Department of Applied Mechanics  
Division of Material and Computational Mechanics  
Chalmers University of Technology  
SE-412 96 Gothenburg  
Sweden  
Telephone: + 46 (0)31-772 1000

Cover:  
Illustration of a walking cycle of the spring orthosis.

Chalmers Reproservice  
Gothenburg, Sweden 2010



Spring orthosis analysis  
Finite element modelling and optimization of a composite material  
Master's Thesis in Solid and Fluid Mechanics  
JOAKIM BERGE  
ERIK LERNERYD  
Department of Applied Mechanics  
Division of Material and Computational Mechanics  
Chalmers University of Technology

### Abstract

This thesis covers finite element (FE) analysis and optimization of a spring orthosis, constructed from a pre-impregnated carbon-fibre epoxy composite material. The spring orthosis is one of the most advanced aids that are used in the orthopedist industry today and is made for people with weak calf muscles. The work has been performed in collaboration with Ortopedteknik, Borås Hospital, at FS Dynamics in Gothenburg.

The purpose of the analyses was to find weaknesses of how the orthosis is built today and to give suggestions of how to change its properties and behaviour. The orthosis has two major interesting areas, the spring and the toe. Both of these areas were analysed regarding rotation angles of the plies, ply stacking sequence and manufacturing procedure. The geometry of the orthosis, material type and number of composite plies in toe and spring were kept constant during the analysis.

The material was modelled as a balanced orthotropic lamina, with a plane stress assumption. To validate the material model a four point bending test of a composite plate was modelled in Abaqus/CAE and compared with experimental data. The interactive Tsai-Wu failure criterion was used as a relative stress measurement.

The FE model of the orthosis was created from a scan of the real orthosis. From this the front surface was extracted and used as a thin shell model. The composite layup of the orthosis was created in the way to best imitate the manufacturing procedure used by the engineers at Ortopedteknik.

To be able to analyse the orthosis a walking cycle was recorded from a person wearing the orthosis. This walking cycle was then applied to the model in Abaqus by prescribing reference points and using boundary conditions and multi point constraints. The maximum Tsai-Wu values in the toe and spring part during this walking cycle indicating that the orthosis is not close to failure.

The Design Of Experiment (DOE) methodology was used to analyse how the stacking sequences of both the spring (18 plies) and the toe (5 plies) affects the bending stiffness. This was done for the four point bending test in Abaqus where the vertical reaktion force was used as stiffness measure. It was found that the angle variation of the outermost plies of the spring has the most effect on the bending stiffness and that the six innermost plies can be rotated arbitrary without significantly affecting the bending stiffness. For the toe the rotation of the two outermost plies are almost alone deciding the bending stiffness of the toe.

From the DOE data approximations were created and then used to optimize stacking sequences based on requested bending stiffnesses. This was used to investigate how various bending stiffnesses of the spring and toe affect the deformation of the spring and toe. The result showed that an increased bending stiffness of the spring will increase the deformation of the toe and vice versa. The bending stiffness of the toe has no significant effect on the deformation of the spring. A study of the Tsai-Wu value also showed that the toe cannot be too weak since this resulted in failure.

Keywords: Abaqus CAE, Carbon fibre, Composite material, Composite modeler, Design of experiment, Draping, Finite element analysis, Four point bending test, Isight, Laminate, Optimization, Orthosis, Ply, Shell, Tsai-Wu



# Contents

<b>Abstract</b>	<b>I</b>
<b>Contents</b>	<b>III</b>
<b>Preface</b>	<b>V</b>
<b>1 Introduction</b>	<b>1</b>
1.1 Background . . . . .	1
1.2 Purpose . . . . .	2
1.3 Scope and limitations . . . . .	2
1.4 Methodology . . . . .	3
1.5 Thesis outline . . . . .	3
<b>2 Theory</b>	<b>4</b>
2.1 Composite materials . . . . .	4
2.1.1 Micromechanics . . . . .	4
2.1.2 Macromechanics . . . . .	6
2.1.3 Lamina Strength . . . . .	10
2.1.4 Laminate theory . . . . .	12
2.1.5 Interlaminar stresses . . . . .	13
2.1.6 Laminate strength . . . . .	14
2.2 Contact mechanics . . . . .	16
2.3 Computer experiments . . . . .	18
<b>3 Material modelling</b>	<b>20</b>
3.1 Four point bending test . . . . .	21
3.1.1 Setup of Abaqus model . . . . .	22
3.1.2 Material Model . . . . .	23
3.1.3 Geometry and boundary conditions . . . . .	24
3.1.4 Element selection . . . . .	26
3.1.5 Contact interaction . . . . .	27
<b>4 Orthosis model</b>	<b>29</b>
4.1 Model geometry . . . . .	29
4.1.1 Mesh . . . . .	30
4.2 Composite layup . . . . .	30
4.2.1 Creating original composite layup . . . . .	31
4.3 Walking cycle . . . . .	35
4.3.1 Localising maximum stress during the walking cycle . . . . .	37
4.3.2 Creating reference states from the walking cycle . . . . .	37
4.4 Creating new composite layups . . . . .	38
<b>5 Laminate stacking sequence analysis</b>	<b>39</b>
5.1 Creating approximation . . . . .	40
5.2 Stiffness optimization . . . . .	42
5.3 Analysis of relative motion of toe and spring . . . . .	43

<b>6</b>	<b>Results</b>	<b>45</b>
6.1	Four point bending test . . . . .	45
6.2	Maximum Tsai-Wu during walking cycle . . . . .	47
6.3	Composite layup with no drop offs in heel area . . . . .	49
6.4	Laminate stacking sequence . . . . .	51
6.5	Stiffness optimization . . . . .	54
6.6	Relative motion results . . . . .	55
<b>7</b>	<b>Conclusions</b>	<b>58</b>
<b>8</b>	<b>Discussion</b>	<b>60</b>
<b>9</b>	<b>Recommendations</b>	<b>62</b>
<b>10</b>	<b>References</b>	<b>63</b>
<b>A</b>	<b>Calculation of volume percent carbon fibre in test specimen</b>	<b>64</b>
<b>B</b>	<b>Analysis of test set up parameters</b>	<b>65</b>
B.1	Element type . . . . .	65
B.2	Constraint enforcement method . . . . .	66
B.3	Friction . . . . .	68
<b>C</b>	<b>Curve-fitted amplitudes</b>	<b>70</b>
<b>D</b>	<b>Python Script</b>	<b>71</b>
<b>E</b>	<b>Geometry clean up</b>	<b>74</b>
<b>F</b>	<b>Stacking sequences</b>	<b>76</b>
<b>G</b>	<b>Main effect</b>	<b>77</b>

# Preface

In this study FE analyses and optimization of a spring orthosis has been performed. The work has been carried out from January to June 2010 at FS Dynamics, Gothenburg, Sweden. Magnus Ekh, Docent at the Department of Applied Mechanics, Division of Material and Computational Mechanics, Chalmers University of Technology, Gothenburg, Sweden was supervisor and examiner and Dr. Per Heintz was supervisor representing FS Dynamics.

# Acknowledgements

We would like to say our thanks to both our supervisors Magnus Ekh and Per Heintz for their guidance and support. We appreciate all the help received from our co-workers at FS Dynamics and would also like to send a special thank you to Jan Rydin, Consulting engineer at Simulia.

Gothenburg June 2010  
Joakim Berge, Erik Lerneryd



# 1 Introduction

This thesis covers FE-analysis and optimization of a spring orthosis<sup>1</sup>. A spring orthosis is one of the most advanced aids that are used in the orthopedist industry today. The work has been performed in collaboration with Ortopedteknik, Borås Hospital.

## 1.1 Background

In recent years the usage of carbon fibre materials in orthoses has increased. Carbon fibre has the highest strength and stiffness of any composite-reinforcements [1]. The major advantages of carbon fibre is its high stiffness to density ratio. One disadvantage is its brittleness.

The orthoses are designed individually to match the needs of each unique patient. The orthosis is made from a pre-preg material (pre-impregnated carbon fibre with epoxy) and is manufactured by hand by the engineers at Ortopedteknik. Today experiences from previously built orthoses form the ground of how new orthoses are built [Interview with engineers at Ortopedteknik, February-May, 2010]. In order to develop the product further and deeper, analysis is needed, which includes calculations using FEM. A deeper understanding would improve the possibilities of creating a better aid for each individual patient.

The spring orthosis is primarily used to keep the user in an upright position. The majority of the persons using the product have weak calf muscles, most of them are suffering from Myelo Meningocele (MMC) also known as spinal cord hernia [Interview with engineers at Ortopedteknik, February-May, 2010]. Figure 1.1(a) shows how the orthosis looks when its ready to be used and Figure 1.1(b) shows how the orthosis looks when all buckles are removed. The attached reflectors in Figure 1(b) were used when recording the walking cycle with position cameras.

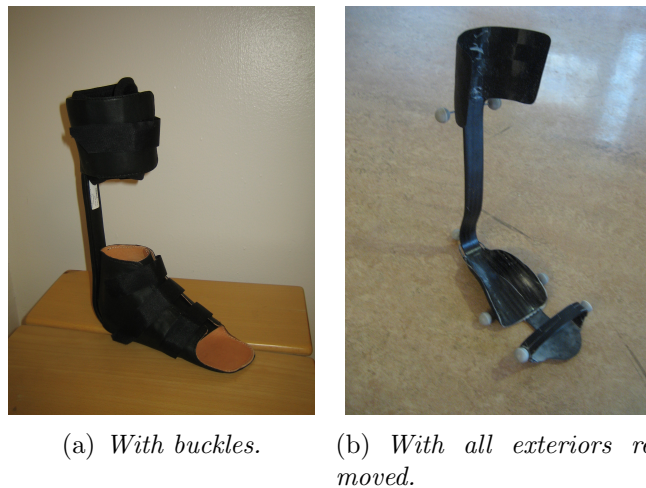


*Figure 1.1: Photos of the spring orthosis.*

---

<sup>1</sup>An orthosis is an artificial device or brace, worn by a patient. The word orthosis is derived from the Greek word ortho which means "to straighten".

## 1.2 Purpose

The purpose of the FEM analysis is to find weaknesses of how the orthosis is built today and to give suggestions in order to change its behaviour and properties. The orthosis has two major interesting areas, the spring part and toe part, marked in Figure 1.2. In these areas the main part of the deformation occur. The spring deforms when there is a relative motion between the arch of the foot and the calf. The toe part deforms when there is relative motion between the arch and the toes.

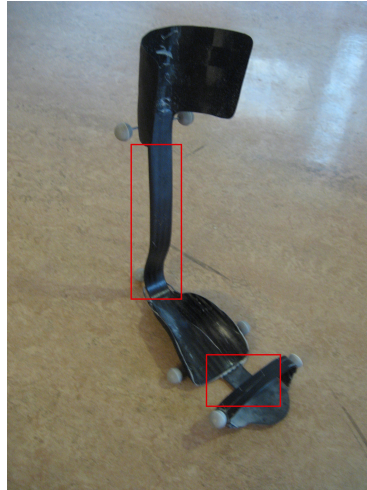


*Figure 1.2: Marking of the two areas of interest, the spring and the toe.*

The following questions are investigated:

- Where and when do the largest stresses occur during an ordinary walking cycle?
- How does the orientation of the composite plies change the bending stiffness of the spring and the toe?
- Which plies have most impact of the bending stiffness of the toe and the spring?
- Is there a way to obtain a ply stacking sequence based on requested bending stiffness?
- How does the composite layup affect the relation of the deformation between toe and spring?
- How does the manufacturing procedure affect the stress distribution in the spring and the toe.

## 1.3 Scope and limitations

To change the behaviour and properties of the orthosis the change of the following parameters were analysed:

- Ply rotational angles
- Ply stacking sequence
- Manufacturing procedure



Not more than one orthosis was analysed in this thesis and the following parameters were not taken into account but kept constant during the project:

- Geometry of the orthosis
- Type of material
- Number of plies in toe and spring

Only one walking cycle was recorded, performed by a person without disabilities. The following softwares were used; Abaqus/CAE v.6.9-1 , Composite modeler v.1.0h ANSA v.13.0.2, Isight v.4.0 and Matlab R2009b.

## 1.4 Methodology

The FEM model of the orthosis was created by using ANSA starting from a scanned geometry in stl-format. The model was set up using Abaqus/CAE and Composite Modeler. Composite Modeler (CM) is an Abaqus plug-in and was used to create composite layups for the orthosis. The orthosis with original composite layup was subjected to static analysis of each single time step from a recorded walking cycle. The time steps with maximum stresses both in the spring and the toe were extracted and used as a reference state, for comparison to other layups.

To validate the composite material model a four point bending test was simulated and compared to a real test. The model of the bending test was also used to investigate how the composite layup affects the bending stiffness. This was done by creating DOEs (design of experiments) using Isight.

## 1.5 Thesis outline

This thesis starts with a theory chapter (chapter 2), describing composite-, contact- and computer experiment theories. Further it follows three chapters describing the methods used when analysing the material and the orthosis: Material modelling (3), Orthosis model (4) and Laminate stacking sequence analysis (5). Then the results are presented (6), which is followed by conclusions (7), discussion (8) and finally recommendations (9).

## 2 Theory

This theory chapter will cover theories of composite materials, contact mechanics and computer experiments. The composite section describes micro- and macromechanics and different strength theories. The contact theories describe different contact methods used when modelling the four point bending test. The computer experiment section describes theories and vital concepts needed to be able to follow the stacking sequence analyses.

### 2.1 Composite materials

A composite material is built from laminas containing matrix- and reinforcement materials. A lamina can also be denoted as a ply, whereas ply is more used when referring to the sheets of material received from manufacturers. The matrix material binds the reinforcement together and gives the composite its shape, surface and environmental tolerance. The objective of the fibrous reinforcement is to carry most of the structural loads. A composite lamina can have different configurations. The fibres can be continuous or discontinuous, aligned or randomly oriented, unidirectional or woven, see Figure 2.1(a)-2.1(e) [1].

Composites are heterogeneous materials where the stress-strain relations changes from one point to another, i.e. the elastic modulus for the fibre differs from the elastic modulus of the matrix. Thus, when analysing composites it is more convenient to deal with averaged stresses and strains which are related by the "effective modulus" of an equivalent homogenous material. Analysis of composite materials is often divided into micro- and macromechanics. Micromechanics is about defining effective material parameters of the composite while macromechanics describe the constitutive relations [2].

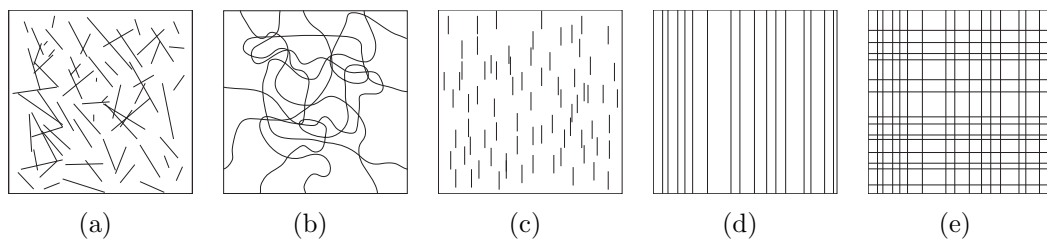


Figure 2.1: Different configurations of composite materials. The configuration of the fibres is important regarding the macroscopic properties of the composite. The configurations are; (a) Discontinuous, randomly oriented (b) Continuous, randomly oriented (c) Discontinuous, aligned (d) Continuous, aligned, unidirectional (e) Continuous, aligned, woven

#### 2.1.1 Micromechanics

Micromechanics of composite materials is the analysis of effective composite properties in terms of constituent material properties. One of the key elements in micromechanics analysis is the relative volume. For any number of constituent materials,  $n$ , the sum of all volume fractions must be equal to one:

$$\sum_{i=1}^n v_i = 1 \quad (2.1)$$

where  $v_i$  is the volume fraction of the  $i$ :th constituent

$$v_i = \frac{V_i}{V_c}. \quad (2.2)$$

$V_i$  is the volume of the  $i$ :th constituent and  $V_c$  is the total volume of the composite. For a composite material only consisting of matrix- and fibre material, equation (2.1) reduces to

$$v_m + v_f = 1 \quad (2.3)$$

where  $v_m$  and  $v_f$  are the volume fractions of the matrix and fibre respectively. Figure 2.2(a) illustrates a representative volume element of a unidirectional composite, i.e. a composite with fibres running in only one direction. If assuming that the stresses, strains, displacements and dimensions of this composite do not change in the lengthwise direction then area averages can be used accordingly:

$$\bar{\sigma} = \frac{1}{V} \int_V \sigma dV = \frac{1}{A} \int_A \sigma dA \quad (2.4)$$

$$\bar{\epsilon} = \frac{1}{V} \int_V \epsilon dV = \frac{1}{A} \int_A \epsilon dA \quad (2.5)$$

$$\bar{\delta} = \frac{1}{V} \int_V \delta dV = \frac{1}{A} \int_A \delta dA \quad (2.6)$$

where  $\bar{\sigma}$  = average stress,  $\bar{\epsilon}$  = average strain and  $\bar{\delta}$  = average displacement.

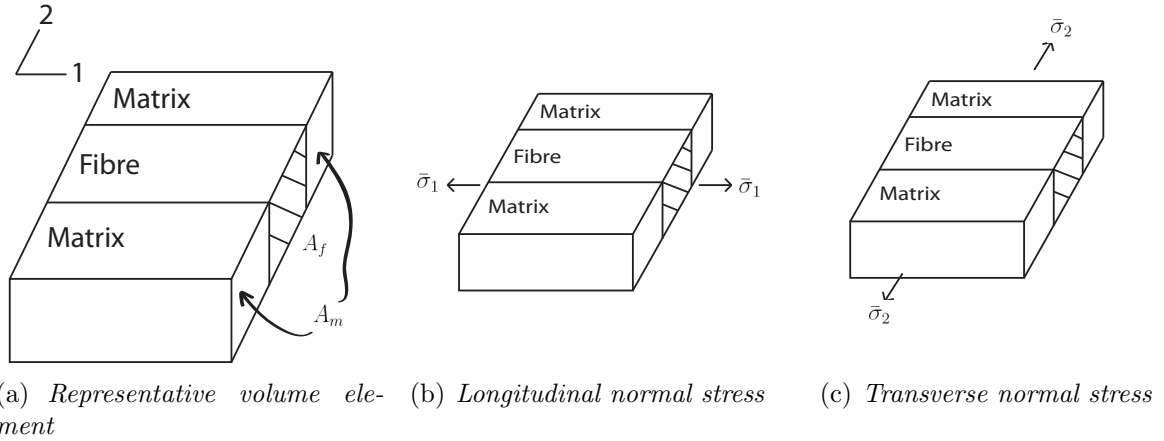


Figure 2.2: Representative volume element and normal stress states

Other assumptions needed to be able to use averages is that there is a no slip condition between the fibres and matrix and that both materials are linearly elastic and homogenous [2]. By considering a longitudinal normal stress, see Figure 2.2(b), and static equilibrium, meaning that the sum of the forces acting on the matrix and fibre equals the total resultant force, the following equation can be stated:

$$\bar{\sigma}_{c1} A_1 = \bar{\sigma}_{f1} A_f + \bar{\sigma}_{m1} A_m \quad (2.7)$$

Since area fractions are equal to volume fractions, equation (2.7) can be rewritten to give the so called rule of mixtures[3].

$$\bar{\sigma}_{c1} = \bar{\sigma}_{f1} v_f + \bar{\sigma}_{m1} v_m \quad (2.8)$$

By using Hooke's law and that

$$\bar{\epsilon}_{c1} = \bar{\epsilon}_{f1} = \bar{\epsilon}_{m1} \quad (2.9)$$

equation (2.8) becomes the rule of mixture for longitudinal effective stiffness modulus:

$$E_1 = E_{f1} v_f + E_{m1} v_m \quad (2.10)$$

The modulus of the fibre has two indices since it can be anisotropic and thus the longitudinal module differs from the transverse. The epoxy matrix material is isotropic. When the composite is subjected to stresses in the transverse direction, see Figure 2.2(c), the total transverse composite displacement must be equal to the sum of the displacements in the fibre and the matrix:

$$\bar{\delta}_{c2} = \bar{\delta}_{f2} + \bar{\delta}_{m2} \quad (2.11)$$

With the definition of normal strain, e.g.  $\bar{\delta}_{c2} = \bar{\epsilon}_{c2}L_2$  and that the length fraction is equal to the volume fraction the rule of mixture for transverse strain is obtained:

$$\bar{\epsilon}_{c2} = \bar{\epsilon}_{f2}v_f + \bar{\epsilon}_{m2}v_m \quad (2.12)$$

By using Hooke's law and that

$$\bar{\sigma}_{c2} = \bar{\sigma}_{f2} = \bar{\sigma}_{m2} \quad (2.13)$$

equation (2.12) becomes the inverse rule of mixture for the transverse modulus:

$$\frac{1}{E_2} = \frac{v_f}{E_{f2}} + \frac{v_m}{E_m} \quad (2.14)$$

However the assumption in equation (2.13) is not accurate for most composites which has lead to the development of semi-empirical equations. These equations result from basis in mechanics but also have curve-fitting parameters from experiments. The most widely used is the Halpin-Tsai equation, which for the transverse modulus yields:

$$\frac{E_2}{E_m} = \frac{1 + \xi\eta v_f}{1 - \eta v_f} \quad (2.15)$$

where

$$\eta = \frac{(E_{f2}/E_m) - 1}{(E_{f2}/E_m) + \xi} \quad (2.16)$$

and  $\xi$  is the curve-fitting parameter. The shear modulus,  $G_{12}$ , is obtained by simply replacing  $E_2, E_{f2}$  and  $E_m$  with  $G_{12}, G_f$  and  $G_m$  in equations (2.15)-(2.16). The major (in-plane) Poisson's ratio is calculated by another rule of mixture formulation:

$$\nu_{12} = v_f\nu_f + v_m\nu_m \quad [2] \quad (2.17)$$

In the following sections all stresses are averaged stresses according to equation (2.4), but denoted  $\sigma$  instead of  $\bar{\sigma}$ .

### 2.1.2 Macromechanics

The most general stress-strain relations at a point in an elastic material is given by the equation

$$\sigma_{ij} = C_{ijkl}\epsilon_{kl}, \quad i, j, k, l = 1, 2, 3 \quad (2.18)$$

where  $\sigma_{ij}$  and  $\epsilon_{kl}$  are the stress and strain tensor with 9 components each and  $C_{ijkl}$  is the stiffness matrix with 81 components. If no further restrictions are made the material is called anisotropic and equation (2.18) is known as the generalized Hooke's law for anisotropic material.

In practice there is no need to deal with all the 81 components since various symmetry conditions simplify the equations. Firstly, the stress and strain tensors are symmetric and reduces the number of independent stress and strain components to 6 and the number of nonzero elastic constants to 36, i.e. symmetry with respect to the the first two subscript and with respect to the last two subscript  $C_{ijkl} = C_{jikl}$  and  $C_{ijkl} = C_{ijlk}$ .

Secondly, the stresses can be derived from the strain energy density function,  $\mathbf{W} = \frac{1}{2}C_{ijkl}\epsilon_{ij}\epsilon_{kl}$ , according to

$$\sigma_i = \frac{\partial \mathbf{W}}{\partial \epsilon_{ij}} = C_{ijkl}\epsilon_{kl} \quad (2.19)$$

and then by taking the second derivative:

$$\frac{\partial^2 \mathbf{W}}{\partial \epsilon_{ij} \partial \epsilon_{kl}} = C_{ijkl} \Leftrightarrow \frac{\partial^2 \mathbf{W}}{\partial \epsilon_{kl} \partial \epsilon_{ij}} = C_{klij} \quad (2.20)$$

Since the results of the differentiation is the same regardless of the order it shows that the stiffness matrix is symmetric,  $C_{ijkl} = C_{klij}$ . Now, there are 21 of the 36 anisotropic components that are independent. Those symmetry conditions are derived without saying anything about the symmetry of the material. All real materials have some form of symmetry which will reduce the number of nonzero components further, no known material is completely anisotropic[2].

A continuous fibrous composite ply having unidirectional fibres has two mutually perpendicular planes of material property symmetry, see Figure 2.3, and is said to be an orthotropic material<sup>2</sup>. Since a woven ply is also an orthotropic material all the expression for the unidirectional ply will be equally valid for a woven ply [4]. Unlike the anisotropic stiffness matrix in equation (2.18), which is independent of how the principal directions are defined, an orthotropic material stiffness matrix is dependent on how the principal axes are defined. When dealing with composites the principal material coordinate axes are referred since they are directed in and transverse the reinforcement direction, see Figure 2.3. An orthotropic material defined in this way is called a specially orthotropic material.

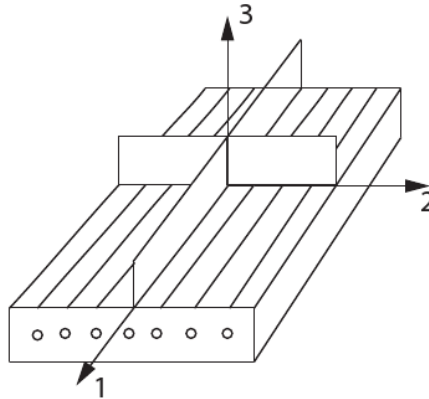


Figure 2.3: Lamina showing the principal material coordinate axes and symmetry planes. The 1-axis is directed in the reinforcement direction, 2- and 3-axis are directed transversely to the reinforcement.

Now there are 12 nonzero elastic constants and 9 independent elastic constants for the specially orthotropic material. If the coordinate system is not in the material principal direction the stiffness matrix takes the same form as for the anisotropic material with 36 nonzero elastic components, 21 independent, this type of material is called a generally orthotropic material [2].

When a composite has a plane with isotropic material properties, i.e for parallel fibres with the 1-direction along the fibres, the 23-plane will be the isotropic plane: This type of material is called transversely isotropic.

<sup>2</sup>An orthotropic material is a material that has different material properties in different directions, i.e x,y and z. The three planes xy,yz and zx must form the three mutually perpendicular planes of material property symmetry [4].

Engineering constants are measured experimentally to describe the stress-strain relations of a material. The stiffness matrix will then be populated of engineering constants such as Young's modulus, shear modulus and Poisson's ratio instead of  $C_{ijkl}$ . For an isotropic material where the material properties are the same in all directions there is no need of subscript for the engineering constants. This is not the case for the orthotropic material because of the different properties in the different directions, e.g.  $E_1 \neq E_2$  and  $\nu_{12} \neq \nu_{21}$ . For the specially orthotropic material, with principal axis 1 along the fibre reinforcement, normal stresses only induces normal strains and all shear strains are equal to zero as with isotropic material. For any other set of coordinate system for an orthotropic material this will not be the case, i.e. a "shear-coupling" effect will be present. In a general three-dimensional state with all possible normal and shear stresses associated with the 1-2-3 axes the stress-strain relations can be written as

$$\begin{bmatrix} \epsilon_1 \\ \epsilon_2 \\ \epsilon_3 \\ \gamma_{23} \\ \gamma_{31} \\ \gamma_{12} \end{bmatrix} = \begin{bmatrix} 1/E_1 & -\nu_{21}/E_2 & -\nu_{31}/E_3 & 0 & 0 & 0 \\ -\nu_{12}/E_1 & 1/E_2 & -\nu_{32}/E_3 & 0 & 0 & 0 \\ -\nu_{13}/E_1 & -\nu_{23}/E_2 & 1/E_3 & 0 & 0 & 0 \\ 0 & 0 & 0 & 1/G_{23} & 0 & 0 \\ 0 & 0 & 0 & 0 & 1/G_{31} & 0 \\ 0 & 0 & 0 & 0 & 0 & 1/G_{12} \end{bmatrix} \begin{bmatrix} \sigma_1 \\ \sigma_2 \\ \sigma_3 \\ \tau_{23} \\ \tau_{31} \\ \tau_{12} \end{bmatrix} \quad (2.21)$$

Due to symmetry of the compliance matrix,  $\nu_{ij}/E_i = \nu_{ji}/E_j$ , nine of the engineering constants are independent for the specially orthotropic material. As previously mentioned the generally orthotropic material has 21 dependent elastic components because of its off principal axes defined coordinate system and all the components of the compliance matrix in equation (2.21) will be populated. All the components of the generally orthotropic material can be derived from the engineering constants from a testing of a specially orthotropic material along the principal material directions, according to equation (2.25). Hence, when testing a material it is preferable to do the testing for a specially orthotropic material. If the material is transversely isotropic and specially orthotropic the subscript 2 and 3 are interchangeable in equation (2.21) which means that  $G_{13} = G_{12}$ ,  $E_2 = E_3$ ,  $\nu_{21} = \nu_{31}$  and  $\nu_{23} = \nu_{32}$ . Because of the isotropic material properties in this plane the relations for the shear modulus for an isotropic material can be used

$$G_{23} = \frac{E_2}{2(1 + \nu_{32})} \quad (2.22)$$

leaving it to 5 independent constants. In laminate analysis, the lamina is often assumed to be in a two-dimensional plane stress state. This reduces the relations in equation (2.21) to

$$\begin{bmatrix} \epsilon_1 \\ \epsilon_2 \\ \gamma_{12} \end{bmatrix} = \begin{bmatrix} 1/E_1 & -\nu_{21}/E_2 & 0 \\ -\nu_{12}/E_1 & 1/E_2 & 0 \\ 0 & 0 & 1/G_{12} \end{bmatrix} \begin{bmatrix} \sigma_1 \\ \sigma_2 \\ \tau_{12} \end{bmatrix} \quad (2.23)$$

since in plane stress  $\sigma_3 = \tau_{23} = \tau_{31} = 0$ . Now there are 4 independent constants for the plane stress specially orthotropic transversely isotropic lamina. The experimental characterisation of the orthotropic lamina involves the measurement of 4 different engineering constants  $E_1$ ,  $E_2$ ,  $G_{12}$  and  $\nu_{12}$ . Those are the engineering constants needed in equation (2.23). In cases when a three dimensional analysis is required for an orthotropic material having a plane of isotropy more than those four constants are needed. The constants  $E_3$ ,  $G_{13}$ ,  $G_{23}$  and  $\nu_{23}$  are also needed, 5 of them being independent. In absence of these values it is usually assumed that  $\nu_{23} = \nu_{12}(= \nu_{13})$  and  $G_{23} = G_{12}(= G_{13})$  [4]. For the case of woven lamina or cross-plyed at  $0^\circ$  and  $90^\circ$  the number of independent elastic constants

reduces to 3 since  $E_1 = E_2$ , because of the double symmetry of properties with respect to the 1 and 2 axes [2]. This type of material is called a balanced orthotropic lamina.

When analysing a laminate, containing multiple laminas, the stress-strain relations for the off axis laminas are needed. Those can be expressed with four independent elastic constants in the principal coordinates and the lamina orientation angle. With the sign convention used in Figure 2.4 the static equilibrium for an element can be written as

$$\begin{aligned}\sigma_1 &= \sigma_x \cos^2\theta + \sigma_y \sin^2\theta + 2\tau_{xy} \sin\theta \cos\theta \\ \sigma_2 &= \sigma_x \sin^2\theta + \sigma_y \cos^2\theta - 2\tau_{xy} \sin\theta \cos\theta \\ \tau_{12} &= -\sigma_x \sin\theta \cos\theta + \sigma_y \sin\theta \cos\theta + \tau_{xy}(\cos^2\theta - \sin^2\theta)\end{aligned}\quad (2.24)$$

or in matrix form

$$\begin{bmatrix} \sigma_1 \\ \sigma_2 \\ \tau_{12} \end{bmatrix} = \begin{bmatrix} \cos^2\theta & \sin^2\theta & 2\sin\theta \cos\theta \\ \sin^2\theta & \cos^2\theta & -2\sin\theta \cos\theta \\ -\sin\theta \cos\theta & \sin\theta \cos\theta & \cos^2\theta - \sin^2\theta \end{bmatrix} \begin{bmatrix} \sigma_x \\ \sigma_y \\ \tau_{xy} \end{bmatrix} \quad (2.25)$$

where the matrix in equation (2.25) is the transformation matrix from the principle to the off-axis coordinate system[5]. It can also be shown that the strain tensor transforms in the same way.

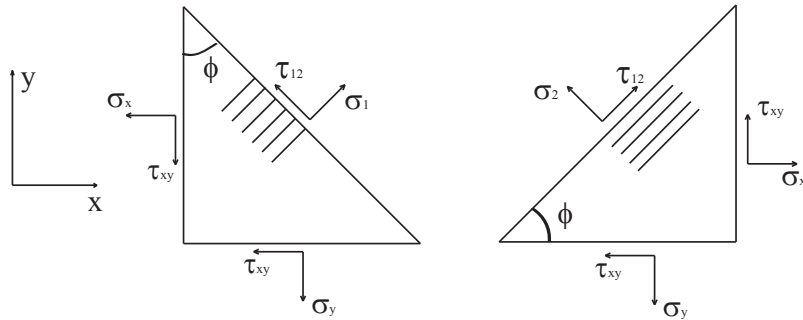
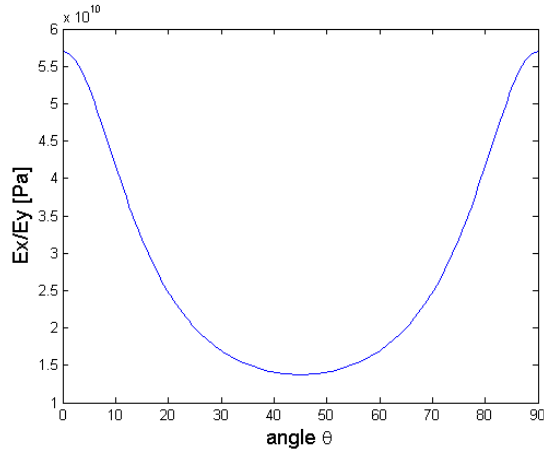


Figure 2.4: Triangular element showing the different stresses in an off axis coordinate system. The 1-direction is in the reinforcement direction and 2-direction is transverse the reinforcement.

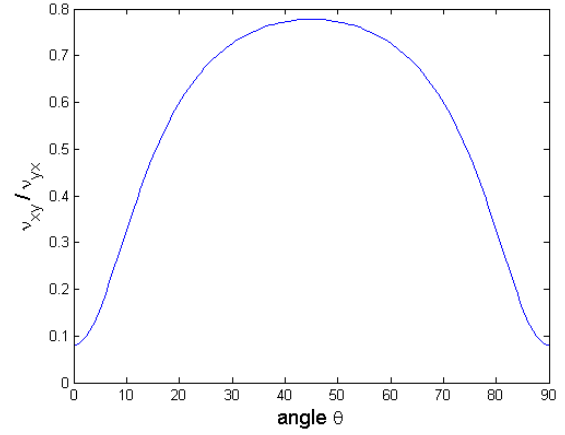
In the same way the engineering constants can be transformed from the principal axes to the off axes coordinate system. The stress-strain relation transformation from a principal coordinate system (1,2,3) to the off-axis coordinate system (x,y,z), when the transformation matrix is denoted by  $\mathbf{T}$  and the compliance matrix in equation (2.23) is denoted by  $\mathbf{S}$ , can be written as

$$\epsilon = \mathbf{T}^T \mathbf{S} \mathbf{T} \sigma \quad (2.26)$$

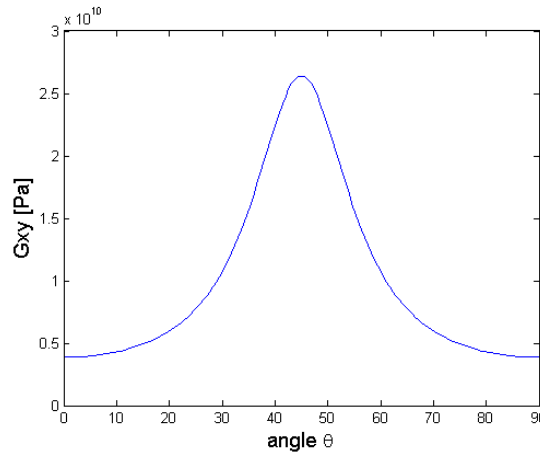
Here  $\sigma$  and  $\epsilon$  are the stresses and strains for the off axis coordinate system (x,y,z). For example, equation (2.26) inserted into Hooke's law,  $E_x = \frac{\sigma_x}{\epsilon_x}$ , will give the equation for the Young's modulus in an off axes coordinate system under uniaxial loading. Figure 2.5 shows the Young's modulus  $E_x/E_y$ , shear modulus  $G_{xy}$  and the Poisson's ratio  $\nu_{xy}/\nu_{yx}$  variation over the angle for a woven ply.



(a) Young's modulus  $E_x/E_y$ .



(b) Poisson's ratio  $\nu_{xy}/\nu_{yx}$ .



(c) In plane shear modulus  $G_{xy}$ .

Figure 2.5: Different variables variation over the angle for a woven ply, where the fibres are running in two directions perpendicular to each other.

### 2.1.3 Lamina Strength

In section 2.1.1 the stress-strain relations have been described by effective moduli, representing a homogenous material instead of a heterogeneous material. This can also be done for the strength of the material. The effective strength is defined as the ultimate value of the volume averaged stresses which causes failure of the lamina under the averaged state of stress. When analysing the strength of the lamina the compressive longitudinal  $s_L^{(-)}$  and transversal  $s_T^{(-)}$ , tensile longitudinal  $s_L^{(+)}$  and transversal  $s_T^{(+)}$  and the in-plane shear strength  $s_{LT}$  are used. The longitudinal, L, direction is in the fibre direction and the transverse, T, direction is transverse to the unidirectional fibres. The stress-strain relations, in the case of uniaxial stress and pure shear stress respectively, can then be written as

$$s_{\alpha}^{(-)/(+)} = E_{\alpha} e_{\alpha}^{(-)/(+)}, \quad \alpha = L, T \quad (2.27)$$

$$s_{LT} = G_{LT} e_{LT} \quad (2.28)$$

where  $e$  is the corresponding strain. The shear strength  $s_{LT}$  is independent of the sign.

For unidirectional fibres the longitudinal tensile strength is generally greater than the compressive and in the transverse direction the compressive strength is generally greater



than the tensile strength which is the lowest of all strengths [2]. There is also an inter-laminar strength parameter that does not follow the plane stress assumption often used when analysing laminas. Those stresses can create delamination and is further discussed in section 2.1.5.

**2.1.3.1 Failure criteria** There are different semi-empirical failure criteria that are used to estimate when lamina failure will occur. These criteria apply even under complex loading conditions other than uniaxial or shear stresses and involves the strengths described in section 2.1.3. They do not take into account the details of specific micro-mechanical failure modes such as fibre pullout, fibre breakage, fibre micro-buckling, matrix cracking or delamination. The failure process is very complex since these micro-failure modes may occur in various combinations and sections. The existence and growth of cracks and other defects in the composite are also ignored in these approaches. To take into account such failure modes a fracture mechanical approach is needed. None of the available theories have been shown to accurately predict failure for all materials and loading conditions, and there is no agreement on which is the best [2].

Many of the failure criteria for anisotropic composite materials are based on previously developed criteria for predicting the transition from elastic to plastic behaviour in anisotropic metallic materials. They use the concept of failure surface or failure envelope generated by plotting stress components in stress space. The axes usually represent the material principal axes. Failure are predicted when the combination of stresses fall on or outside the failure surface. Example of failure criteria are the maximum stress criterion and maximum strain criterion that are non interactive criteria, i.e. they do not take into account the interaction between the different stress components.

The interactive failure criteria Tsai-Wu and Tsai-Hill take into account the interaction between the different stress components, for more literature about failure criteria see for example [2]. The Tsai-Wu and Tsai-Hill theories are based on the macromechanical behaviour of the composite without regard for the micromechanical behaviour of the fibre and matrix materials. The main difference between the interactive stress criteria mentioned is that Tsai-Wu takes into account different strengths in tension and compression, of which Tsai-Hill does not.

**2.1.3.2 Tsai-Wu failure criterion** The failure surface for the Tsai-Wu stress theory in stress space is described by

$$F_i \sigma_i + F_{ij} \sigma_i \sigma_j = 1, \quad i, j = 1, 2, \dots, 6 \quad (2.29)$$

where  $F_i$  and  $F_{ij}$  are experimentally determined strength tensors of the second and fourth order respectively. The stresses  $\sigma_i$  represent the symmetric part of the stress tensor in Voigt notation. Failure is predicted when the LHS of equation (2.29) is  $\geq 1$ . In the case of plane stress, equation (2.29) reduces to

$$F_{11} \sigma_1^2 + F_{22} \sigma_2^2 + F_{66} \sigma_6^2 + F_1 \sigma_1 + F_2 \sigma_2 + 2F_{12} \sigma_1 \sigma_2 = 1 \quad (2.30)$$

The linear terms for  $\sigma_1 = \sigma_{11}$  and  $\sigma_2 = \sigma_{22}$  takes into account the different strengths in tension and compression. These terms are not included in the Tsai-Hill failure criterion. The term  $2F_{12} \sigma_1 \sigma_2$  takes into account the interaction between the normal stresses. All the components of the strength tensor in equation (2.30) can be expressed in the different

strengths according to

$$F_{11} = \frac{1}{s_L^{(+)} s_L^{(-)}}; \quad F_1 = \frac{1}{s_L^{(+)}} - \frac{1}{s_L^{(-)}} \quad (2.31)$$

$$F_{22} = \frac{1}{s_T^{(+)} s_T^{(-)}}; \quad F_2 = \frac{1}{s_T^{(+)}} - \frac{1}{s_T^{(-)}}; \quad F_{66} = \frac{1}{s_{LT}^2} \quad (2.32)$$

$$F_{12} = F_{12}^* \sqrt{F_{11} F_{22}} \quad (2.33)$$

where the numerical values of  $s_T^{(-)}$  and  $s_L^{(-)}$ , defined in section 2.1.3.1, are assumed to be positive.

The coefficient  $F_{12}^*$  is often estimated, otherwise it has to be determined from a bi-axial test that is not straightforward to perform. In the absence of a measured value the coefficient is generally set to  $-1/2$  without any significant loss in accuracy [4]. The Tsai-Wu failure criteria is called a quadratic interaction criteria and the failure surface has the shape of an ellipse and because of the differences in tensile and compressive strength the elliptic shape becomes convex.

#### 2.1.4 Laminate theory

A coordinate system is put in the middle surface of the laminate with the  $z$ -axis being parallel to the normal of the laminate. The laminate will then have the height  $h$  and  $z$  goes from  $-h/2 \leq z \leq h/2$ . The forces and moment acting on the laminate can be integrated as

$$\mathbf{N} = \begin{bmatrix} N_x \\ N_y \\ N_{xy} \end{bmatrix} = \int_{-h/2}^{h/2} \boldsymbol{\sigma} dz; \quad \mathbf{M} = \begin{bmatrix} M_x \\ M_y \\ M_{xy} \end{bmatrix} = \int_{-h/2}^{h/2} \boldsymbol{\sigma} z dz; \quad \boldsymbol{\sigma} = \begin{bmatrix} \sigma_x \\ \sigma_y \\ \tau_{xy} \end{bmatrix} \quad (2.34)$$

The deformation of the laminates is defined from the strains and curvatures of the middle surface according to

$$\boldsymbol{\epsilon} = \begin{bmatrix} \epsilon_x \\ \epsilon_y \\ \gamma_{xy} \end{bmatrix} = \boldsymbol{\epsilon}_0 + \boldsymbol{\kappa} z. \quad (2.35)$$

This gives the stress strain relation in a lamina according to

$$\boldsymbol{\sigma} = \mathbf{Q}(\boldsymbol{\epsilon}_0 + \boldsymbol{\kappa} z) \quad (2.36)$$

where  $\mathbf{Q}$  is the stiffness matrix. With this inserted into equation ((2.34)) and integrating between  $-h/2 \leq z \leq h/2$ , with the stiffness matrix being constant in each lamina then the forces and moments can be written as

$$\mathbf{N} = \mathbf{A}\boldsymbol{\epsilon}_0 + \mathbf{B}\boldsymbol{\kappa} \quad (2.37)$$

$$\mathbf{M} = \mathbf{B}\boldsymbol{\epsilon}_0 + \mathbf{D}\boldsymbol{\kappa} \quad (2.38)$$

where

$$\mathbf{A} = \sum_k \mathbf{Q}_k h_k \quad (2.39)$$

$$\mathbf{B} = \sum_k \mathbf{Q}_k h_k \bar{z}_k \quad (2.40)$$

$$\mathbf{D} = \sum_k \mathbf{Q}_k h_k (\bar{z}_k^2 + 1/12 h_k^2) \quad (2.41)$$

and the subscript  $k$  denotes laminae number  $k$  and  $\bar{z}$  is the distance to the mid surface of a lamina. Equation (2.37) and (2.38) can be written in matrix form;

$$\begin{bmatrix} \mathbf{N} \\ \mathbf{M} \end{bmatrix} = \begin{bmatrix} \mathbf{A} & \mathbf{B} \\ \mathbf{B} & \mathbf{D} \end{bmatrix} \begin{bmatrix} \boldsymbol{\epsilon}_0 \\ \boldsymbol{\kappa} \end{bmatrix}. \quad (2.42)$$

This describes the linear relation between the loads  $\mathbf{N}$  and  $\mathbf{M}$  and the deformations  $\boldsymbol{\epsilon}_0$  and  $\boldsymbol{\kappa}$  [5]. The extensional stiffness matrix  $\mathbf{A}$  relates the force  $\mathbf{N}$  to the strains  $\boldsymbol{\epsilon}$  and the bending stiffness matrix  $\mathbf{D}$  relates the moments  $\mathbf{M}$  to the curvature  $\boldsymbol{\kappa}$ . The coupling stiffness matrix  $\mathbf{B}$  couples the membrane bending behaviour of the laminate, i.e. relates the forces  $\mathbf{N}$  to the curvature  $\boldsymbol{\kappa}$  and the moments  $\mathbf{M}$  to the strains  $\boldsymbol{\epsilon}$ . Dependent on how the plies are stacked the matrices will be populated in different ways. For example in some cases, depending on the ply angle and the stacking sequence, the moment  $M_x$  can cause a twisting curvature  $\kappa_{xy}$  in addition to the bending curvatures  $\kappa_x$  and  $\kappa_y$ .

The correlation between the predicted values from the laminate theory of the stiffness, described in section 2.1.4, and test data for all kinds of symmetric laminate configurations is consistently very satisfactory. The accuracy of the prediction depends on the accuracy of the basic elastic properties  $E_1$ ,  $E_2$ ,  $G_{12}$  and  $\nu_{12}$  [4].

### 2.1.5 Interlaminar stresses

In the plane stress assumption, made in section 2.1.2, all the stresses in the  $z$ -direction are neglected. A state of plane stress does exist in the laminas of a laminate in regions sufficiently far away from discontinuities such as free ends. The plane stress assumption is most accurate for structures with thin walled elements [4]. It has been shown that even for laminates under uniaxial loading there is a boundary layer region along the free edges where a 3-dimensional state of stress exists, a boundary layer region approximately equal to the laminate thickness [2]. These so called interlaminar stresses associated with the  $z$ -axis can cause delamination, or separation of the laminas. According to [2] the interlaminar stresses are

$$\tau_{xz}(z) = - \int_{-t/2}^z \frac{\partial \tau_{xy}}{\partial y} dz \quad (2.43)$$

$$\tau_{yz}(z) = - \int_{-t/2}^z \frac{\partial \sigma_y}{\partial y} dz \quad (2.44)$$

$$\sigma_z(z) = - \int_{-t/2}^z \frac{\partial \tau_{yz}}{\partial y} dz \quad (2.45)$$

and they are visualised in Figure 2.6. The interlaminar shear stress  $\tau_{xz}$  goes from zero in the interior region to a very large value approaching the free end, which follows from equation (2.43). All the interlaminar stresses are equal to zero in the interior region.

Interlaminar stresses in layered laminates arises from the consideration of relative ply elastic constants in adjacent plies. It can also arise from a consideration of stress equilibrium along the free edge faces of the laminate subjected to load. Since failure due to these stresses can occur they have to be taken into account in the designing process [4]. Since this is a three dimensional problem and the laminate analysis only predicts in-plane stresses additional analysis is required to predict those stresses. How those stresses can be estimated can be found in [4].

It has been shown both analytically and experimentally that the influence of the interlaminar stresses are dependent on the stacking sequence. The stacking sequence can change the interlaminar normal stress  $\sigma_z$  from tensile to compressive. Since tensile interlaminar normal stresses tend to separate the plies and compressive stresses would tend to

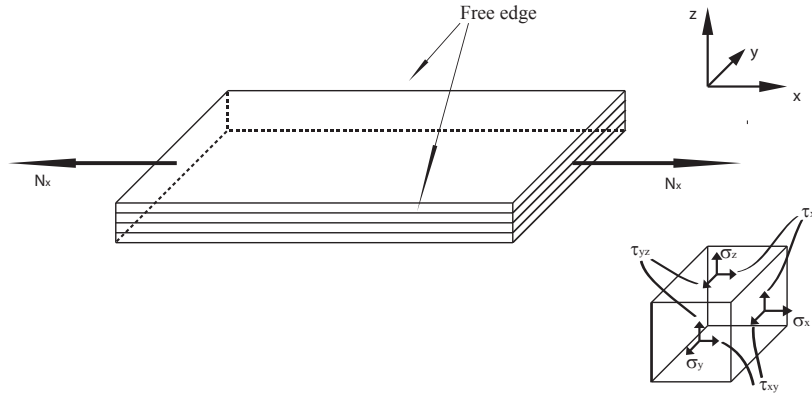


Figure 2.6: In-plane and interlaminar stresses in a layered laminate.

keep the plies together the stacking sequence producing tensile stresses would then have lower strength.

### 2.1.6 Laminate strength

In section 2.1.3.1 different types of failure criteria for a lamina were discussed. When analysing a laminate one has to translate the stresses and strains to the lamina level to use the failure criteria for a lamina. Failure can occur both due to in-plane stresses and due to interlaminar stresses. As have been discussed in section 2.1.5 the interlaminar stresses can lead to a mode of failure known as delamination.

In many laminated constructions the ultimate failure occurs soon after first lamina failure. For many other laminates the stress level of the first lamina failure and the ultimate stress level differ quite much. Thus, to predict laminate failure based on first lamina failure may be too conservative [6]. There will usually be a sequence of lamina failures, because laminates often have the different laminas oriented in different angles, leading to an ultimate failure when all laminas have failed.

To model the failure of the different plies the stiffness for the failed ply and the corresponding laminate stiffness matrix has to be modified to reflect the effect of these failures. Calculation of this modified laminate stiffness requires the knowledge of the modified ply stiffness. To know this stiffness the type of failure must be known. Alternatively all the stiffnesses for the failed ply may be set to zero when calculation of the modified laminate stiffness [2]. When setting the stiffness for the ply to zero this assumes that the ply fails instantaneously when the failure stress level has been reached. This will create knees in the load-deformation curves that is sharp for each ply that fails, see Figure 2.7. This may not be the case in reality when the failure occurs gradually over a finite strain range.

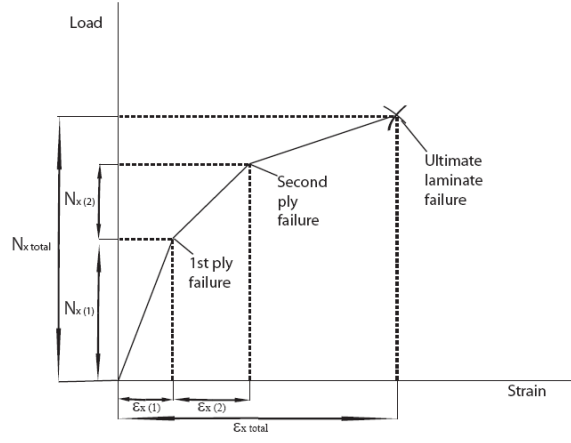


Figure 2.7: Load-strain curve for an uniaxial loaded laminate showing multiple ply failure up to ultimate laminate failure.

When delamination occurs due to interlaminar stresses the failure stress of the laminate can be reduced below the value predicted by the in-plane failure criteria. The initiation of delamination is often followed by stable delamination which grows to unstable delamination and ultimate failure. Hence, initiation and failure are not the same. A fracture mechanics approach is preferred when dealing with delamination growth and failure stages while mechanics of material is preferred when dealing with prediction of delamination initiation [2]. A quadratic failure criteria, a mechanics of material approach, predicting initiation of delamination can be stated as

$$\left(\frac{\bar{\tau}_{xz}}{s_{XZ}}\right)^2 + \left(\frac{\bar{\tau}_{yz}}{s_{YZ}}\right)^2 + \left(\frac{\bar{\sigma}_z^t}{s_Z^{(+)}}\right)^2 + \left(\frac{\bar{\sigma}_z^c}{s_Z^{(-)}}\right)^2 = 1 \quad (2.46)$$

where the overbar means averaging of the interlaminar stresses and  $s$  stands for strengths[2]. The averaging in this case is defined as

$$\bar{\sigma}_{ij} = \frac{1}{\lambda_{avg}} \int_0^{\lambda_{avg}} \sigma_{ij} d\lambda \quad (2.47)$$

where  $\lambda_{avg}$  stands for the averaging dimension, e.g distance from the free edge, and  $\sigma_{ij}$  stands for the stress components. Since the data for interlaminar strengths are not usually available the strength value  $s_Z = s_T$ , in the case of transversely isotropy [2], and the parameters  $s_{XZ} = s_{YZ} = s_{LT}$  [6] can be used instead. Interlaminar stresses can not only cause delamination near free edges in laminates, it may also occur at other discontinuities such as ply drop offs, see Figure 2.8.

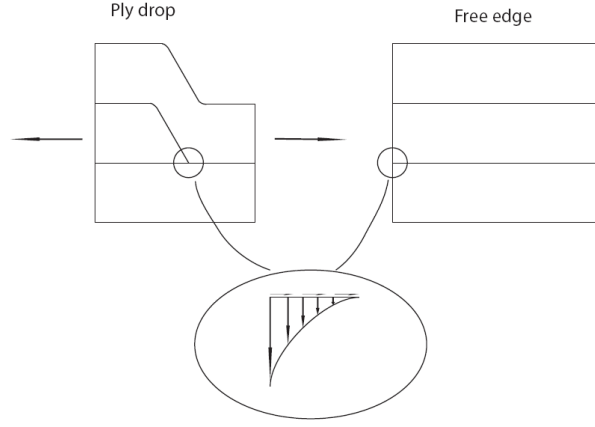


Figure 2.8: Interlaminar stresses in two different discontinuities, drop off and free edges.

Failure is not the only undesired result of delamination. Delamination does also cause reduced stiffness which can make the structure unsafe even if fracture does not occur. Stiffness loss can be used to characterise the growth of delamination and a model for this is described in [2].

## 2.2 Contact mechanics

Based on a simple one-dimensional example, this section gives brief descriptions of various methods used to solve contact problems. Assume that a point mass  $m$  is attached to a spring, stiffness  $k$ , which is clamped at the end according to Figure 2.9. Gravity  $g$  is acting on the system and the deflection of the mass is restricted by a rigid surface below the mass.

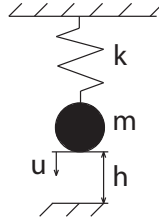


Figure 2.9: Point mass supported by spring.

The total energy of the system without considering any constraint can be written as

$$\Pi(u) = \frac{1}{2}ku^2 - mgu. \quad (2.48)$$

The restriction of the motion of the mass due to the rigid surface can be described by

$$c(u) = h - u \geq 0 \quad (2.49)$$

which prevents penetration to occur. For  $c(u) > 0$  there is a gap between the mass and the surface, for  $c(u) = 0$  the gap is closed. As the mass is in contact with the surface a reaction force  $f_R$  appears. It is always assumed to be negative, hence the contact pressure can only be compression. Thus the following statement yields:

$$c(u) \geq 0, \quad f_R \leq 0 \quad \text{and} \quad f_R c(u) = 0 \quad (2.50)$$

The Lagrange multiplier method adds this constraint to the energy equation:

$$\Pi(u, \lambda) = \frac{1}{2}ku^2 - mgu + \lambda c(u). \quad (2.51)$$

where  $\lambda = f_R$ . The variation of equation (2.51) leads to two equations, since  $\delta u$  and  $\delta \lambda$  can be varied independently.

$$ku\delta u - mg\delta u - \lambda\delta u = 0 \quad (2.52)$$

$$c(u)\delta\lambda = 0 \quad (2.53)$$

Equation (2.52) represents the equilibrium for the mass and equation (2.53) states the fulfilment of the kinematic constraint. By assuming that  $c(u) = 0$  one can now solve for Lagrange multiplier  $\lambda$

$$\lambda = kh - mg = f_R. \quad (2.54)$$

Still  $f_r \leq 0$  needs to be fulfilled of the solution to equation (2.54) [7] [8].

The penalty method is another contact formulation. Here a penalty term is added to equation (2.48) (only if  $c(u) > 0$ ) as follows:

$$\Pi(u) = \frac{1}{2}ku^2 - mgu + \frac{1}{2}\epsilon[c(u)]^2 \quad \text{with } \epsilon > 0 \quad (2.55)$$

The penalty parameter  $\epsilon$  can be interpreted as a spring stiffness in the contact interface between the mass and the rigid surface, see Figure 2.10.

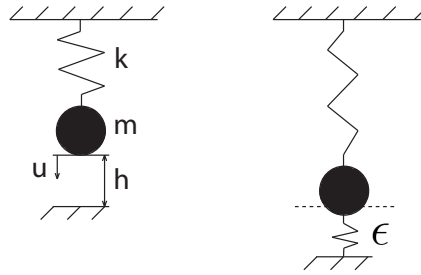


Figure 2.10: Illustration of the penalty spring that appears due to the penalty term.

The variation of equation (2.55) yields

$$ku\delta u - mg\delta u - \epsilon c(u)\delta u = 0 \quad (2.56)$$

from which the following solution can be derived:

$$u = \frac{mg + \epsilon h}{k + \epsilon} \quad (2.57)$$

The constraint equation is then

$$c(u) = h - u = \frac{kh - mg}{k + \epsilon} \quad (2.58)$$

Since  $mg \geq kh$  in the case of contact, equation (2.58) means that a penetration of the mass into the rigid surface occurs. This is physically equivalent to a compression of the spring with stiffness  $\epsilon$  in Figure 2.10. The penetration depends upon the penalty parameter  $\epsilon$ . A high value of  $\epsilon$  leads to small penetrations and vice versa.

The Direct method and the augmented Lagrange method are two other contact methods. Augmented Lagrange combines the penalty method with the Lagrange multiplier method. The direct method is based on the fact that the contact constraint is enforced directly, i.e. that the gap is assumed to be closed immediately [7]. For more detailed description of the above mentioned methods, see [7] and [8].

## 2.3 Computer experiments

A good experimental design should minimise the number of runs to acquire as much information as possible. There are two types of experiments, physical and computer experiments. There always exist random errors in physical experiments, e.g. physical experiment can give different outputs for the identical experimental settings. Therefore when setting up and analysing the experiments, statistical experimental designs may be used. Many physical experiments can often be expensive and time consuming and the experiments can be modelled by some mathematical model.

An engineering model trying to describe the physics can be of the form

$$y = f(x_1, \dots, x_s) = f(\mathbf{x}), \quad \mathbf{x} = (x_1, \dots, x_s)' \in T \quad (2.59)$$

where  $\mathbf{x}$  is the input variable,  $y$  is the output variable, the function  $f$  is the physical system to be described and  $T$  is the input variable space. Equation (2.59) can be regarded as a solution to many types of equations; linear, nonlinear, ordinary, and/or partial differential which often can be impossible to solve analytically. To find the relation of the input  $x_i$  and  $y$  can be time consuming and expensive for the physical model. One of the goals of computer experiments is to find an approximate model, a metamodel, see equation (2.60), that is much simpler than the true one [9].

$$y = g(x_1, \dots, x_s), \quad \mathbf{x} \in T \quad (2.60)$$

A schematic model of this can be seen in Figure 2.11. The characteristics of the computer experiments compared to the physical are for example that each experiment can be reproduced and the same inputs will give identical outputs and it often involves larger numbers of variables compared to those of a physical experiment[9].

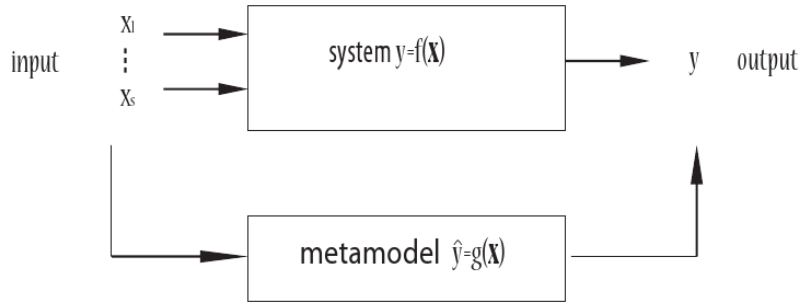


Figure 2.11: Schematic illustration of the system and the metamodel.

For a given number of runs,  $n$ , one wants to find a good design  $D_n = \mathbf{x}_1, \dots, \mathbf{x}_n$ , where  $\mathbf{x}$  are the input parameters, that minimises the deviations of the metamodel and the function  $f$  in equation (2.59). One method to estimate the deviation is the sample mean method, for more information see [9]. There are different ways to generate  $D_n$  for the sample mean method, one of them that has been shown to have a good space-filling design is the latin hypercube sampling (LHS) and its modifications[9].

When the data from the computer experiments have been collected one wants to find a metamodel that describes the relationship between the input and the output. The aim is to create an analytical formula that approximates the system in equation (2.59). For a given true model there are many possible metamodels and it is difficult to say which is the



best. The purpose is to find a useful model. Two types of metamodels are the polynomial models that approximates the model with polynomial bases and the radial basis function (RBF) methods, for more information about metamodels see [9].

There are different ways of estimating the prediction error for the metamodel,  $g$ , one way is to have direct evaluation of the error which is very time consuming. A method for this that evaluates the approximate error over the whole experimental region is called the mean squared error (MSE) and is defined as

$$MSE(g) = \int_T \{f(\mathbf{x}) - g(\mathbf{x})\}^2 d\mathbf{x}. \quad (2.61)$$

For large models that computationally intensive the Cross Validation (CV) procedure is often used. The CV score is defined as

$$CV_n = \frac{1}{n} \sum_{i=1}^n \{f(x_i) - g(x_i)\}^2. \quad (2.62)$$

This method can give good approximation of the predicted error of  $g$  and is referred to as "leave-one-out cross validation" [9].

### 3 Material modelling

This section describes the material used and how the material model used in Abaqus was obtained.

The spring orthosis is made from a pre-impregnated(pre-preg) high strength carbon fibre composite material. The composite is woven as a 4x4 twill, see Figure 3.1, with material parameters according to Table 3.1. The material parameters were provided by the manufacturers, Advanced Composite Group. Note that these data are normalised for 50 volume percent carbon fibre, except for in-plane shear and inter laminar shear strength (ILSS). 50% of the fibres run in one direction and the other 50% run in the perpendicular direction. This means that  $\nu_f = 25\%$  in one direction.

Woven composites are often assigned one warp and one weft direction, where the weft direction is transverse the warp direction (often, but not necessarily, perpendicular to each other). Depending on how the weft fibres are woven relative the warp fibres different properties can be obtained in different directions. The 4x4 twill has no differences between the warp and weft direction.

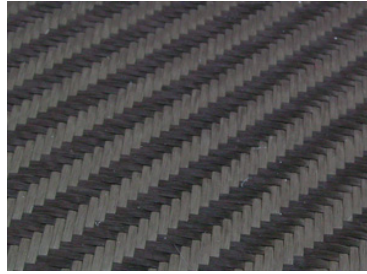


Figure 3.1: 4x4 twill

Table 3.1: Material parameters for 4x4 twill VTM266/CF0100,  $\nu_f = 50\%$

$E_1^{tensile}$	60.0	GPa
$E_1^{compressive}$	54.1	GPa
$E_2^{tensile}$	60.0	GPa
$E_2^{compressive}$	54.1	GPa
Tensile strength	700	MPa
Compressive strength	541	MPa
$\nu_{12}$	0.08	
$G_{12}$	3.87	GPa
In-Plane shear strength	95.5	MPa
Interlaminar shear strength	71.4	MPa

The spring orthosis is created from 24 separate plies, or laminas, together forming a laminate. Of these plies, 18 are used to construct the spring, whereas the rest 6 plies are mainly to provide comfort for the user. The plies forming the spring are cut to rectangular strips from a large sheet of carbon fibre received from manufacturer. Each ply is then separately applied onto a cast of the patient's foot, this procedure is called draping. Since this is done by hand the draping procedure varies from one job to another, depending on who is performing it and the variation of pressure applied by the constructing engineer. The layup of the plies and further information on how the plies are draped is covered in section 4.2.

The variation of applied pressure will result in a variation of amount epoxy pouring out, i.e. the volume fraction carbon fibre,  $v_f$ , changes value. As can be read in section 2.1.1 this will affect the material properties. By using micromechanics theory described in section 2.1.1 these parameters can be determined as a function of fibre volume fraction,  $v_f$ , and the corresponding material parameters from carbon fibre and epoxy. The effective stiffnesses  $E_1$  and  $E_2$  can be fairly approximated by using equation (2.10). If applying equation (2.10) with data from carbon fibre and epoxy according to Table 3.2 and using  $v_f = 25\%$  this will result in the following value:

$$E_1 = E_{f1}v_f + E_mv_m = 60.5 \text{ GPa} \quad (3.1)$$

*Table 3.2: Young's modulus for carbon fibre and epoxy*

Carbon fibre	Epoxy
230 GPa	4 GPa

The effective value in equation (3.1) is close to the tensile modulus stated in Table 3.1. However the other parameters, e.g. Poisson's ratio, shear modulus, tensile and compressive strengths, will be difficult to calculate for different volume fractions of fibre. This is mainly because of the uncertainties of how much the weft will affect the composite's behaviour. The best choice is to use the material parameters supplied by the manufacturers. Since epoxy material is lost during manufacturing one has to make sure to use data obtained from a test specimen with  $v_f \approx 50\%$ .

### 3.1 Four point bending test

The test was conducted by the Technical Research Institute of Sweden. Nine different test specimens were separately subjected to a four point bending test according to Figure 3.2. The specimens consist of 18 plies, stacked  $[45^\circ/0^\circ]$ , and they were hand made in the same way as the orthosis and thus have varying thickness depending on the pressure applied during manufacturing. Higher pressure will result in a thinner and a stiffer plate. The length and width of all specimens were 246 mm and between 43.9 – 44.0 mm respectively while the varying thickness of the plates can be seen in Table 3.3.

The load was applied on the two middle supports until failure occurred, i.e. when the test specimen lost all its strength. The vertical velocity of the two middle supports was 5 mm/min downwards and the displacement as well as the applied force were recorded throughout the entire test period. The results of each test can be seen in Table 3.3, where the maximum load and displacement were obtained at the time when ultimate failure occurred. c

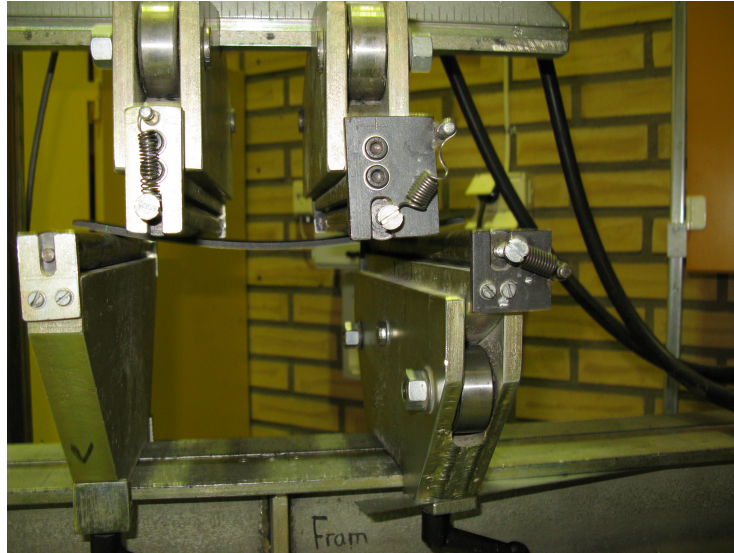


Figure 3.2: Set-up of 4-point bending test

Table 3.3: Test results for all nine test specimens from four point bending test

Specimen number	Thickness [mm]	Max Load [kN]	Max displacement [mm]
1	5.58	5.30	20.5
2	5.28	4.39	21.6
3	5.60	4.80	18.0
4	5.30	4.75	23.9
5	5.18	4.40	24.2
6	5.19	4.35	26.9
7	4.78	4.05	27.5
8	4.73	4.17	26.4
9	4.78	3.99	29.2

To be able to verify the material model the four point bending test was reconstructed in Abaqus/CAE. Calculations, which can be found in Appendix A, show that a test specimen with  $v_f = 50\%$  should have a thickness of 5.70 mm. Test specimen number 3 in Table 3.3 has a thickness of 5.60mm which differs less than 2% from a test specimen with  $v_f = 50\%$ . Thus it seems reasonable to use material data received from manufacturers and comparing with test data from specimen number 3.

### 3.1.1 Setup of Abaqus model

The four point bending experiment described in section 3.1 was used to validate the material model in Abaqus/CAE. This was done by comparing the force/displacement curve of the middle supports from the experiment to the force/displacement curve from the finite element simulations in Abaqus/CAE.

Since the compressive strength is less than the tensile strength, see Table 3.1, the initial failure was assumed to have occurred at the top of the plate where compressive stresses are present. This was also detected in the experiments made by SP, and can be seen in Figure 3.3 where force versus displacement is plotted. After the assumed compressive failure the strength of the structure was reduced and this appears as a small dip in the curve. After the first ply failure different types of failure modes could be present, which

was not modelled. The force, 3.3kN, and the displacement, -11.3mm, recorded at this dip was used as a reference.

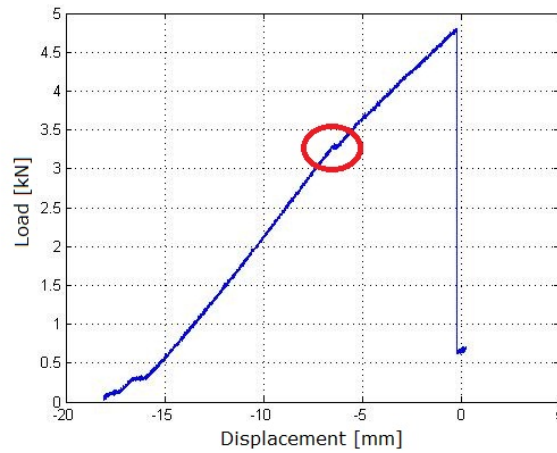


Figure 3.3: Recorded force of test specimen number 3. The dip that is assumed to have occurred due to compression failure of the top lamina is highlighted. Due to the brittleness of carbon fibre the dip is quite sharp and sudden.

To set up the test in Abaqus, the following parameters had to be determined:

- Material model and material parameters
- Dimensions of the rolls and the plate
- Boundary conditions
- Finite element mesh
- Element type
- Friction coefficient,  $\mu$
- Contact formulation

The following parameters are given; material data sheet, dimensions of rolls and plate, stacking sequence. The test suppliers have confirmed that there is friction present between the rolls and the plates, but not the magnitude of it.

### 3.1.2 Material Model

The material was modelled according to equation (2.23) as a balanced orthotropic lamina with  $E_1 = E_2$  described in section 2.1.2. This corresponds to the material model "lamina" in Abaqus/CAE, see [10], which is a plane stress orthotropic elasticity material model. Required parameters in this model are  $E_1 (= E_2)$ ,  $\nu_{12} (= \nu_{21})$ ,  $G_{12}$  and  $G_{13} (= G_{23})$ . The out of plane shear moduli  $G_{13}$  and  $G_{23}$ , which are not included in equation (2.23), are needed for the out of plane stiffness needed to model the transverse shear deformation. This means that there are 4 independent material parameters to determine. Since  $G_{13}$  and  $G_{23}$  are not given in the material data sheet they were tuned so that the vertical reaction force would match the force obtained from the test, see Figure 3.3.

The Tsai-Wu failure criterion, described in section 2.1.3.2, was used as an equivalent stress measure. It was used when comparing different test parameters and to investigate where and when failure has occurred. The parameters required in the criterion can be seen in Table 3.4.

Table 3.4: Parameters used in the Tsai-Wu failure criterion.

$F_{11}$ [ $MPa^{-2}$ ]	$F_{22}$ [ $MPa^{-2}$ ]	$F_1$ [ $MPa^{-1}$ ]	$F_2$ [ $MPa^{-1}$ ]	$F_{66}$ [ $MPa^{-2}$ ]	$F_{12}$ [ $MPa^{-2}$ ]
$3 * 10^{-6}$	$3 * 10^{-6}$	$-0.42 * 10^{-3}$	$-0.42 * 10^{-3}$	$0.11 * 10^{-3}$	$-\frac{3}{2} * 10^{-6}$

From the material data sheet one can see that Young's modulus differs in compression and tension. There is no possibility to model this in Abaqus. To compensate for this an average of  $E_1$  and  $E_2$  was calculated accordingly:

$$E_{1,2} = \frac{1}{2} (E_{1,2}^{compressive} + E_{1,2}^{tensile}) \quad (3.2)$$

The stacking sequence used is the same as for the original layup of the spring, 18 plies with  $[45^\circ/0^\circ]$ , see Figure 3.4.

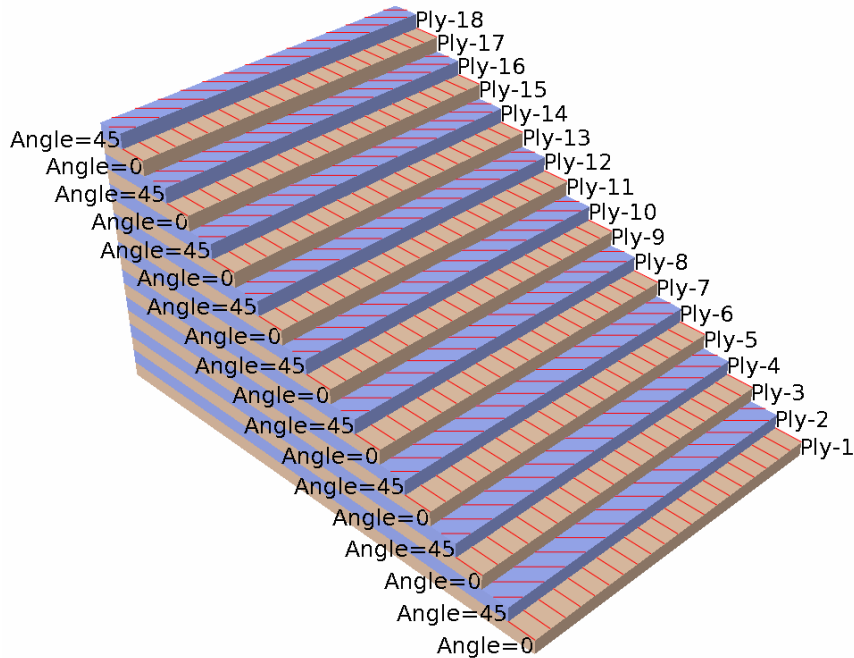


Figure 3.4: Ply stack plot of the plate. The normal of the shell is pointing downwards so ply 1 is on the top and ply 18 is on the bottom of the plate.

### 3.1.3 Geometry and boundary conditions

The geometry of the rolls and the plate can be seen in Figure 3.6. Dimensions of the plate were taken from test specimen number 3, see Table 3.3, and the rolls diameter,  $D=0.02m$ , was measured from the real equipment used in the test. Since the test set up is symmetric in x- and z-direction, the length and the width was divided into halves i.e from  $0.246m \times 0.044m$  to  $0.123m \times 0.022m$ . This meaning that the reaction force used for comparison will be divided by 4. The thickness of the plate is  $0.0056m$ .

The geometry of the plate was modelled with two different types of shell elements; conventional shells, which is a thin shell, and continuum shell which is a thick shell, see Figure 3.5(a) and Figure 3.55(c). When using a continuum shell the thickness is modelled and it is possible to use one element for each layer of the composite. In the area around the contact a mesh refinement was made to better capture what happens in this area and to

model the contact properly. The mesh refinement was chosen such that further refinement did not affect the result of the simulations.

The rolls were modelled as rigid bodies, see figure 3.55(b). A rigid body is a collection of nodes, elements and/or surfaces whose motion are governed by the motion of the rigid body reference point. The relative positions of the elements and nodes remains constant under the simulations. Therefore, the elements of the rigid body do not deform but can have large rigid body motions [10].

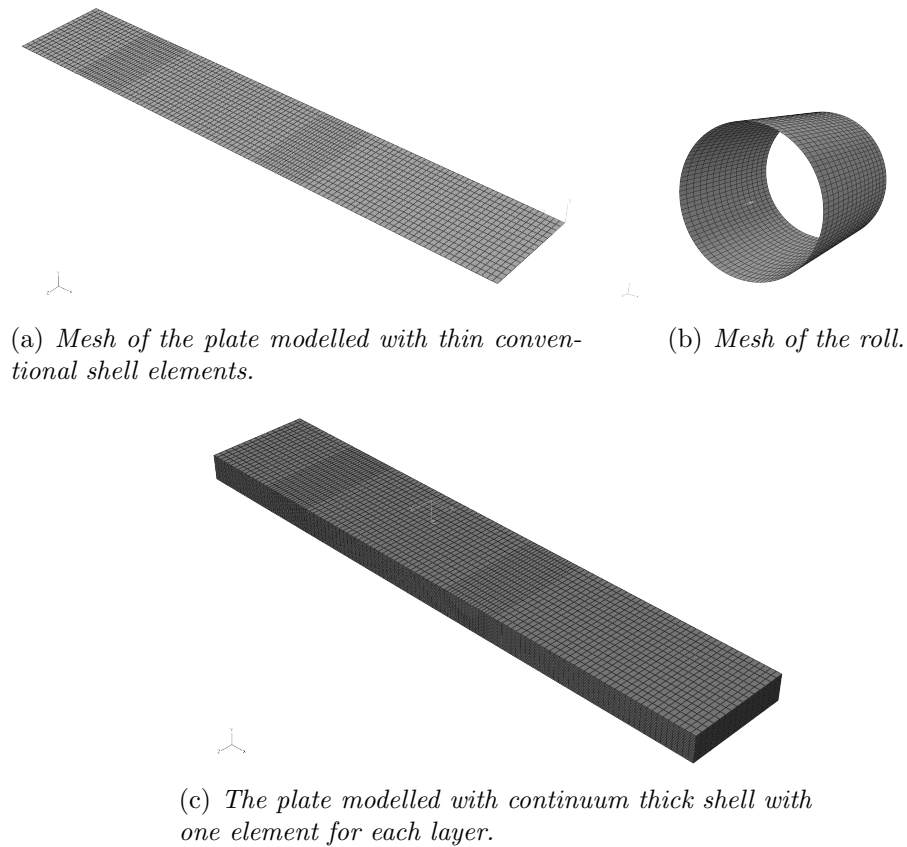


*Figure 3.5: The mesh of the rolls and the plate used in Abaqus/CAE.*

Boundary conditions for the rolls were applied to the reference points of the rolls. For the roll that is acting as a support all the degrees of freedom were fixed and the roll that moves downwards had a prescribed displacement in the negative vertical direction and all other degrees of freedoms fixed. All boundary conditions for the four point bending test can be seen in Figure 3.6 and Table 3.5.

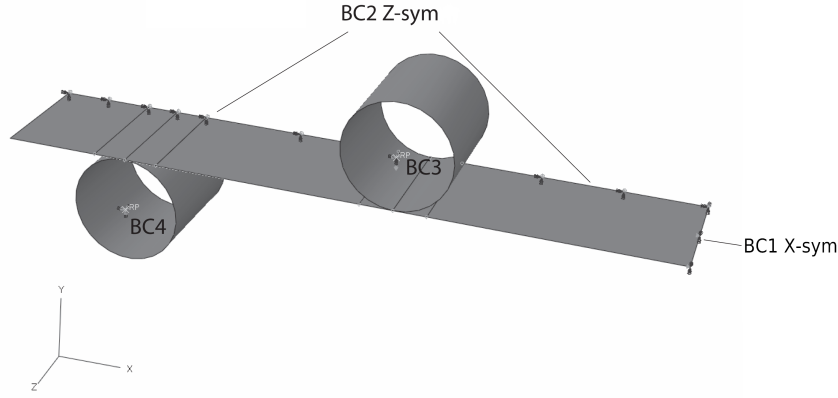


Figure 3.6: Test setup in Abaqus. Dimensions of the plate are  $0.246 \times 0.044 \times 0.0056$  and the roll diameter is  $0.02\text{m}$ . The boundary conditions for the test setup are also shown, the different boundary conditions can be seen in Table 3.5.

Table 3.5: Boundary conditions tabulated for the four point bending test model.

Boundary	$u_x$	$u_y$	$u_z$	$rot_x$	$rot_y$	$rot_z$
BC1, X-symm	0	free	free	free	0	0
BC2, Z-symm	free	free	0	0	0	free
BC3	0	-0.0113	0	0	0	0
BC4	0	0	0	0	0	0

### 3.1.4 Element selection

For the continuum shell the linear continuum shell element with reduced integration SC8R was used. There are three different types of thin quadrilateral shell elements supporting computations with layered composites; S8R, S4R and S4. The elements S4 and S4R are linear elements with 4 nodes and S8R is a 2nd order element with 8 nodes, R stands for reduced integration. Reduced integration means that a lower order integration is used to form the element stiffness matrix[10]. For more information about the elements in Abaqus see [10].

Abaqus will integrate over the thickness of the shell to establish the matrices described in section 2.1.4. When estimating the transverse shear stiffness and interlaminar shear stresses Abaqus assumes that the shell section directions are the principal bending directions. If the layered orthotropic laminate is not symmetric around the mid surface, it may be so that the shell section direction is not the principal bending direction, which will make the approximation of the transverse shear stiffness and interlaminar shear stresses less accurate [10]. The interlaminar shear stresses are only calculated in Abaqus when the elastic material model is used for each layer of the shell section.

To calculate interlaminar shear stresses it is required that Simpson's integration rule and not Gauss quadrature is used. This is since Simpson's rule has an integration point at the interface between the composite layers which Gauss quadrature does not have [10]. The concept of calculating the interlaminar shear stresses relies on the concept of a "stack" of a continuum shell elements. A stack is defined as a continuous set of continuum shells with the first and last element on a free boundary and that are connected through shared nodes on the top and bottom element surfaces, for more information about stacked continuum



shells see [10].

Because of the loss in accuracy when modelling the transverse shear stiffness with elements having asymmetric layered laminate layup, the computations with conventional shell elements are less accurate. The continuum shell on the other hand models each ply with one layer of elements, thus each ply is symmetric in itself and there is no loss of accuracy. A comparison of how the different element types affect the stiffness was made. The same test setup was used to compare the reaction force of the roll in y-direction. The results are presented in Table 3.6 and shows that the reaction forces of all thin conventional shells are equal and the difference when using a continuum shell is less than 0.5%.

*Table 3.6: Reaction forces when using different element types for a prescribed y-displacement of -0.0113m.*

Element type	S4	S4R	S8R	SC8R
Reaction force	-833N	-833N	-833N	-829N

The computational time of an analysis with a continuum shell (SC8R) is approximately 20 times the computational time of an analysis with a conventional shell (S4R). The main reasons are that the continuum shell model uses one element per ply to model the thickness and that more integration points are used.

Failure can occur as an interaction between different failure modes, e.g. delamination due to interlaminar stresses and failure due to in plane stresses as described in section 2.1.6. Therefore the continuum shell (SC8R) was chosen when analysing the failure that occurred in the four point bending test. The differences of modelling the four point bending test with conventional shells with S4, S4R and S8R compared to stacked continuum shells with SC8R was analysed. This was done by comparing the different stresses. The result of these comparisons can be seen in Appendix B, section B.1.

The continuum shell was also used when tuning the value of  $G_{13,23}$ . The conventional element S4R was however used when analysing composite layup effects, see section 5. This is because of the shorter computational time and the good estimation of the reaction force.

### 3.1.5 Contact interaction

To simulate the interaction between the rolls and the plate a contact interaction formulation is needed. Each contact formulation in Abaqus is based on a choice of a contact discretization, a tracking approach and assignment of master and slave surfaces. A surface-to-surface type of contact was chosen as contact discretization. As a tracking approach finite sliding was used, which allows for arbitrary separation, sliding and rotation of the surfaces[10]. The rolls were set as the master surfaces and the upper and lower part of the plate as slave surfaces. According to [10] discrete rigid surfaces must always be the master surfaces.

A contact constraint model and the frictional behaviour are also needed, for the normal and tangential behaviour respectively. If no friction is requested a frictionless type of tangential behaviour can be used. To model friction, a penalty type of friction behaviour was used, which Abaqus recommends since the Lagrange multiplier method will give convergence problems[10].

The contact constraint enforcement can be modelled in different ways. The direct method strictly enforces the constraints without approximations or use of augmented iterations, which may lead to over constraint issues. The Penalty method, briefly described in section 2.2, approximates the constraints and some degree of penetration will occur. This method reduces the number of iterations needed in the analysis. The linear penalty

method used here uses one value for the penalty stiffness. To lower the amount of penetration this value can be increased. The augmented Lagrange method uses the linear penalty method with augmented iterations that will lower the penetration tolerance and improve the accuracy of the approximation. This method may need more iterations but it avoids the problem with over constraints while lowering penetration. (The penalty and augmented Lagrange constraint enforcement methods sometimes provides more efficient solutions compared to the direct method, due to reduced calculation costs per iteration and a lower number of overall iterations per analysis at some typically small sacrifice in solution accuracy). For more information about the contact formulations in Abaqus see [10].

How the constraints enforcement methods for the normal behaviour and the friction coefficient influenced the results in the simulations were analysed as follows:

- Friction coefficient was changed between  $0 \leq \mu \leq 0.3$ . Stress distribution of the plate with and without friction and how the stresses changes for different values of friction was analysed.
- A comparison between augmented Lagrange, linear penalty and direct contact with friction being fixed,  $\mu = 0.2$ . In this comparison the value of the penetration in the contact area was compared. Also how the methods influenced the stress distribution in the area around the contact was analysed. The requirement was that the contact interaction definition should model reality in the best possible way according to the failure of the test specimen.

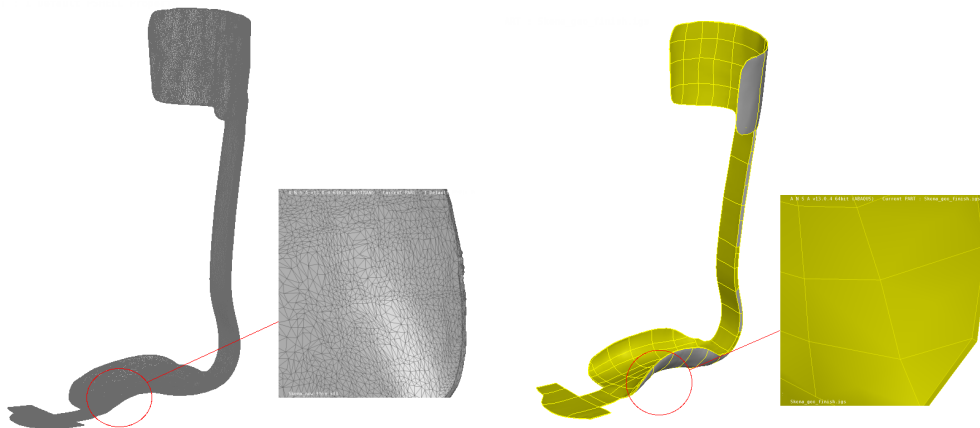
The friction coefficient  $\mu$  was set to 0.2 and augmented Lagrange was chosen as the contact method. The comparisons can be found in Appendix B, section B.2 and B.3.

## 4 Orthosis model

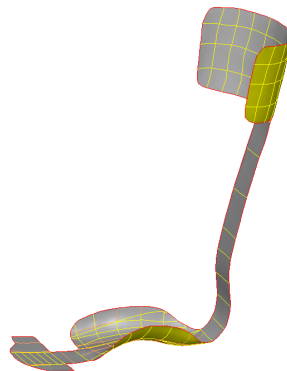
This chapter describes how the FE-model of the orthosis was created, how the walking cycle was applied, how the maximum stresses during the walking cycle were generated and how difference composite layups were selected, created and analysed.

### 4.1 Model geometry

To be able to analyse the orthosis a geometry of the model was needed. The model was scanned and an stl-file was obtained. This file format describes the raw, unstructured, triangulated surface by a unit normal and vertices of the triangles using a three-dimensional Cartesian coordinate system. This format does not have any common CAD attributes so it has to be reconstructed. As can be seen in Figure 1(a) the edges of the model were uneven and rough in the stl file. This is because the scan catches all the irregularities that exist in the model. To obtain a geometry that is easier to work with the pre processor ANSA was used to create surfaces and to smooth the edges. A shell surface was then extracted. The created geometry and the extracted front surface can be seen in Figure 1(b) and 1(c). The main steps in the geometry clean up and shell extraction can be found in Appendix E. Because of the irregularities at the bottom of the orthosis the extracted middle and bottom surfaces were irregular in some regions. Therefore the top surface was used.



(a) Scanned geometry as an stl-file. The (b) Cleaned up geometry. The zoomed in area shows the irregularities at the area shows the edges after the clean up.

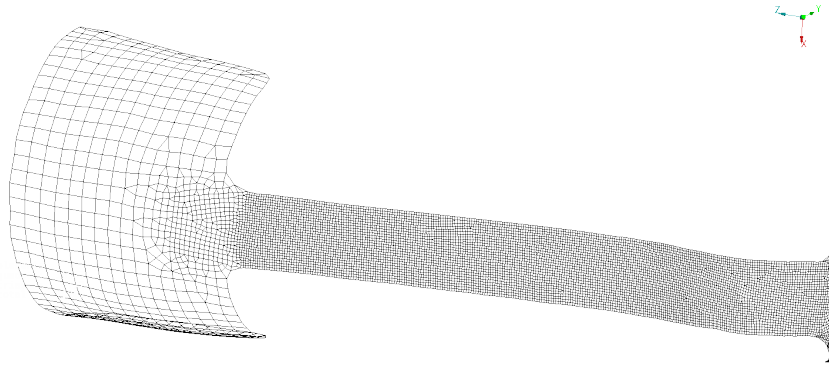


(c) Front surface that was used in the simulations.

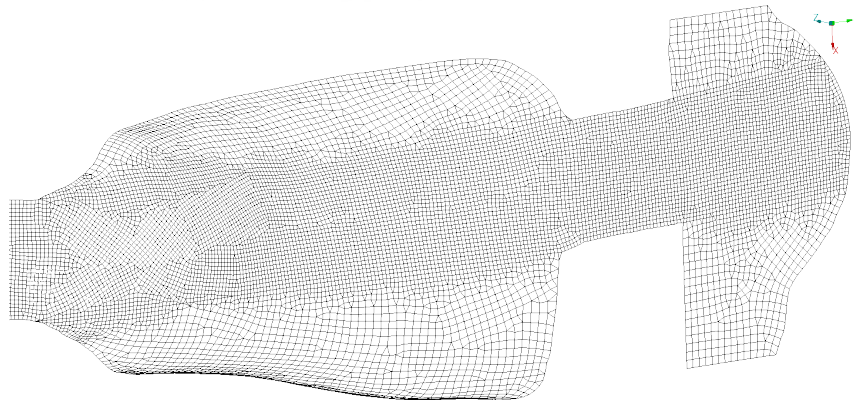
Figure 4.1: Different states of the orthosis model.

### 4.1.1 Mesh

The mesh created in ANSA can be seen in Figure 4.2. A mesh refinement was done in the spring and toe since these areas are of most interest, since this is where most of the deformations occur. The upper support of the orthosis will not be affected during the walking cycle, so this part has a rougher mesh. The sides of the arch of the foot have finer mesh than the top support but rougher than the spring. The elements used are the linear elements S4 and S3. The second order element S8R was rejected due to poor convergence properties of the analyses performed.



(a) *The mesh of the top and the spring.*



(b) *The mesh of the arch of the foot and the toe.*

*Figure 4.2: The mesh used in the analysis.*

## 4.2 Composite layup

The composite layup was created in Composite Modeller (CM), which is an Abaqus plugin. CM allows you to create composite plies with varying properties and orientations. An advantage of CM compared to creating a composite layup in Abaqus/CAE is that it allows you to choose how the plies are draped onto the model. One option is to let a ply orientation follow a seed curve. A seed curve is a curve defined on element edges that can be used to constrain the draping over a surface[11]. By letting the warp of the woven ply follow a single seed curve the orientation angle of the ply will change along the curve. If draping without using a seed curve the ply will be cut to fit the corresponding area and

the angle will remain constant. Figure 4.3 shows the difference between applying a ply with and without seed curve.

Before choosing how the model is draped one has to specify what type of material to use. In this case a biaxial material with 90 degrees between warp and weft was used to model the woven material. A maximum strain angle, the maximum allowed angle between warp and weft when shearing the fabric, also has to be specified and it was set to be 60 degrees, a default value in CM. This was chosen since the this value was unknown from the supplier. When draping the plies on to the model one has to specify which coordinate system that should act as a reference and a point where the seeding should start. The seeding point will then be the starting point, e.g when draping the plies along the seed curves. For more information about draping in CM see [11].

When a ply is stretched to be able to follow a curve the angle between the warp and weft changes, i.e. the warp and weft are no longer perpendicular. CM in Abaqus/CAE gives warnings of this behaviour by making the ply orientation indicator yellow or red. If it shows red it means that the angle is close to the maximum strain angle, see Figure 4.3(a), and that the draping may be changed. This is an advise to the user that this is a bad way of draping. To account for non perpendicular angles between warp and weft the user must define multiple mechanical property sets for a reference material and specify the shear state for each set [11]. These properties must be measured from material tests. Since there were no data for these property sets, Abaqus will not take the shear into account. Abaqus will however take into account the rotation of the ply that follows by draping along a seed curve.

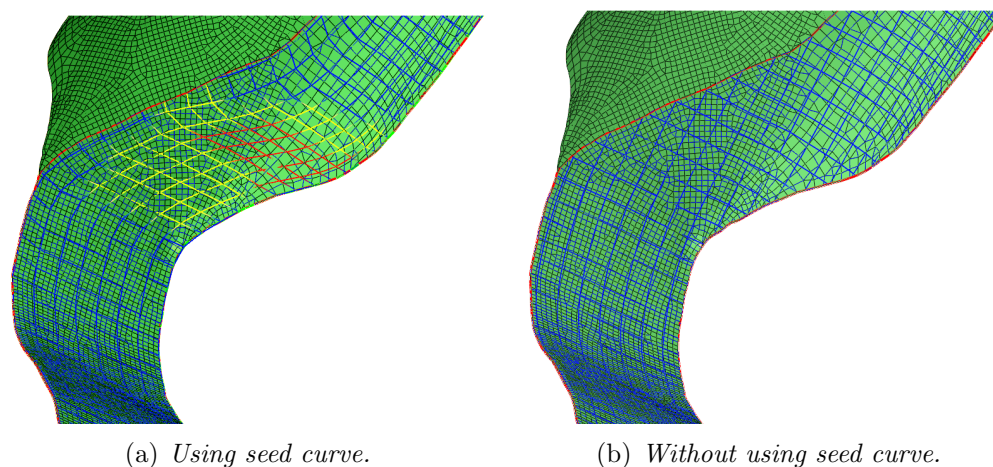


*Figure 4.3: Effect of using seed curve on ply orientation. The same area is draped in both cases, but there is a clear difference between the orientations of the ply.*

#### 4.2.1 Creating original composite layup

Based on interviews and observations of the engineers at Ortopedteknik the draping procedure was reproduced, this is later referred to as the original layup. The spring orthosis consists of 24 separate plies draped onto various regions. The stacking sequence used can be seen in Table 4.1. Different element sets were created to match the areas where the different plies are draped onto. Ply 4-21 are used to build the spring and toe. Figure 4.4 shows the corresponding sets or regions that Table 4.1 refers to.

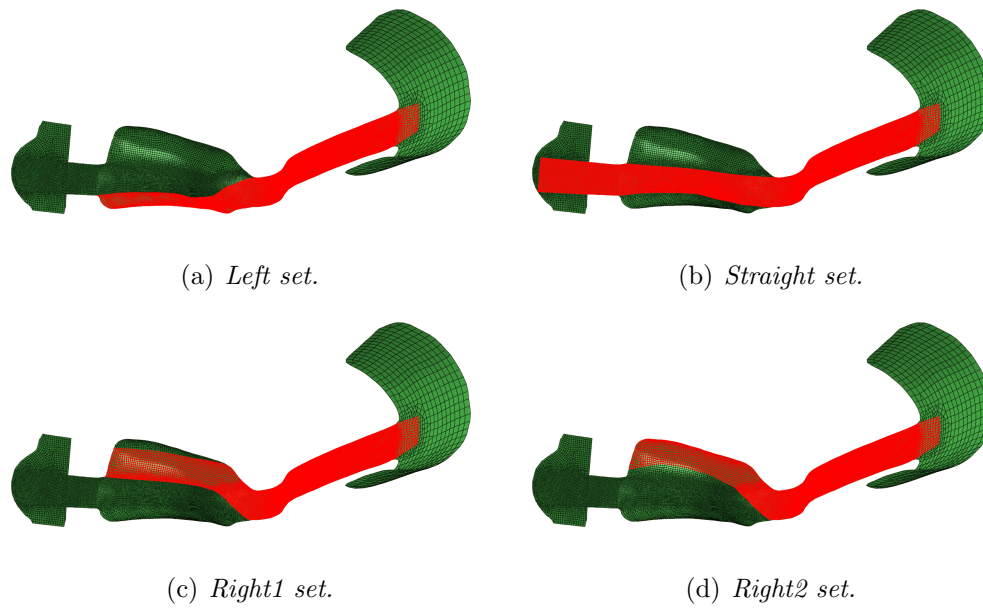


*Figure 4.4: Illustration of different draping regions used when creating the spring.*

The sets in Figure 4.4 were created such that they have approximately equal width all the way from the top of the spring to the toe. The seed curves used can be seen in Figure 4.5. The plies that cover the straight set do not need a seed curve. These plies are not equal, they are cut shorter and shorter to form something that looks like a stair, illustrated in Figure 4.6 with ply 5 being the longest and ply 13 being the shortest. The regions of interest during the analysis are the spring and the toe. These element sets are illustrated in Figure 4.8. These regions are the ones with largest deformations of the orthosis, while the arch of the foot and the top support mainly are for comfort. Ply 1-3 and 22-24 are draped without using seed curves, see Figure 4.7.

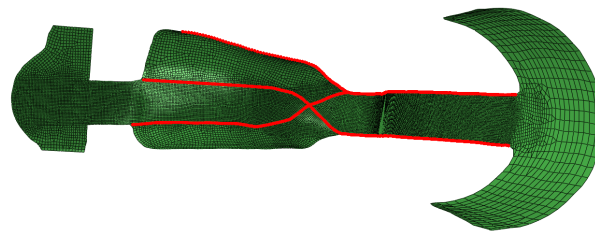


*Figure 4.5: Seed curves used when creating the spring*

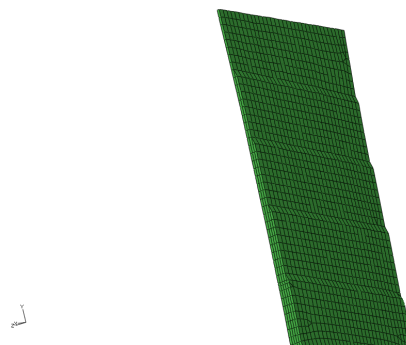


*Figure 4.6: Solid model created to show how the toe part is built.*



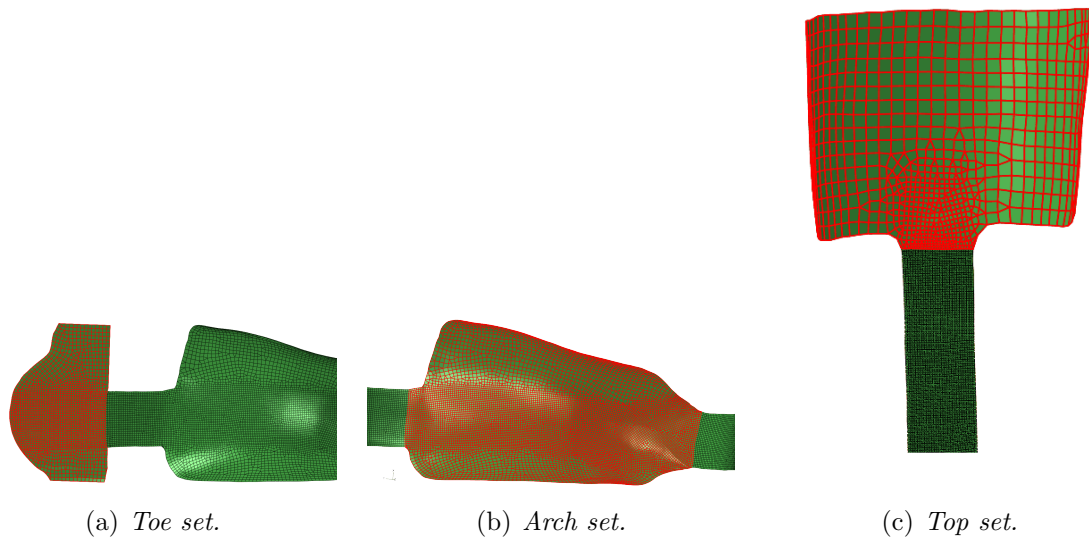


Figure 4.7: Illustration of different draping regions used when creating ply 1-3 and 22-24.

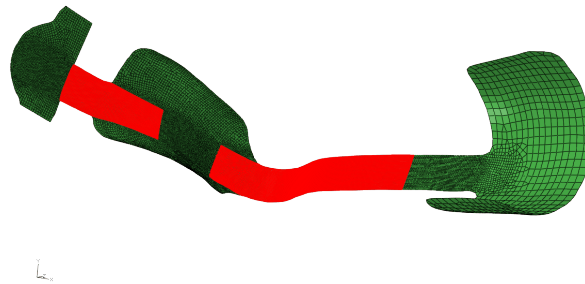


Figure 4.8: Element sets used for analysis, toe element set and spring element set.

The plies were draped in the order of Table 4.1 with ply 1 closest to the foot. They are added in the direction of the normal pointing to the ground, which means that the ply 24 is closest to the ground.

Table 4.1: Ply stacking sequence of spring orthosis original layup. The element sets can be seen in Figure 4.4 and 4.7.

Ply	Orientation	Element set
1	45°	Arch
2	0°	Top
3	0°	Toe
4	45°	Left
5	0°	Straight level 5
6	45°	Right1
7	0°	Straight level 4
8	45°	Right2
9	0°	Straight level 3
10	45°	Left
11	0°	Straight level 2
12	45°	Right1
13	0°	Straight level 1
14	45°	Right2
15	0°	Left
16	45°	Right1
17	0°	Right2
18	45°	Left
19	0°	Right1
20	45°	Right2
21	0°	Left
22	0°	Toe
23	0°	Top
24	45°	Arch



### 4.3 Walking cycle

A walking cycle was recorded at Ortopedteknik to see how the orthosis deforms when being used. There were 7 reflectors attached to the orthosis, with positions and numbering according to Figure 4.9. The reflectors were connected by steel connectors glued onto the orthosis, see Figure 4.10. As the patient walked through the room, there were 8 cameras recording the positions of each reflector. To obtain only one step cycle, 0.88 seconds of the recorded time was extracted, containing 213 time steps. This resulted in 3 time histories each for all 7 reflectors, one for x-movement, y-movement and z-movement.



*Figure 4.9: Positions and numbering of reflectors.*



*(a) Arch of the foot.*



*(b) Toe area.*



*(c) Top of the spring.*

*Figure 4.10: Close up photos of how the reflectors were connected to the orthosis.*

In the Abaqus model the reflectors were replaced by reference points. To control the movement of the reference points each point was assigned three boundary conditions, one for each translation direction. No rotational degrees of freedom were controlled. Each boundary condition has magnitude 1 and is related to an amplitude corresponding to the recorded data for that degree of freedom. This creates a 3-dimensional movement of all reference points. However not all are needed to control the motion of the orthosis. To obtain a statically determined position of the orthosis at least 3 points need to be controlled, otherwise unwanted rotations can occur. Relative motion between the points were discovered to cause high stress levels even at the start of the walking cycle. This relative motion can be explained by measurement inaccuracies. For instance the usage of both reference point 1 and 2 caused unrealistically high stresses due to the relative motion between the two points. The more points used to control the motion the more stress inaccuracies were obtained.

To capture the relative motion between the arch of the foot and the spring as well as between the arch and the toe, reference points 2, 4 and 6 were used to control the motion. To transfer the motion of the points to the orthosis an MPC (Multi Point Constraint) was used. MPCs transfer degrees of freedom from one master node to a slave node set. The MPC used is called "beam" and creates a rigid beam between the reference point and the node set[10]. This will constrain both translations and rotations but since there are no rotational boundary conditions only translations are constrained. The beam constraint was used as an attempt to imitate the steel connectors in Figure 4.10.

However there is a difference between controlling the motion by moving the reference points and using constraints compared to reality where the reflectors moves due to deformations of the orthosis. The area close to the slave nodes will show high stress concentrations, an example of this can be seen in Figure 4.11. This is an issue that is very difficult to get away from. Therefore it was of importance to choose the points so that they would not affect the two areas of interest, seen in Figure 4.8.

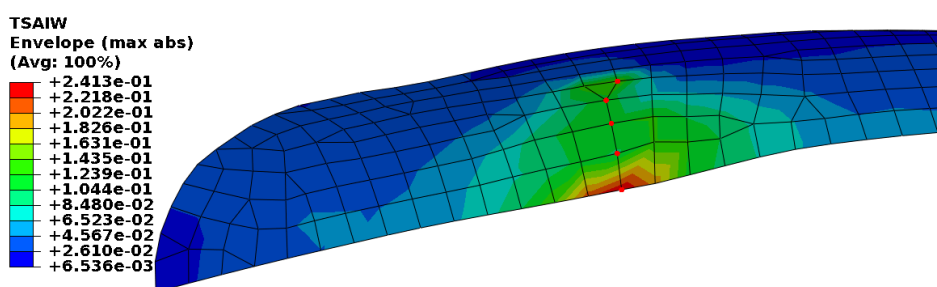


Figure 4.11: An example of stress concentrations that occur in the area around the slave nodes.

The slave nodes used for all constraints can be seen in Figure 4.12. These node sets have been selected to match the areas where the steel connectors are attached to the real model. In Figure 4.12(a) there is also a link constraint between reference point 1 and 2. A link constraint keeps the distance between the points constant. This was used to obtain a more realistic movement of the toe, i.e. to avoid that only the left side of the toe moves in the vertical direction. Still only point 2 is prescribed.

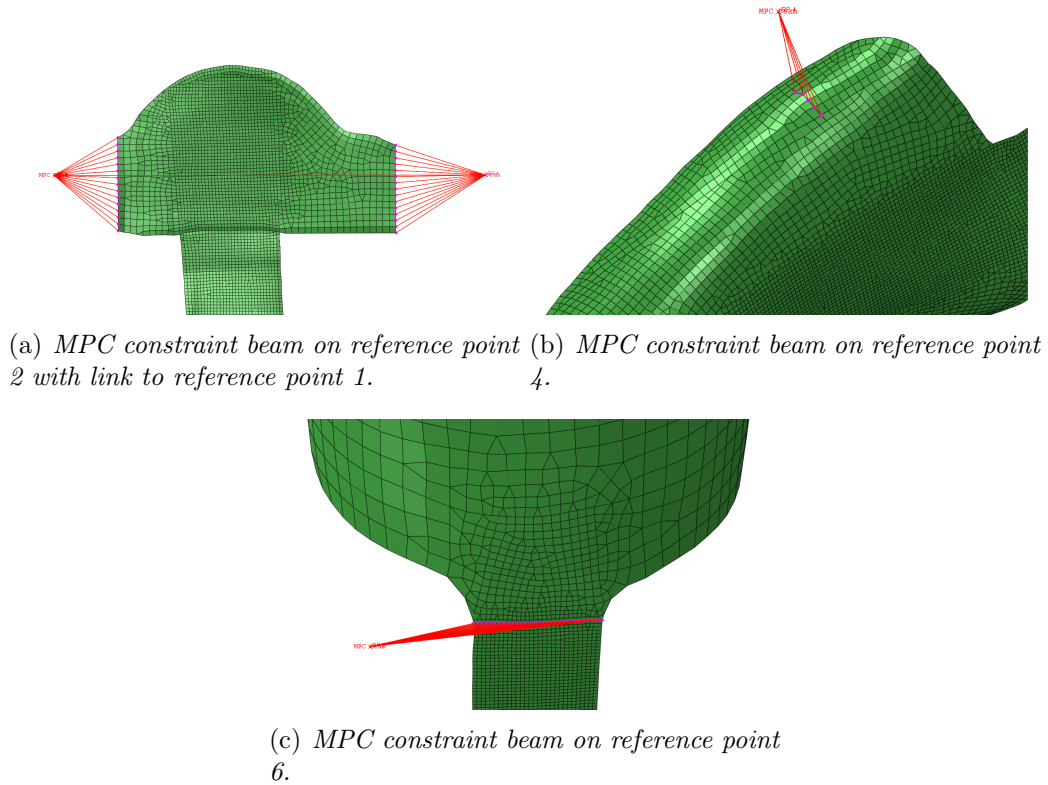


Figure 4.12: The constraints and slave nodes used.

To filter out measurement noise each amplitude was recreated by a curve-fitted 10th order polynomial. The same number of time frames were used. This improved the convergence rate. The original amplitudes are plotted together with the fitted curves in Appendix C, Figure C.1.

To make the orthosis "walk" a general static analysis was performed. The step time period was set to 1 and maximum time increment was set to  $\frac{1}{213} \approx 0.0046948$ . This made sure that each of the 213 recorded time steps will be present in the results.

#### 4.3.1 Localising maximum stress during the walking cycle

One purpose of modelling the walking cycle was to determine where, when and in what ply the maximum stresses occur in both the toe and the spring element set. The Tsai-Wu failure criteria, described in section 2.1.3.2, was used as a parameter for maximum stress. To search the Abaqus odb-file<sup>3</sup> a Python script was created, this can be found in Appendix D. The input to the script is the odb-file and the name of the element set of interest. Outputs are Tsai-Wu value, frame number, element number and ply number. By running the python script two states were obtained, one with maximum Tsai-Wu value in the toe (toe state) and one with maximum Tsai-Wu value in the spring (spring state).

#### 4.3.2 Creating reference states from the walking cycle

The spring and toe state were recreated by performing two single step analyses. To reduce the run time, the translation degrees of freedom of point 6 was set as fixed while point 2 and 4 were subjected to translatory boundary conditions. These boundary conditions consist of the motion of point 2 and 4 relative point 6.

<sup>3</sup>An odb-file is an output data base containing output parameters from a simulation.

To be able to apply these states to other configurations the displacement boundary conditions were replaced by loads. This allows the orthosis to deform differently depending on how the composite layup is configured. The reaction forces in point 2 and 4 were extracted from the analyses made from the recreation of the two states, mentioned above. These forces were then applied on point 2 and 4. To make sure that the model is statistically determined, the rotations of point 6 needs to be prescribed. These rotations were also extracted from the recreation of the two states. The correct rotations of the orthosis about point 6 make sure that the forces acting in point 2 and 4 are oriented in the correct direction. Both when using displacement BCs and forces the same result was obtained as for the original two state of the walking cycle.

#### 4.4 Creating new composite layups

Many orthoses made at Ortopedteknik show tendencies of fracture initialisation in the heel area, i.e. the area just below the heel. To show how the effect of ply drop offs in this area of the spring affects the stress distribution, a different composite layup was created. The same stacking sequence was used as seen in Table 4.1 but different element sets were used for some plies. Ply 1-3,5,7,9,11,13,22-24 were all draped in same way as in section 4.2.1. To avoid the drop offs in the heel area a new element set was created, seen in Figure 4.13. This element set was used when applying plies 4,8,12,15 and 19. All other plies, 6,10,14,16,17,18,20 and 21, were applied on the straight element set seen in Figure 4.4(b) but cut off in different lengths, all ending in the arch of the foot. The spring state described in section 4.3.1 was used in this analysis.

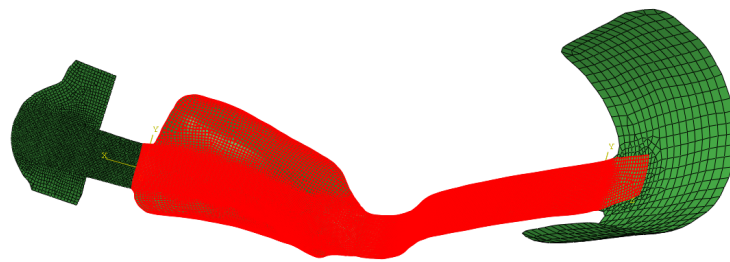


*Figure 4.13: Element set used when creating composite layup with no ply drop offs in the heel area.*

## 5 Laminate stacking sequence analysis

This chapter describes analyses created to show how different stacking sequences, ply angles and draping methods affect the behaviour of the spring orthosis.

To get an understanding of how the laminate stacking sequence and lamina orientation affect the stiffness of the composite the four point bending test described in section 3.1 was used. The test setup for these analyses was the same as when validating the material model but using a thin shell element S4R instead. The reaction force obtained in section 3.1.1 was used as a relative measure, i.e. the original layup has a relative stiffness (RS) of 1. A stacking sequence with relative stiffness larger than one has a larger stiffness than the original layup and vice versa. A copy of the four point bending test but with 5 plies was also created. The displacement of the roll was still  $11.3\text{mm}$  in the y-direction. The reaction force obtained from this model was used as a relative measure for the toe, i.e. the relative stiffness of the toe equals 1 when all plies are oriented  $0^\circ$ .

To get an understanding on how the different plies affect the stiffness the Design Of Experiment (DOE) methodology was used. The DOE technique makes it possible to extract as much information as possible from a limited number of test runs. This was done in Isight and the DOE loop in Isight can be seen in Figure 5.1.

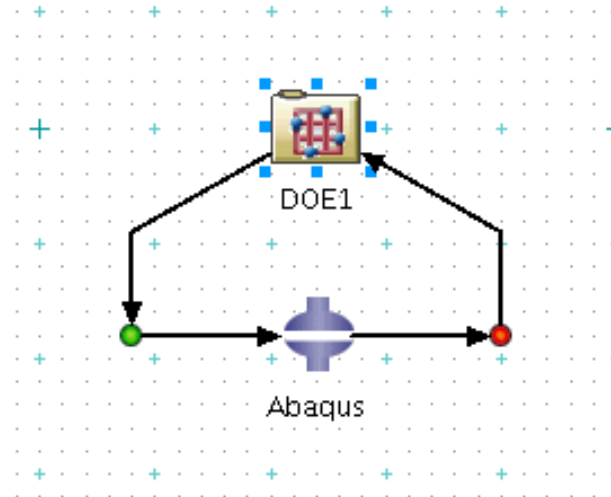


Figure 5.1: DOE loop in Isight. The loop generates stacking sequences according to Latin Hypercube sampling. They are then executed in Abaqus.

The thickest part of the spring of the orthosis has 18 plies and the toe part has at the most 5 plies. Both of these set up of plies were analysed where each ply in the stack can be rotated between  $0^\circ \leq \theta \leq 45^\circ$ . This means that the number of variables in the two analysis are 18 and 5. To cover the different possible stacking sequences for the 18 layers it would be needed almost infinite number of sequences for continuous parameters. The same holds for the 5 layer stacking sequences. There are different methods to pick these stacking sequences to get the best possible design space. For these analyses the Latin hypercube sampling [9] was used. The sample size, and type of analyses that were made are presented in Table 5.1. From the DOE a regression analysis output was requested together with basic statistics. These data were then analysed to find interaction properties between the different plies. The different tools that are available for analysis in Isight are described in [12]. The tools that were used in this analysis are;

- **Pareto plot.** This plot is a bar chart showing normalised coefficients which represent

the percent total effect on the response. If at least  $(N+1)(N+2)/2$  points are available, where  $N$  is the number of inputs, and each inputs have at least 3 distinct levels a full second order polynomial model, including two-way interactions is fitted to the data. For the minimum number of responses  $(N+1)$  it will result in a linear polynomial fit. If the number of data is between  $(N+1)$  and  $(N+1)(N+2)/2$  a partial second-order polynomial is constructed. Before the polynomial is fitted the data are first scaled to between -1 and 1 and a least square fit is made on this data. The coefficients resulting from the least square fit regression data are normalised by dividing each coefficient by the sum of all coefficients[12].

- **Correlation plot** A graphical tool that shows how the parameters are related. The correlation ranges between -1 and 1 where -1 represents a perfect inverse correlation and 1 represents a perfect direct correlation, according to Spearman. A value close to 0 signify a lack of correlation[12].
- **Main effect plot** Graphs that show the effect of a given factor on a response. A larger magnitude gives means that the factor has a greater influence on the response. The slope of the curve indicates if an increase of the factor has a positive or negative influence on the response. For more information see Appendix G and [12].

The tools described above was not used individually to determine the interaction properties between the plies. By evaluating all tools together an indication of how the different plies affect the response was obtained.

*Table 5.1: DOEs that were analysed.*

Number of layers	Number of variables	number of samples	Parameters	NAME
18	18	400	$0^\circ \leq \theta \leq 45^\circ$	DOE A
5	5	100	$0^\circ \leq \theta \leq 45^\circ$	DOE B

## 5.1 Creating approximation

From the DOEs presented in Table 5.1 approximations, i.e. metamodels, were created. For information on metamodels, see theory section 2.3. In Isight there are two different types of approximations to choose between; response surface method (RSM) and radial basis function (RBF). The response surface model approximates the surface with polynomials up the fourth order according to

$$F(x) = a_0 + \sum_{i=1}^N b_i x_i + \sum_{i=1}^N c_{ii} x_i^2 + \sum_{ij(i < j)} c_{ij} x_i x_j + \sum_{i=1}^N d_i x_i^3 + \sum_{i=1}^N e_i x_i^4 \quad (5.1)$$

where  $N$  is the number of model inputs,  $x_i$  is the set of model inputs and  $a, b, c, d$  and  $e$  are the polynomial coefficients.

The accuracy of the prediction relies on the amount of data used when constructing the polynomial, the shape of the exact response function that is approximated and the volume of the design space in which the model is constructed. The RBF method uses radial basis function to approximate the function. The RSM and RBF methods in Isight are described in [12].

To validate how good an approximation created out of the estimation is, different error estimation graphs and error estimation number will be analysed. A cross validation error



analysis procedure is used with 20 randomly chosen points from the data set. Four different types of error estimations were considered.

- **Average.** Average of the difference between the actual (from Abaqus simulations) and predicted (from approximation) values for all error samples. Low values are desired.
- **Maximum.** Maximum difference between the predicted (from approximation) and actual (from Abaqus simulations) value for all error samples. Low values are desired.
- **Root mean square.** The squared difference between the actual (from Abaqus simulations) and predicted (from approximation) values for all error samples are averaged and then taken the square root of. Low values are desired.
- **R-squared.** Coefficient of determination. Provides a measure of how well future outcomes are likely to be predicted by the model. Ranges from 0 to 1, where 1 represents a perfect fit.

The average, maximum and root mean square are normalised by the range of the actual values for each response[12]. The graph used to analyse the error estimation in Isight was;

- **Response fit.** This graph shows the actual versus the predicted values. The diagonal line represents a perfect fit. If all points fall on or close to the line the approximation model predicts well based on the error points.

Those plots show how the predicted results deviates from the actual results graphically. From those values the error estimation numbers are computed, for more information see [12].

To determine which approximation method to use, a comparison between an RBF and a 1st and 2nd order RSM approximation were made for both DOE A and B. Higher order approximations were not considered since they were likely to give unphysical behaviour between the curve fitted data points. In Table 5.2 the error estimations for the chosen approximations for DOE A and B are shown. The interval of the relative stiffness that was captured in the test data for the approximation are also shown. The approximation will not be used to predict responses outside those intervals. In Figure 5.2 the response fit for the approximations of the these sets are shown.

*Table 5.2: Error estimations for DOE A and B*

RUN	Method	Average	Maximum	Root mean square	R-squared	Interval
A	RSM 2nd order	0.04411	0.08344	0.05061	0.97046	$0.554 \leq RS \leq 1.129$
B	RBF	0.02802	0.06551	0.03352	0.98767	$0.343 \leq RS \leq 0.955$

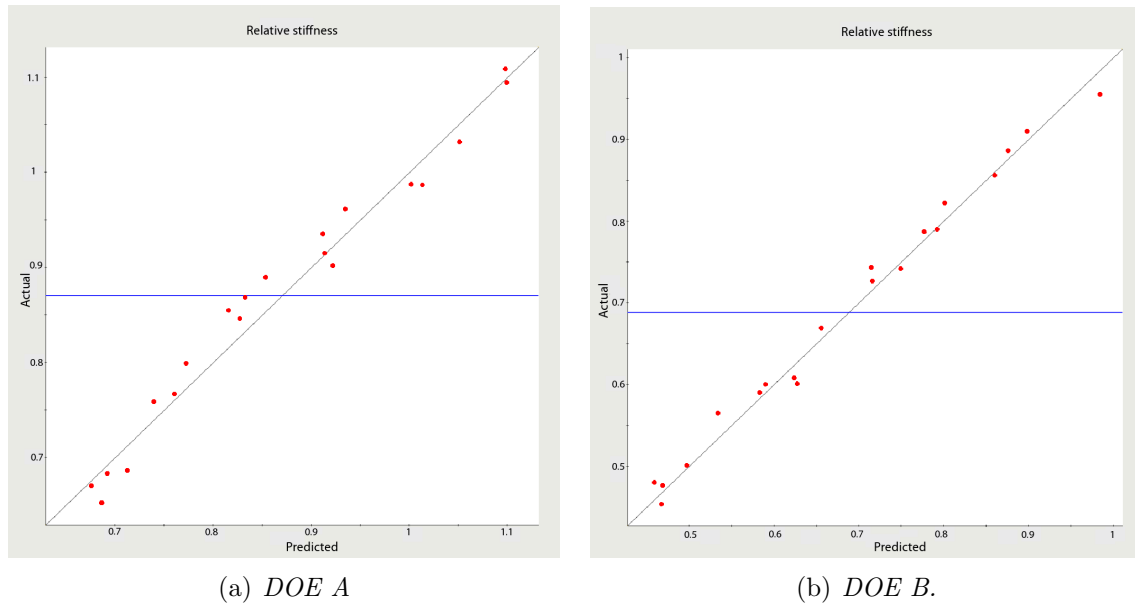


Figure 5.2: *The response fit for DOE A and B. The dots represent the 20 randomly chosen points in the cross validation error analysis procedure.*

## 5.2 Stiffness optimization

The approximations created were used to create optimization loops to generate a stacking sequence for a predefined value of the relative stiffness. This is then compared to the result for the same stacking sequence in Abaqus. The optimization algorithms used for this are Multi-Island GA and ASA, described in [12]. The criteria that were used when choosing these algorithms were that they should be stable and generate values close to the target. If the target is reached the optimization method works. Outside those loops an DOE are running where it is possible to define a matrix of values that should be generated and compared. The Design Gateway from Isight that shows the optimization schedule is shown in Figure 5.3.

Discrete parameters were used in the optimization of stacking sequences. This was done due to the fact that the plies are cut by hand. The chosen parameter values are  $\theta = 0^\circ, 15^\circ, 30^\circ, 45^\circ$ . Note that one could also use continuous parameters.



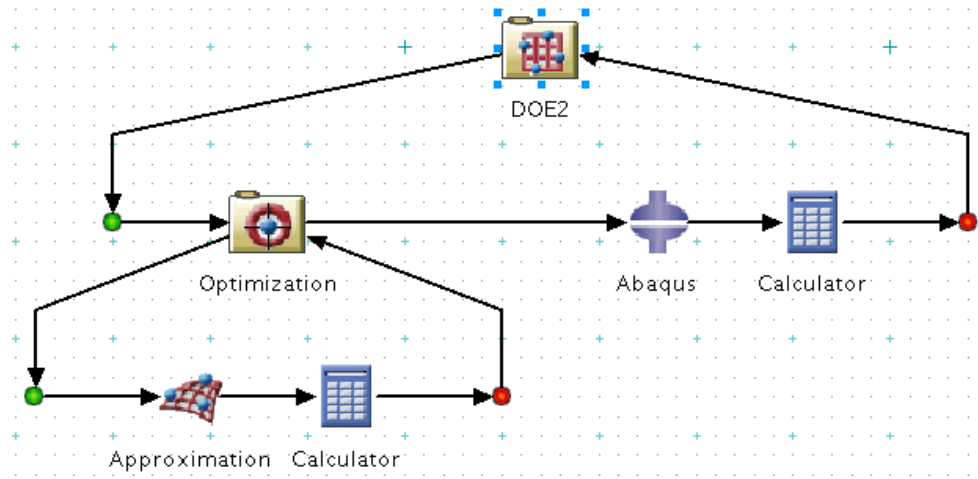


Figure 5.3: Optimization loop in Isight. The main loop generates relative stiffnesses that will be targets in the optimization of stacking sequences from the curve fitting approximation created from data in the DOE A or B. The resulting stacking sequences are then compared to the result using the same stacking sequence in Abaqus.

To see if the approximations would give predicted values close to the actual values, 30 different relative stiffnesses were chosen for the spring part. These values were equally distributed from the lowest to the highest value in the approximation, see Table 5.2. The same thing was done for the toe part with 5 plies but with 10 different relative stiffnesses. The stacking sequences generated from the optimization based on these values were compared to the actual results from Abaqus.

### 5.3 Analysis of relative motion of toe and spring

To show how different stacking sequences affect how the orthosis deforms, 9 different setups were analysed. These setups were created by combining 3 different spring setups with 3 different toe setups. One weak (denoted 1), one intermediate (denoted 2) and one stiff setup (denoted 3) were chosen for both the spring and the toe. The combinations of the setups can be seen in Table 5.3.

Table 5.3: Combinations used when creating the 9 setups. The spring and toe setups can be seen in Table 6.3.

Setup	S1	S2	S3	S4	S5	S6	S7	S8	S9
Spring setup	1	1	1	2	2	2	3	3	3
Toe setup	1	2	3	1	2	3	1	2	3

The purpose of this analysis was to detect how the relative motion between the toe and the arch foot as well as between the spring and the arch of the foot changes. The two reference states described in section 4.3.1 were used in the analysis. The toe state was used when comparing the deformation of the toe and the spring state was used when comparing the deformation of the spring. To get a good measurement of the relative motion, reference point 3, see Figure 4.9, was forced to move with the orthosis via a constraint. The change of distance between point 2 and 3, for the toe, as well as between 3 and 6, for the spring, was then compared. To account for the stress level of each layup the maximum Tsai-Wu value was localised in both the toe and the spring.

One issue that arises when creating a setup from a spring setup and a toe setup is that a new draping procedure must be applied. When creating the layup of the toe, one is restricted to use plies that are present in the spring layup. To decide how to create the spring and toe layup results from the analyses in section 5 were used.

## 6 Results

In this chapter the results from the analyses described in section 3, 4 and 5. The results from Abaqus simulations presented as averaged contour plots are plotted as max absolute envelopes. An envelope plot of the absolute maximum value plots the highest absolute value of all plies in the current element, i.e.  $\max(x_i)$ ,  $i = 1, 2, 3, \dots$ , number of plies in each element. For information about contour plot averaging see [10].

### 6.1 Four point bending test

Tuning the shear stiffness parameters  $G_{13}$  and  $G_{23}$  it was done manually by obtaining a force  $\approx -830N$  at a displacement of  $-0.0113m$ . This force corresponds to a total force of  $\approx -3300N$  for the plate with full dimensions. In Figure 6.1 the obtained force-displacement curve from the Abaqus simulations together with the curve from the experiments are shown. The tuned value of  $G_{13}$  and  $G_{23}$  was  $0.22GPa$ . Note the drop of the force-displacement curve that shows that a compressive failure probably occurred for the first ply. The compressive failure of the upper side of the test specimen was also noticed in the fatigue test done by SP. After this it loses strength until the ultimate failure at  $\approx -0.018m$ .

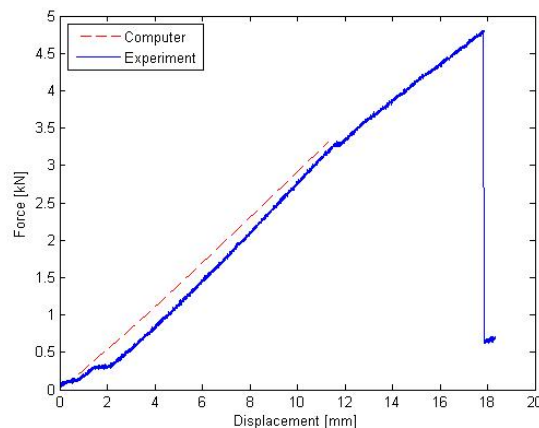


*Figure 6.1: Force displacement curve from the experiment together with the curve from Abaqus simulations.*

In Figure 6.2 a picture of the test specimen 3 of Table 3.3 is shown. As can be seen the failure probably started in the area where the rolls are in contact with the test specimen and were then spread out to the edges. It could also be seen that shear stresses probably contributed to the failure, a presence of delamination at the edges is obvious.

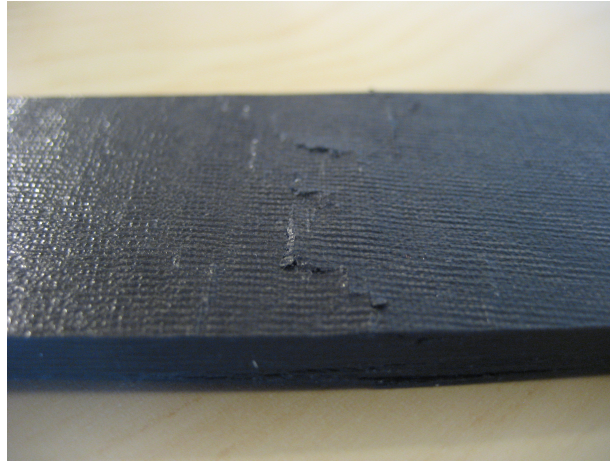


*Figure 6.2: Photo of test specimen 3.*

The four point bending test in Abaqus predicted the compressive failure at the displacement of -0.0113m with Tsai-Wu values around 1 for the upper ply, see Figure 6.3. These values were obtained in the contact area around the roll that pushes the plate downwards. In Figure 6.4 the interlaminar stresses for the four point bending test in Abaqus are shown with an extraction of the ply with the largest interlaminar stresses are shown. The maximum values of those stresses are around 20MPa, far under the ILSS value of 71.4 MPa. For this analysis the interlaminar stress that can cause separation of the plies  $\sigma_{zz}$  could not be computed.

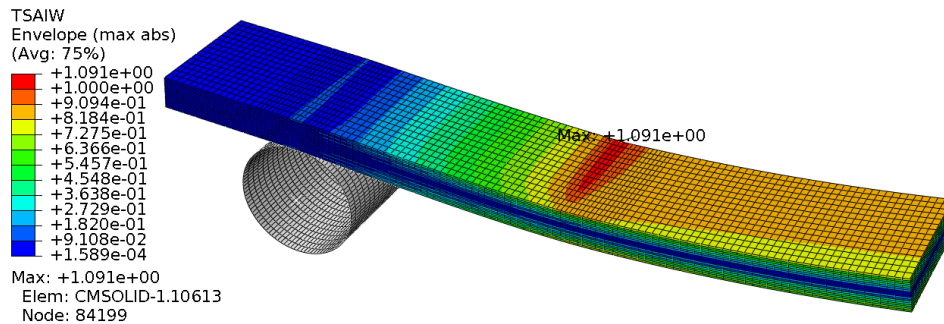
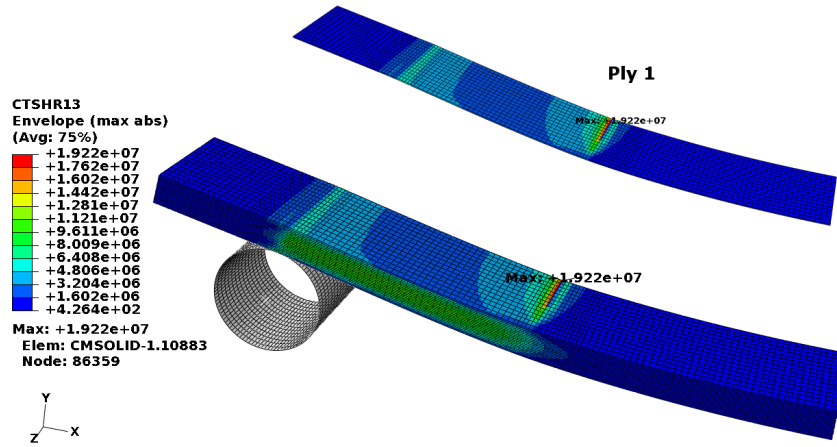
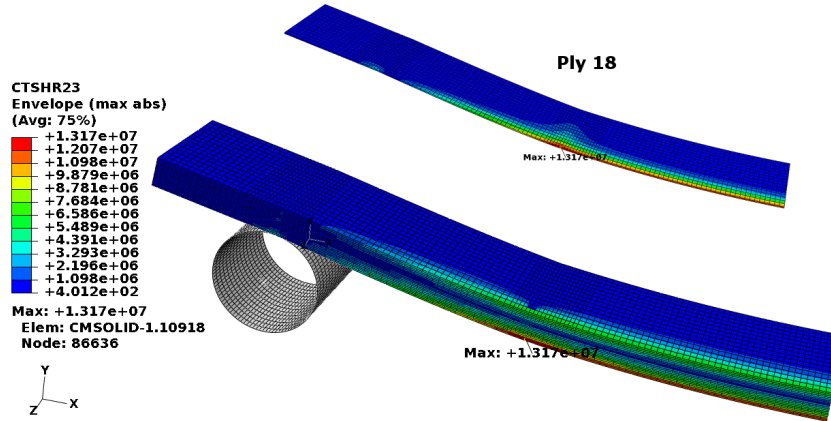


*Figure 6.3: Tsai-Wu for the four point bending test.*



(a) Interlaminar stress  $\tau_{xz}$ .



(b) Interlaminar stress  $\tau_{yz}$ .

Figure 6.4: The interlaminar shear stresses  $\tau_{yz}$  and  $\tau_{xz}$  shown for the Four point bending test in Abaqus. The ply with the largest interlaminar shear stress is extracted.

## 6.2 Maximum Tsai-Wu during walking cycle

Figure 6.5 shows an envelope plot of the maximum absolute Tsai-Wu value. The maximum Tsai-Wu value for the toe element set is 0.4657 located in ply 5 of Table 4.1. This ply is subjected to compressive stresses due to bending. The location of the maximum is just by a ply drop off, i.e. where ply 1 and 24 are cut off. The number of plies in each area can be seen in Figure 6.5. The time frame for this value is 176 which corresponds to a time 70.03 % of the total step time. Figure 6.6 shows what time state that frame corresponds to. This is around where the patient uses his/her toes to push off the ground.

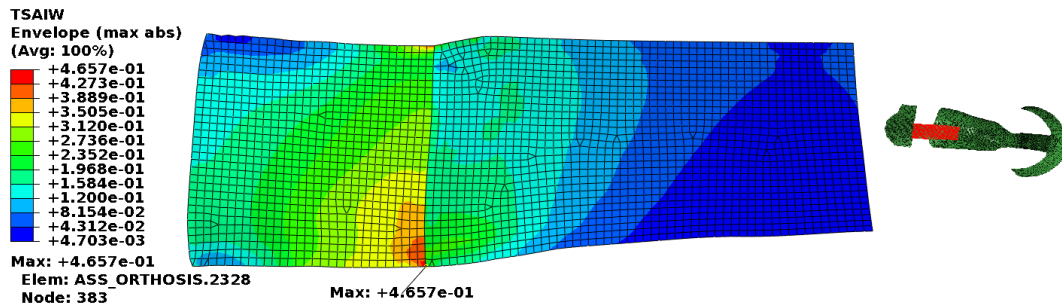


Figure 6.5: Plot of maximum Tsai-Wu value in toe element set (seen from above) and reference to location of the set in the model.

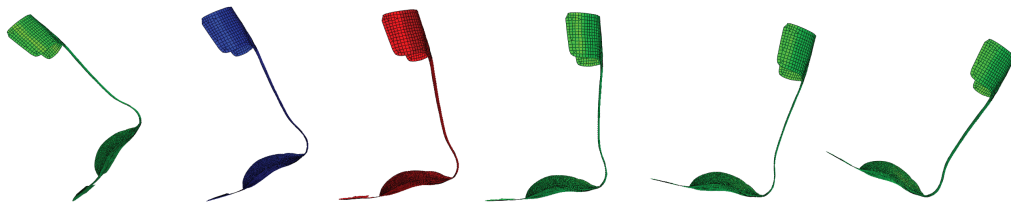
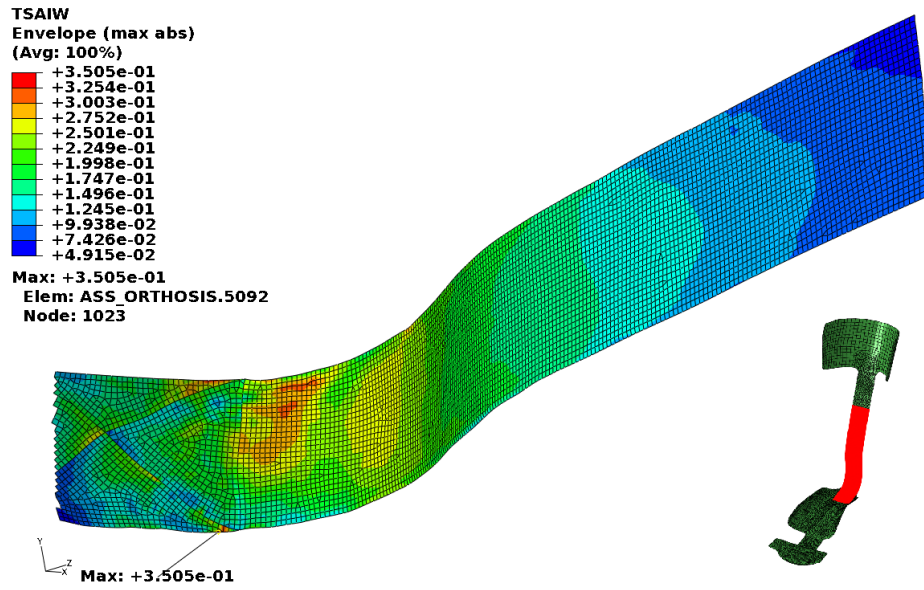


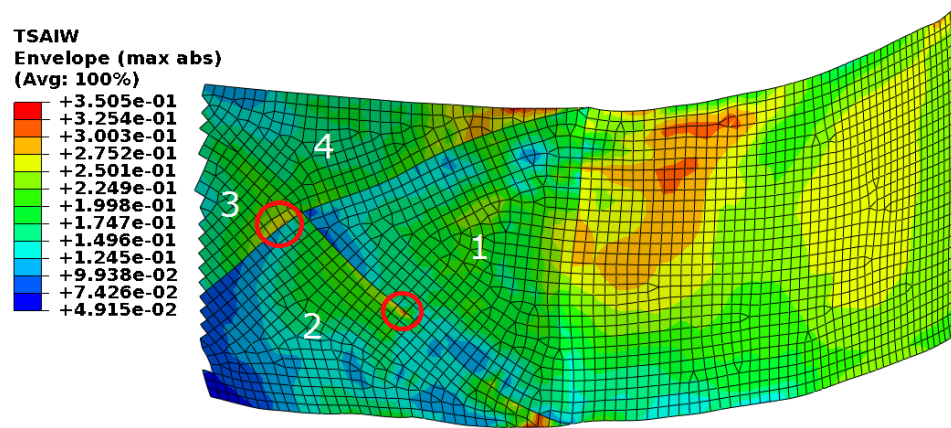
Figure 6.6: Different states of the walking cycle. The red state corresponds to when maximum stresses occur in the spring while the blue state corresponds to when maximum stresses occur in the toe.

The highest Tsai-Wu value for the spring element set can be seen in Figure 6.7(a). The maximum value of 0.3505 is located in ply 1 of Table 4.1. This ply is subjected to compressive stresses due to bending. The time frame for this value is 201 which corresponds to a time 81.77 % of the total step time. Figure 6.6 shows what time state that frame corresponds to. This is around where the heel leaves the ground. Notable is that there are two other regions that have almost the same Tsai-Wu value as the maximum, more clearly visible in Figure 6.7(b). At the opposite side of the shown maximum the same ply has a Tsai-Wu value of 0.3486. The larger red area just to the right in the figure has a maximum Tsai-Wu value of 0.3501 localised in ply 4 of Table 4.1.

The highlighted areas in Figure 6.7(b) show stress concentrations that appear due to drop offs. The different regions of the heel in Figure have various number of plies according to Table 6.1.



(a) The entire spring and reference to location in the model.



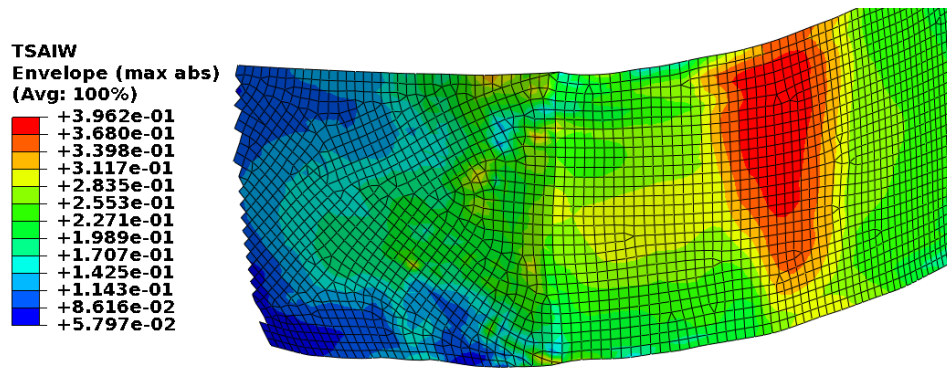
(b) Close up of heel area.

Figure 6.7: Plot of maximum Tsai-Wu values in the spring element set.

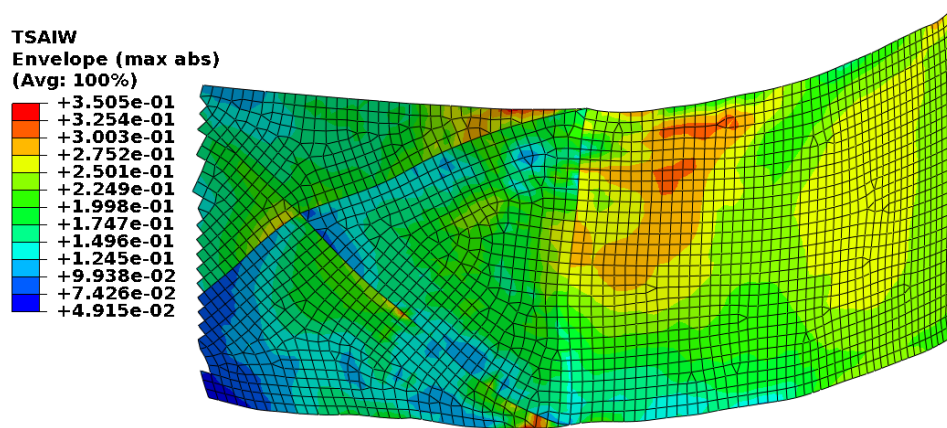
### 6.3 Composite layup with no drop offs in heel area

The result for the composite layup with no drop offs in the heel area is plotted together with the original layup in Figure 6.8. The stress concentrations seen in Figure 6.8(b) are not present in Figure 6.8(a). Noticeable is that the maximum stress is higher and is located in another area in the model with the new layup. Figure 6.9 shows that the new drop offs in the arch of the foot does not lead to any stress concentrations.





(a) Layup with no drop offs in heel area.



(b) Original layup.

Figure 6.8: Plot of spring state for different composite layups.

Table 6.1: Number of plies in different regions of the heel for the original layup, see Figure 6.8(b) to see regions.

Region	1	2	3	4
Number of plies	20	12	7	10

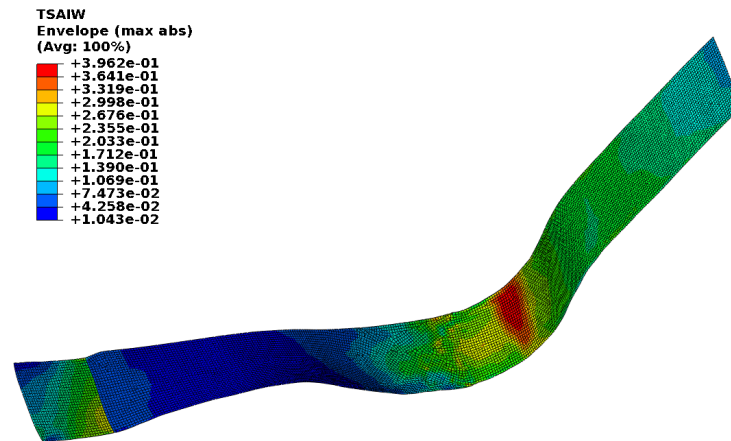
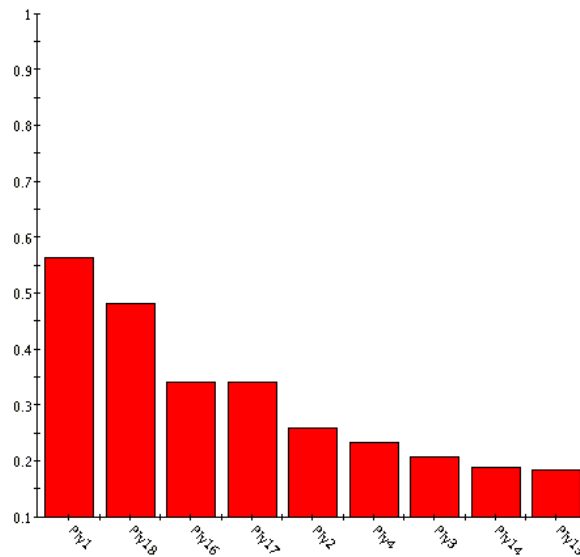


Figure 6.9: Plot of spring state for the entire spring.

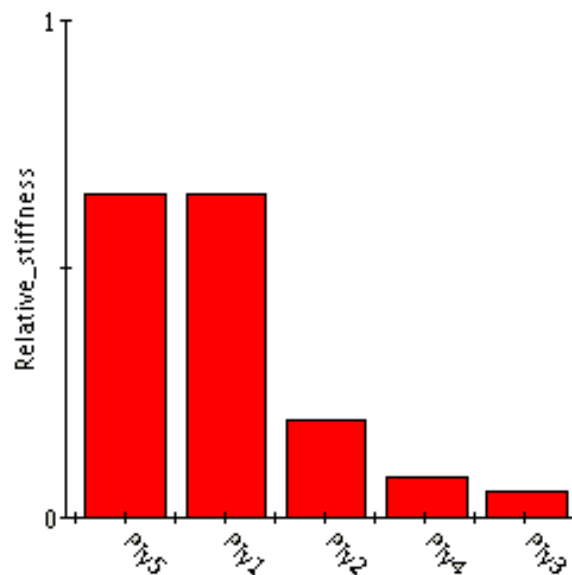


## 6.4 Laminate stacking sequence

In Figure 6.10 correlation coefficients for the approximation are shown for DOE A and B, see section 5.1 for more information on the DOEs. In these figures only the plies with the largest correlation are shown. All the correlations are negative which means that a larger angle has a negative influence on the relative stiffness. The correlation for DOE A shows that the outermost layers has the largest correlation to the response. Note that the inner plies are not represented. For DOE B one can see the same trend. Note that the outermost plies in DOE B have significantly higher correlation compared to the others.



(a) DOE A.



(b) DOE B.

Figure 6.10: Correlation for DOE A and B.

Pareto plots for DOE A and B are shown in Figure 6.11. The ten coefficients showing the largest affect of the response are shown. These plots have been computed from the coefficients of the second order polynomial fits from the regression data. The bars pointing to the left give a negative effect to the response (relative stiffness) for an increasing angle

and vice versa. For DOE A the linear terms of the outer most plies have the largest effect, i.e. ply 1 and 18. After that the effect of the linear terms are decaying for ply 2,3,16 and 17 but they are still affecting nearly as much as the two outer plies. The second order coefficients for ply 1,2,17 and 18 have almost the same affect but positive. For DOE B one can see that the outer most plies are dominant compared to the other plies.

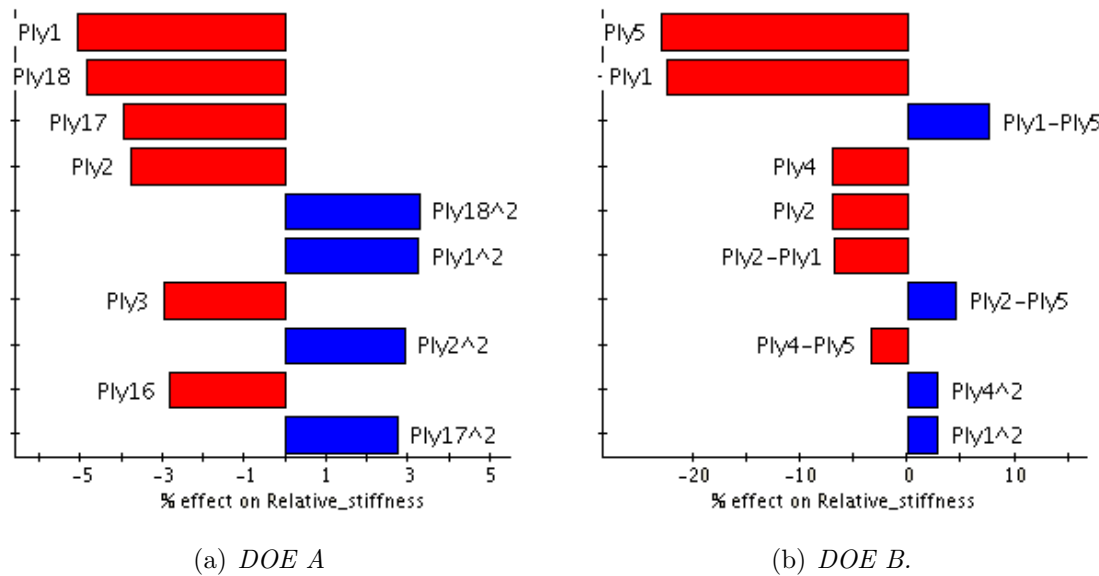
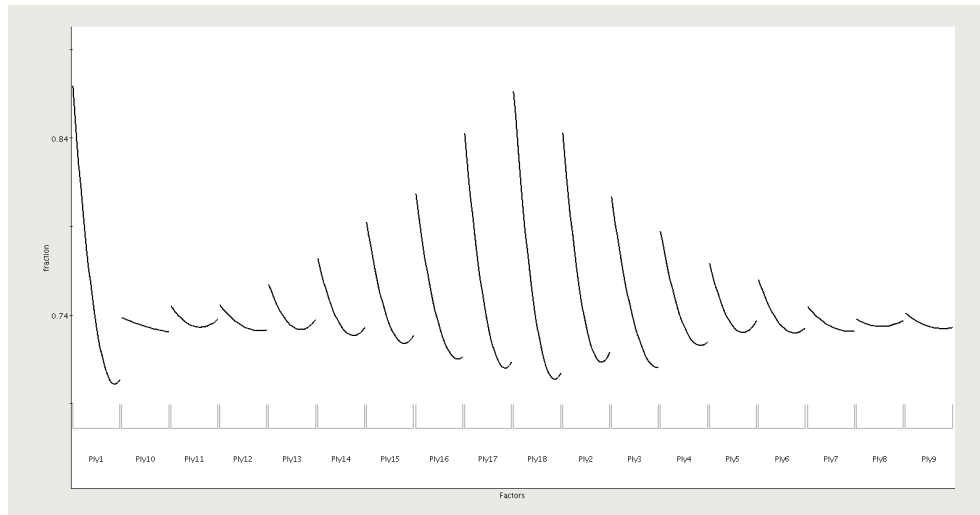
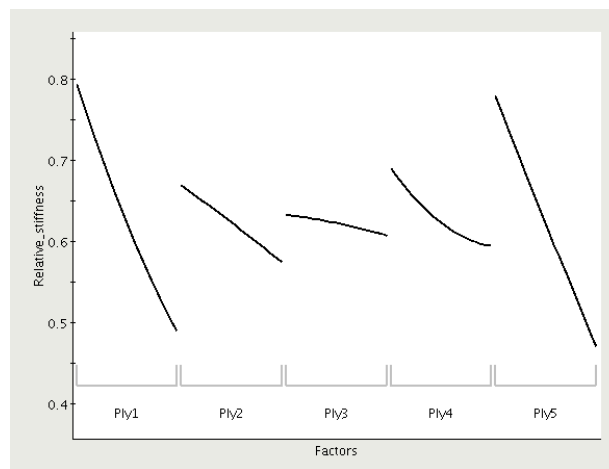


Figure 6.11: Pareto plots for DOE A and B.

In Figure 6.12 main effect graphs are shown. These graphs can be seen as an estimation on how a change in angle will influence the response. It seems like an increased angle leads to a lower relative stiffness for almost all plies. Also in this plot one can see that the outermost plies have more effect on the relative stiffness of the laminate for both DOE A and B.



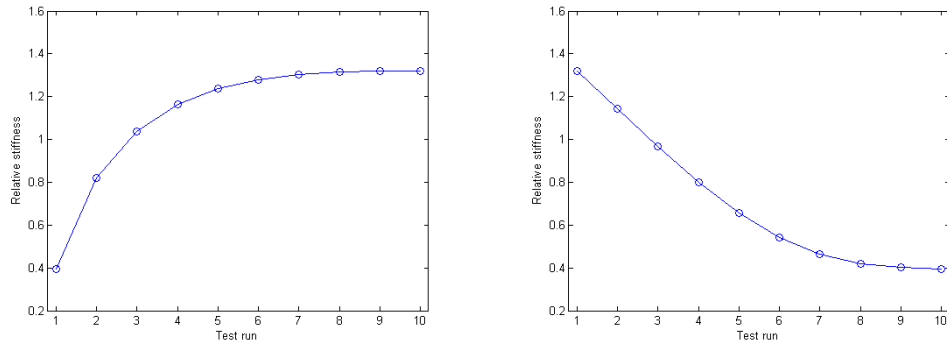
(a) DOE A



(b) DOE B.

Figure 6.12: Main effect graphs for DOE A and B.

To further investigate which plies that have the most influence of the relative stiffness and to see where in the stacking sequence the plies are losing major effect to the relative stiffness, two different tests were submitted. The 18 ply spring layup was used. Based on previous results the assumed weakest,  $45^\circ$ , and assumed strongest,  $0^\circ$ , orientation angles were stacked together. In the first test all plies were set to  $45^\circ$  and then the inner plies where changed to  $0^\circ$  two by two until all plies were rotated  $0^\circ$ . In the second test all the plies where set to  $0^\circ$  and the inner plies where changed to  $45^\circ$  two by two until all plies were rotated  $45^\circ$ . The results of these tests are presented in Figure 6.13. The complete stacking sequences can be found in Appendix F. As can be seen in the figures, test run 8,9 and 10 for both cases result in almost the same relative stiffness. This implies that changing the six innermost plies does not affect the relative stiffness.



(a) Test 1, changing plies from  $45^\circ$  to  $0^\circ$ . (b) Test 2, changing plies from  $0^\circ$  to  $45^\circ$ .

Figure 6.13: Response of relative stiffness for two different tests.

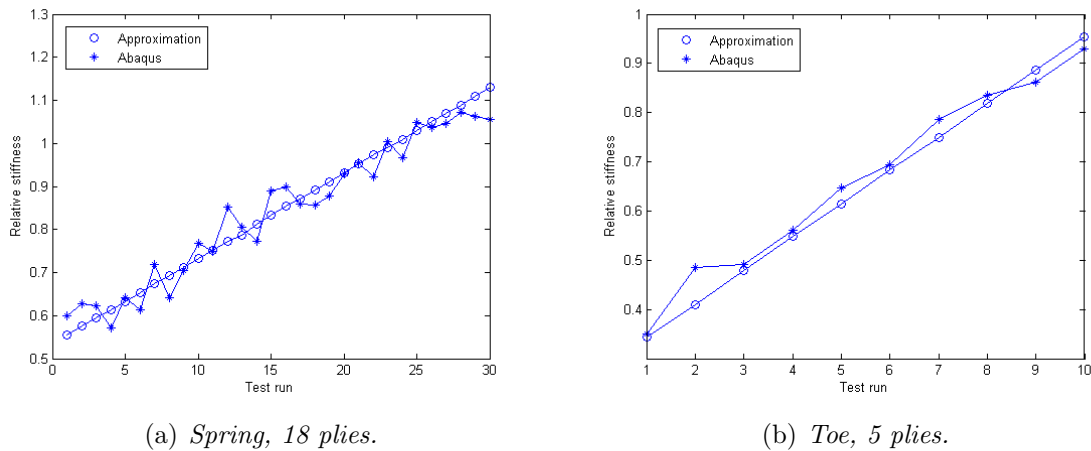
By studying Figures 13(a) and 13(b) and assuming that an increasing angle of all plies leads to a lower relative stiffness one can obtain the maximum and minimum relative stiffness of the spring. These are presented in Table 6.2 together with the maximum and minimum relative stiffness of the toe, obtained by setting all plies to  $45^\circ$  and  $90^\circ$ .

Table 6.2: Maximum and minimum relative stiffness for spring and toe.

	Spring	Toe
Maximum	1.32	1
Minimum	0.40	0.35

## 6.5 Stiffness optimization

How well the different approximations match a requested relative stiffness can be seen in Figure 6.14. The stiffnesses were selected to cover the entire span of the both approximations, for more detailed description of how the comparison was made see section 5.2.



(a) Spring, 18 plies.

(b) Toe, 5 plies.

Figure 6.14: Comparison of relative stiffness response between the approximation and Abaqus.

## 6.6 Relative motion results

This section contains the results of the analysis described in section 5.3. To decide which of the plies of the spring that would be used for the toe part of the orthosis, the results from section 6.4 were used. Those results show that the plies in the middle of the spring laminate had little effect of the relative stiffness. Therefore these plies can be substituted arbitrary without significantly affecting the bending stiffness of the spring. The relative stiffnesses used for the toe and the spring, combined in Table 5.3, as well as the corresponding stacking sequences can be seen in Figure 6.3. Ply 8,9,10,11 and 12 of the spring were substituted to the 5 plies used for the toe. The toe layout could then be chosen without any restrictions. Note that the numbering of the plies in Table 6.3 differs from the numbering of the model used in section 5.2, illustrated in Figure 3.4. The numbers are reversed, meaning that ply 1 in section 5.2 is ply 18 in Table 6.3. This is because the test piece was put up side down in the four point bending test performed by SP, see section 3.1.

*Table 6.3: Relative stiffness and stacking sequence of the 6 setups.*

	Spring 1	Spring 2	Spring 3	Toe 1	Toe 2	Toe 3
Actual relative stiffness	0.60	0.90	1.12	0.38	0.57	0.85
Predicted relative stiffness	0.60	0.85	1.10	0.35	0.60	0.85
Ply 1	45°	45°	0°	45°	30°	0°
Ply 2	45°	15°	15°	30°	0°	15°
Ply 3	45°	45°	15°	30°	30°	30°
Ply 4	45°	45°	30°	30°	15°	15°
Ply 5	15°	45°	15°	45°	30°	15°
Ply 6	0°	15°	15°			
Ply 7	0°	45°	0°			
Ply 8	45°	45°	15°			
Ply 9	45°	30°	0°			
Ply 10	30°	15°	30°			
Ply 11	0°	0°	0°			
Ply 12	45°	0°	30°			
Ply 13	15°	0°	15°			
Ply 14	30°	0°	15°			
Ply 15	45°	0°	30°			
Ply 16	30°	15°	0°			
Ply 17	45°	0°	0°			
Ply 18	30°	0°	15°			

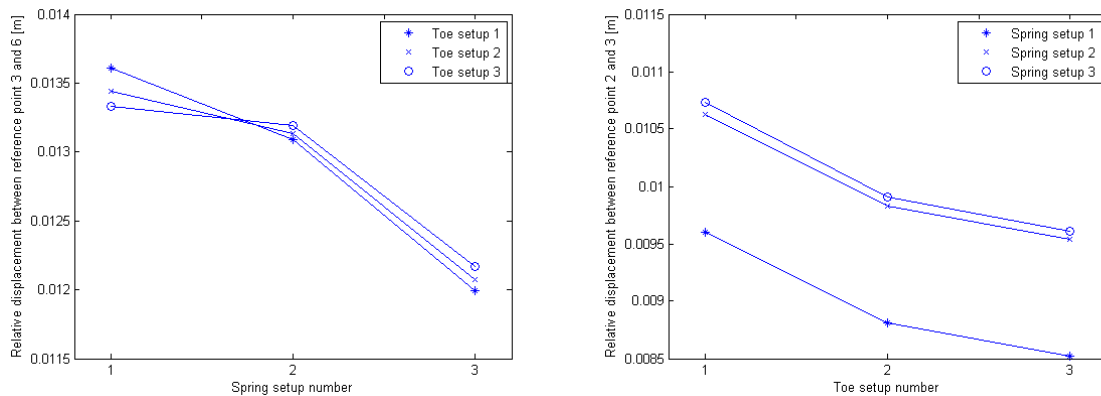
To verify that these substitutions would not have a significant effect of the relative stiffness of the spring the different stacking sequences were compared. The result of this can be seen in Table 6.4 and shows that the relative stiffness remains almost unchanged.

Table 6.4: The relative stiffnesses of the spring when changing ply 8,9,10,11 and 12 to the toe stacking sequence of Table 6.3.

Setup	Original relative stiffness	Modified relative stiffness
S1	0.60	0.59
S2	0.60	0.59
S3	0.60	0.60
S4	0.90	0.91
S5	0.90	0.93
S6	0.90	0.94
S7	1.12	1.11
S8	1.12	1.11
S9	1.12	1.12

The result of change of relative displacement for both the spring and the toe can be seen in Figure 6.15. In Figure 6.15(a) one can see that for a constant toe setup, an increasing stiffness of the spring leads to a decreasing relative displacement of the spring. A stiffer toe setup leads to greater change of relative displacement of the spring when the spring stiffness varies. In Figure 6.15(b) one can see that for a constant spring setup, an increasing stiffness of the toe leads to a decreasing relative displacement of the toe. The magnitude change of relative displacement of the toe decreases almost equally when alternating the toe stiffness. However for a constant toe stiffness there is large difference of relative displacement of the toe between spring setup 2 and 3, but not between spring setup 1 and 2.

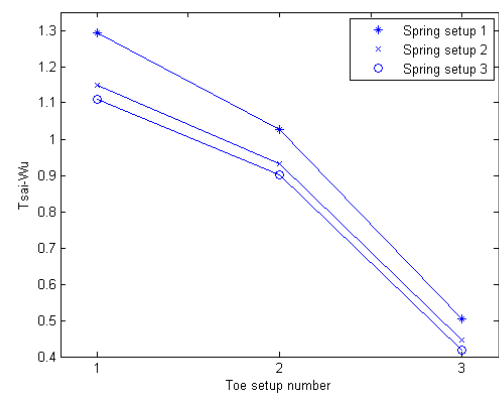
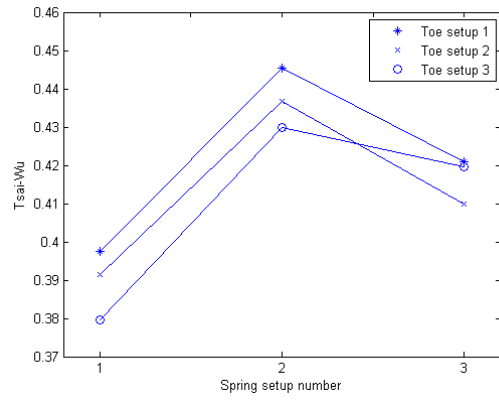
How the maximum Tsai-Wu value was affected by the same analyses can be seen in Figure 6.16. Note that the Tsai-Wu value in Figure 6.16(b) exceeds 1 for some setups, meaning that there lies a restriction of how one can combine spring and tow setups.



(a) The change of the relative displacement of the spring for 3 different toe setups.

(b) The change of the relative displacement of the toe for 3 different spring setups.

Figure 6.15: Relative displacement response of the 9 setups.



(a) The change of maximum Tsai-Wu in the spring for 3 different toe setups. (b) The change of maximum Tsai-Wu of the toe for 3 different spring setups.

Figure 6.16: Maximum Tsai-Wu response of the 9 setups.

## 7 Conclusions

The maximum Tsai-Wu value of the orthosis model during a walking cycle is located in the toe as can be seen in Figure 6.5. The location of the maximum stress is just at a ply drop off. Ply drop offs cause discontinuities, so one could suspect that this is where the maximum stress would occur. This phenomena can also be seen by looking at the stress concentrations obtained in the spring, Figure 6.7(b). These effects appear due to the change of stiffness when two neighbouring areas contain different amount of plies. Other examples of discontinuities that often cause stress concentrations are holes and sharp edges. There is often an urge to reduce these discontinuities from FE-models, this should also be applied on the orthosis model.

By studying Figure 8(a) the stress concentrations highlighted in Figure 6.7(b) are not present when drop offs no longer exist in this area. The maximum Tsai-Wu value is higher in Figure 8(a) which might be a result of a various stiffness of the spring obtained when a new draping procedure was used. However the purpose of reducing ply drop offs was to show that the stress concentrations will be reduced. The maximum Tsai-Wu value in the entire model is not close to 1 which indicates that the model is not close to failure during an ordinary walking cycle.

Many of the previously built orthoses showed fractures in the heel area, therefor one should consider to avoid creating ply drop offs here since they can cause crack initiation, due to interlaminar stresses, see section 2.1.6. In reality there will be contact in this area, a factor which is not accounted for in this thesis. This together with the fact that the woven fabric will have large shear strains in the area around the heel when draping the model, see section 4.2.1, motivates that a new draping procedure should be considered. Large shear strains for a woven fabric make the fabric weaker and might increase the stress concentrations further.

The laminate stacking sequence analysis shows that the outermost plies of the spring have the largest effect on the bending stiffness. This seems reasonable considering that the strain magnitude of these plies are larger than the innermost. The results also showed that it is possible set the 6 innermost plies to arbitrary angles without obtaining any significant change of bending stiffness. Since the orthoses are manufactured by hand other factors with larger impact than what the change of these plies entails will be added.

Another conclusion is that increasing a ply angle will lead to a weaker bending stiffness. This is also quite reasonable since a cross-woven ply has a larger Young's modulus along the fibres, this is shown in Figure 2.5(a).

When using the optimization loop to obtain stacking sequences for requested relative stiffnesses one cannot always be certain of that the requested stiffness is obtained. As seen in Figure 6.14 the actual relative stiffness for a stacking sequence can differ from the predicted. However this difference might not be of importance since previously stated factors from manufacturing may cause an even larger error. The most important feature of this model is that it is possible to create an orthosis where one can modify the stiffness within reasonable large tolerances.

When it comes to predicting how the spring and toe deforms due to different stiffnesses some conclusions can be drawn. Although a more thorough analysis might be needed to obtain a more detailed result. A weaker spring will quite obvious result in a larger deformation of the spring. The combination of a weak toe and a weak spring result in the largest deformation and a weak toe and a stiff spring result in the smallest deformation. However the stiffness of the toe does not have any remarkable effect of the spring deformation, thus it mainly depends on the spring stiffness itself.

The deformation of the toe on the other hand is very much affected by the spring



stiffness. Independent of spring stiffness a weak toe will result in a larger deformation and vice versa. How large the toe deformation is depends on how large the spring stiffness is. For the two stiffest springs used in the analysis the toe deformation was almost identical but using a weak spring decreased the toe deformation significantly. This seems reasonable since if a rigid spring would be used, all deformation would take place in the toe.

The Tsai-Wu values plotted indicate that not all toe setups might be used. The stiffnesses creating values close to or exceeding 1 should be avoided. This means that toe relative stiffness should not be less than  $\approx 0.6$ .

## 8 Discussion

The tuned value of  $G_{13}$  and  $G_{23}$  is approximately 1/15 of the in-plane shear modulus,  $G_{12}$ . This may seem a bit low but considering that the material is a cross woven composite it is not unlikely with such a large difference. However there is a number of error sources affecting the accuracy of this value. First of all the setup of the test performed by SP was not symmetric, as can be seen in Figure 3.2. The two arm supports are not equal and the plate does not seem to be centred. When using x- and z-symmetry in the Abaqus model an ideal case is created which does not correspond to reality. The friction between the rolls and the plates is another unknown factor.

By studying the force-displacement curve of the test, seen in Figure 6.1, one can see that the response at the start is not linear. This is almost impossible to model since the factors causing it are difficult to determine. Therefore the curve from the Abaqus model has a different slope than the experimental.

Recall that the material has different Young's modulus in compression and tension. By averaging Young's modulus more loss of accuracy is obtained. There might be some uncertainties of modelling the plate with plane stress since a 3-dimensional stress state occur in the contact area. Therefore one should consider modelling the plate with 3-D solid elements to catch all aspects of the interaction between the rolls and the plate. However this means that more unknown material parameters,  $E_3$  and  $\nu_{13} = \nu_{23}$ , need to be determined. These can be obtained from theories but this means that more approximations are required. The theories to compute stiffnesses and strengths contain approximations and lead to loss of accuracy. Because of this and under the circumstances, the best way of modelling the plate is by using a continuum shell model. This gave a Tsai-Wu value around 1 when the laminate was suppose to have its first ply failure, which indicates that the model gives a fairly good approximation.

The thin shell element S4 used when modelling the orthosis gave a good approximation of the bending stiffness of the plate. The Tsai-Wu value of the first ply failure was approximately 0.9, similar to the value of the thick shell model, which implies that this shell type models the stress state well. Another argument for saying that this type of element models the stress state in a good way is that it is shown that there exists a plane-stress state sufficiently far away from the free edges. The results of where and when the largest stresses occur can be said to be accurate enough to be trustful.

The approximation of DOE A and B (spring and toe) predicts values fairly good, as can be seen in Figure 6.14 where 30 and 10 values were computed respectively. This conclusion can also be made by studying the corresponding error values. One will not get the exact requested value but the model can give a layup that will increase or decrease the stiffness with a reasonable tolerance. The approximation of DOE B is even better than for DOE A. This might be because ply 1 and 5 have so much more affect than the others, seen in the Pareto plots and main effect graph. The relation of numbers of samples versus number of plies is also much higher for DOE B.

The methods used to evaluate the stacking sequence analysis gave unambiguous results that the outermost plies have more affect on the bending stiffness. As concluded this seems reasonable since in pure bending these plies will have larger strain magnitude. The six innermost plies showed to have almost none effect on the bending stiffness. Therefore these plies were used to build the toe part, since they could be rotated arbitrary. However the effect of draping in this way was not analysed. Draping 5 consecutive plies onto the same area will cause a larger drop-off than those that were present in the original model.

The comparison of the deformation of the toe and spring for different layups showed that it is possible to change this relation. The analysis using 9 setups gave tendencies but

to further investigate these tendencies, more setups need to be compared. The loading case used in this analysis can be used to examine other characteristics of the orthosis since the prescribed displacements were substituted to forces. Although if the geometry of the orthosis changes a new walking cycle needs to be recorded, to obtain correct forces.

Finally it can be said that the model in this thesis can be useful when designing a spring orthosis. One can obtain guidance of how to design the spring and the toe in order to obtain desired properties. The model can also predict how the stresses are increased when a design change is made. This can be useful when predicting the lifetime of the orthosis. Almost all questions stated by the engineers at Ortopedteknik were answered and this thesis has opened many doors to future investigations. Some recommendations for future work is presented in section 9.

## 9 Recommendations

Some recommendations for future work are presented below:

- Use continuum shell element SC8R with one element for each ply to get a better estimation of the stresses in the model.
- Use fracture mechanics to describe the behaviour after the first ply failure, to be able to analyse the complete failure.
- Make design changes of the orthosis to investigate how the design could change the stress distribution during the walking cycle.
- Use an iterative process where also real experiments are used to verify the results from the prediction of the designs.
- Use the current model to optimise the spring orthosis regarding the torsional behaviour as well.
- Make an investigation of the fatigue properties of the model, using data from the four point bending test.
- Investigate which failure criteria that is to recommend for this case. Tsai-Wu was chosen with motivation that it is often used and that it takes into account different strengths in tension and compression.
- Use a walking cycle measured from a disabled person to get a more realistic motion of the orthosis.
- Try to minimise the effect of the measurement uncertainties from the walking cycle, so that more points can be used to control the motion. Consider using another method to deform the orthosis to avoid stress concentrations.
- Construct a standardized test to test different design and loading cases for the spring orthosis.
- Use more samples in the DOE approximation. Both for the investigation of the interaction between the plies and to be able to cover the entire span of relative stiffness.
- A deeper analysis to see how the different plies affect the response may be preferred. This would make it possible to easier make changes for the manufacturer by changing minimal number of ply orientations.

## 10 References

### References

- [1] Åström, B.,T. (1997): Manufacturing of polymer composites. Chapman & Hall, London, England.
- [2] Gibson,R.,F. (1994): Principles of composite material mechanics. McGraaw-Hill Inc, USA.
- [3] Li, C., Rychwalski, R. (2010): Composite and nanocomposite materials, Ed. 4, Chalmers university of technology, Gothenburg, Sweden.
- [4] Dattoo, M., D. (1991): Mechanics of fibrous composites. Elsevier Science Publishers Ltd, Barking, Essex, England.
- [5] Bjarnehed, H., Hult, J. (1992): Styvhet och styrka (Stiffness and strength. In Swedish). Chalmers Tekniska Högskola, Avd Hållfasthetslära, Göteborg, Sweden.
- [6] Mallik, P., K. (1993): Fiber reinforced composites. Marcell Dekker inc, New York, USA.
- [7] Wriggers, P. (2002): Computational contact mechanics. John Wiley & Sons Ltd, West Sussex, England.
- [8] Bathe, K-J. (1996): Finite element procedures. Prentice-Hall inc, New Jersey, USA.
- [9] Fang, K-T., Li, R., Sudjianto, A. (2006): Design and modeling for computer experiments. Chapman & Hall/CRC, London, England.
- [10] Hibbitt, Karlsson, Sörensen, Abaqus version 6.9, 2009
- [11] Composite modeler manual, version 1.0H
- [12] Isight manual, version 4.0

## A Calculation of volume percent carbon fibre in test specimen

Material parameters for Epoxy:

$$E_m = 4 \text{ GPa} \quad (\text{A.1})$$

$$\rho_m = 1260 \text{ kg/m}^3 \quad (\text{A.2})$$

$$\nu_m = 0.35 \quad (\text{A.3})$$

$$G_m = \frac{E_m}{2(1 + \nu_m)} \quad (\text{A.4})$$

Material parameters for Carbon fibre:

$$E_f = 230 \text{ GPa} \quad (\text{A.5})$$

$$\rho_f = 1750 \text{ kg/m}^3 \quad (\text{A.6})$$

$$\nu_f = 0.3 \quad (\text{A.7})$$

$$G_f = \frac{E_f}{2(1 + \nu_f)} \quad (\text{A.8})$$

Data for test specimen 8

$$\text{Mass, } M_{TS} = 77.07 * 10^{-3} \text{ kg} \quad (\text{A.9})$$

$$\text{Length, } L_{TS} = 248 * 10^{-3} \text{ m} \quad (\text{A.10})$$

$$\text{Width, } W_{TS} = 44 * 10^{-3} \text{ m} \quad (\text{A.11})$$

$$\text{Thickness, } T_{TS} = 4.73 * 10^{-3} \text{ m} \quad (\text{A.12})$$

$$\text{Volume, } V_{TS} = L_{TS}W_{TS}H_{TS} \quad (\text{A.13})$$

$$\text{Density, } \rho_{TS} = \frac{M_{TS}}{V_{TS}} \quad (\text{A.14})$$

$$\text{Number of layers, } n = 18 \quad (\text{A.15})$$

Data for one layer of prepreg

$$\text{Mass, } M_{Layer} = 8.88 * 10^{-3} \text{ kg} \quad (\text{A.16})$$

$$\text{Length, } L_{Layer} = 142 * 10^{-3} \text{ m} \quad (\text{A.17})$$

$$\text{Width, } W_{Layer} = 132 * 10^{-3} \text{ m} \quad (\text{A.18})$$

$$\text{Area, } A_{Layer} = L_{Layer}W_{Layer} \quad (\text{A.19})$$

$$\text{Mass per unit area, } M_{PUA} = \frac{M_{Layer}}{A_{Layer}} \quad (\text{A.20})$$

$$v_f = 50 \% \quad (\text{A.21})$$

$$\text{Mass of layer with same area as test specimen, } M_{LS} = M_{PUA}L_{TS}W_{TS} \quad (\text{A.22})$$

$$\text{Volume of layer with same size as test specimen, } V_{LS} = \frac{M_{LS}}{v_f\rho_f + (1 - v_f)\rho_m} \quad (\text{A.23})$$

Volume percent calculations

$$\text{Volume of specimen if no loss of matrix material, } V_{opt} = nV_{Layer} \quad (\text{A.24})$$

$$\text{Height of specimen if no loss of matrix material, } H_{opt} = \frac{V_{opt}}{L_{TS}W_{TS}} \quad (\text{A.25})$$

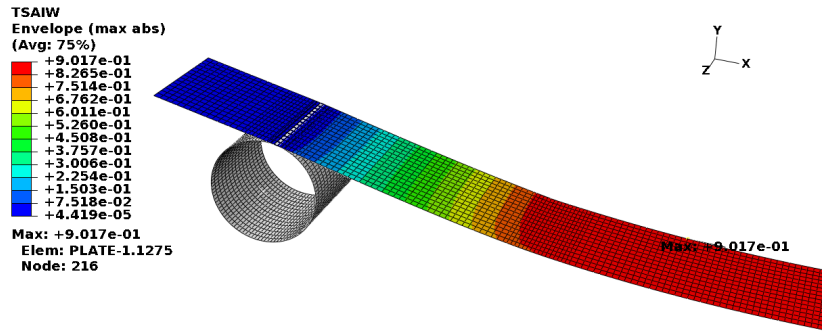
The calculations above result in  $H_{opt} = 5.70 * 10^{-3} \text{ m}$ .

## B Analysis of test set up parameters

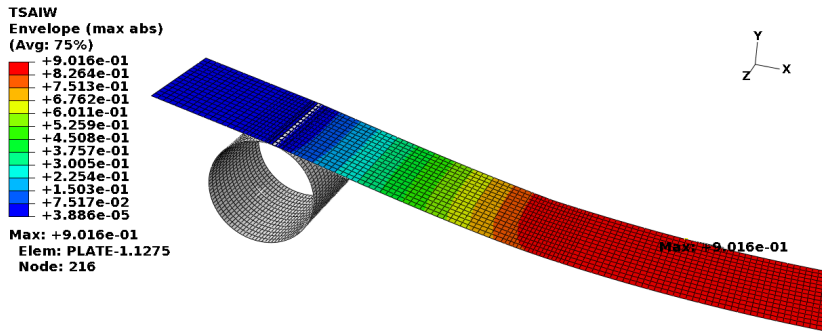
This appendix contains the resulting plots from the analyses of how element type, different contact constraint enforcement methods and friction affect the results of the four point bending test. The analyses are described in section 3.1.4 and 3.1.5.

### B.1 Element type

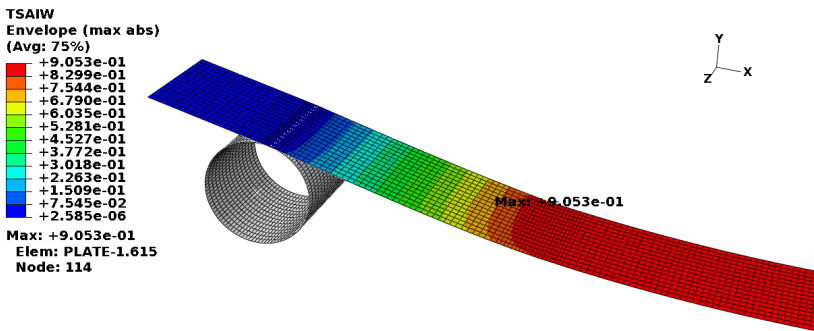
Figure B.1 illustrates the differences of using different elements. When comparing them one can see that the thin shell elements do not model the change in stress distribution due to the contact and friction in the same way as the stacked continuum shell. The only thin conventional shell element type that predicted the highest Tsai-Wu value in the contact was the 2nd order quadratic element S8R. None of the conventional shell elements predicted failure, i.e. a Tsai-Wu value larger than 1.



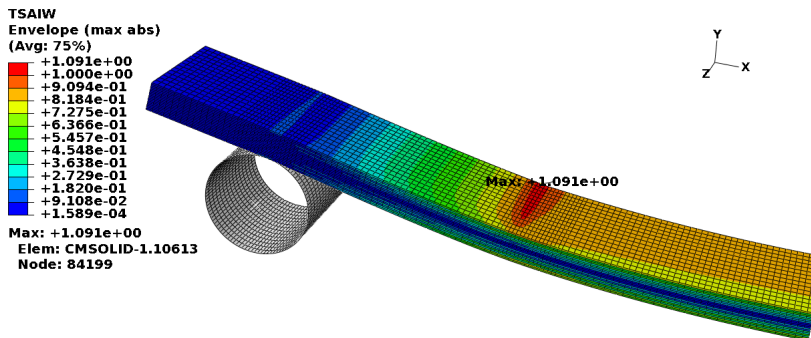
(a) Tsai-Wu values for the element type  $S4$ .



(b) Tsai-Wu values for the element type  $S4R$ .



(c) Tsai-Wu values for the element type  $S8R$ .



(d) Tsai-Wu values for the element type  $SC8R$ .

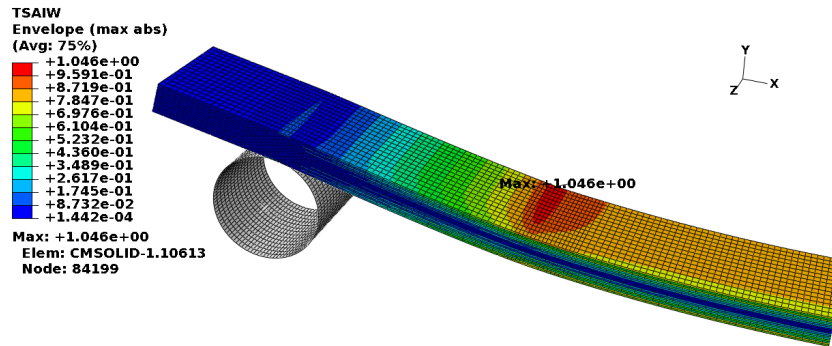
Figure B.1: Comparison of how different element types affect the Tsai-Wu value.

## B.2 Constraint enforcement method

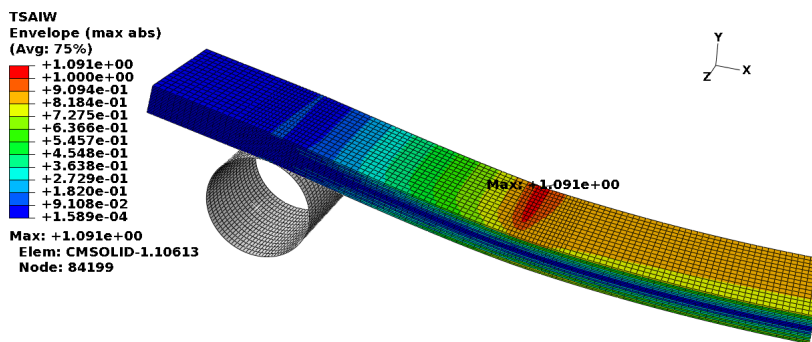
The three different types of constraint enforcement methods; penalty, augmented Lagrange and direct were analysed, the analysis are described in section 3.1.5. In reality there is



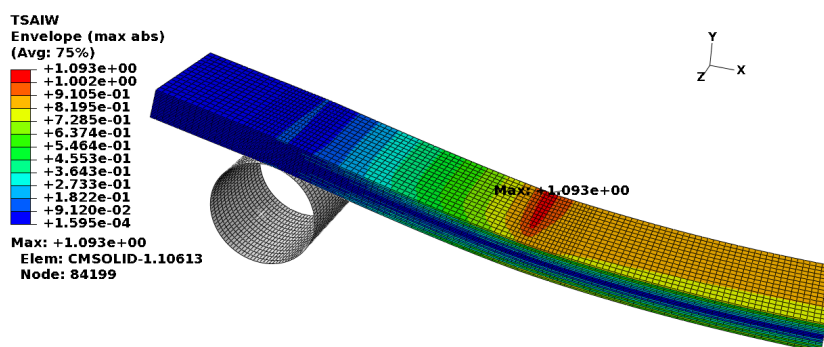
no penetration between the rolls and the plate. Therefore the direct method is best for modelling this reality. The augmented Lagrange method tries to minimise the penetration while the penalty allows penetration. The Tsai Wu value and the contact opening for the three types of contact enforcement methods can be seen in Figure B.2 and Figure B.3. The differences were analysed using the stacked continuum shell. Note the penetration that occurred for the penalty method, this could be reduced with a higher penalty stiffness. Note also the differences in Tsai Wu values. Because of the penetration of the penalty method and due to the bad convergence rate of the direct method, augmented Lagrange was used.



(a) *Tsai Wu shown for penalty method.*

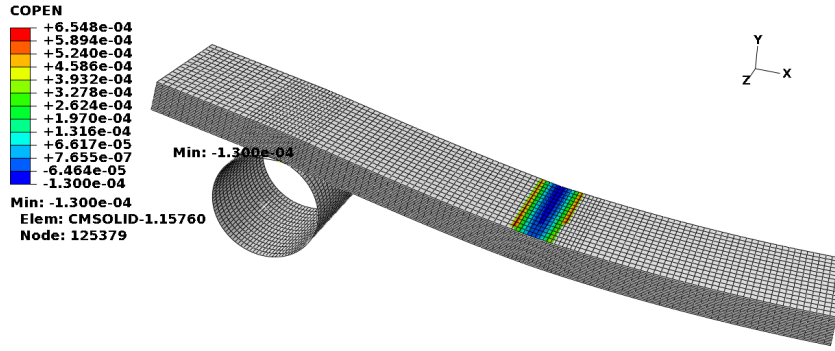


(b) *Tsai-Wu shown for augmented lagrange method.*

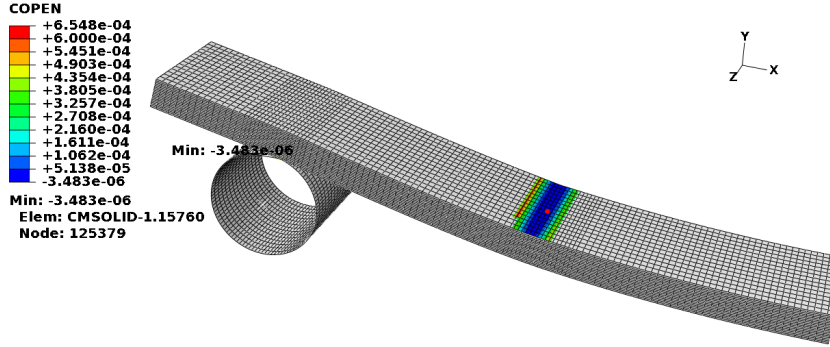


(c) *Tsai-Wu shown for direct method.*

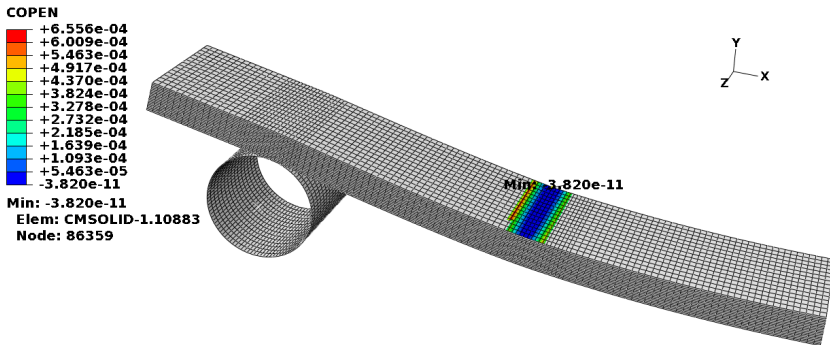
Figure B.2: *Tsai Wu values for the three different types of contact enforcement methods shown for stacked continuum shells.*



(a) Penetration shown for penalty method.



(b) Penetration shown for augmented lagrange method.



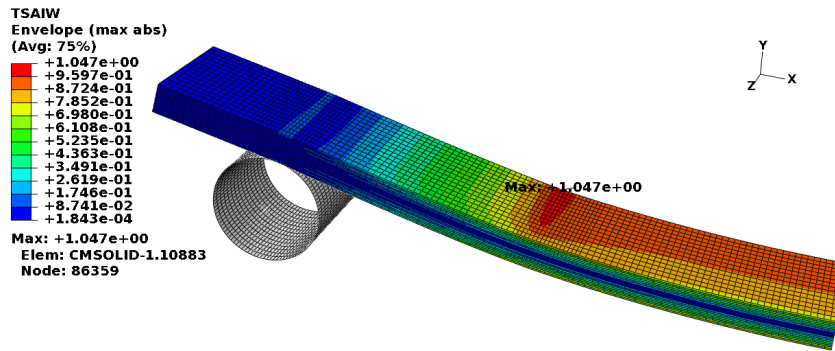
(c) Penetration shown for direct method.

Figure B.3: Penetration shown for the three different types of contact enforcement methods shown for stacked continuum shells.

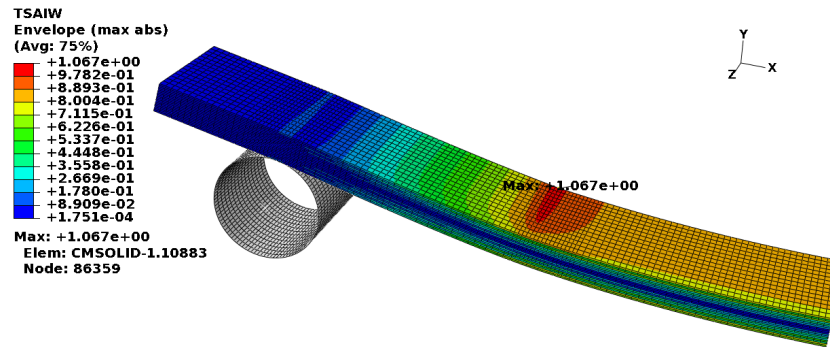
## B.3 Friction

In this part, the contact enforcement method is augmented Lagrange and the element type is SC8R which is a continuum shell element. The element type SC8R was chosen in this analysis because it models the effect of contact in the most accurate way.

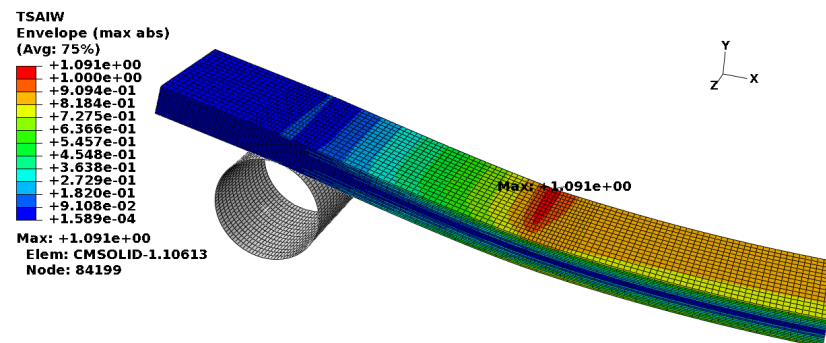
As can be seen when comparing the figures, see Figure B.4, with  $\mu = 0.1$  and with no friction the Tsai-Wu value increases quite a small amount in the area around the contact. It should also be noticed that the distribution of the Tsai-Wu value changes when taking friction into account. When the friction coefficient is raised the distribution changes even more. Since there was friction between the rolls and the plate, the effect of friction had to be taken into account.  $\mu$  was set to 0.2 due to the convergence problems that occurred for higher values.



(a) Stacked continuum shells without friction.



(b) Stacked continuum shells with friction,  $\mu = 0.1$ .



(c) Stacked continuum shells with friction,  $\mu = 0.2$

Figure B.4: Showing how friction affects the stress distribution for  $0 \leq \mu \leq 0.2$

## C Curve-fitted amplitudes

Figure C.1 show the 9 curve fitted polynomials plotted together with the original amplitudes. The curve fit was done in Matlab using 10th order polynomials.

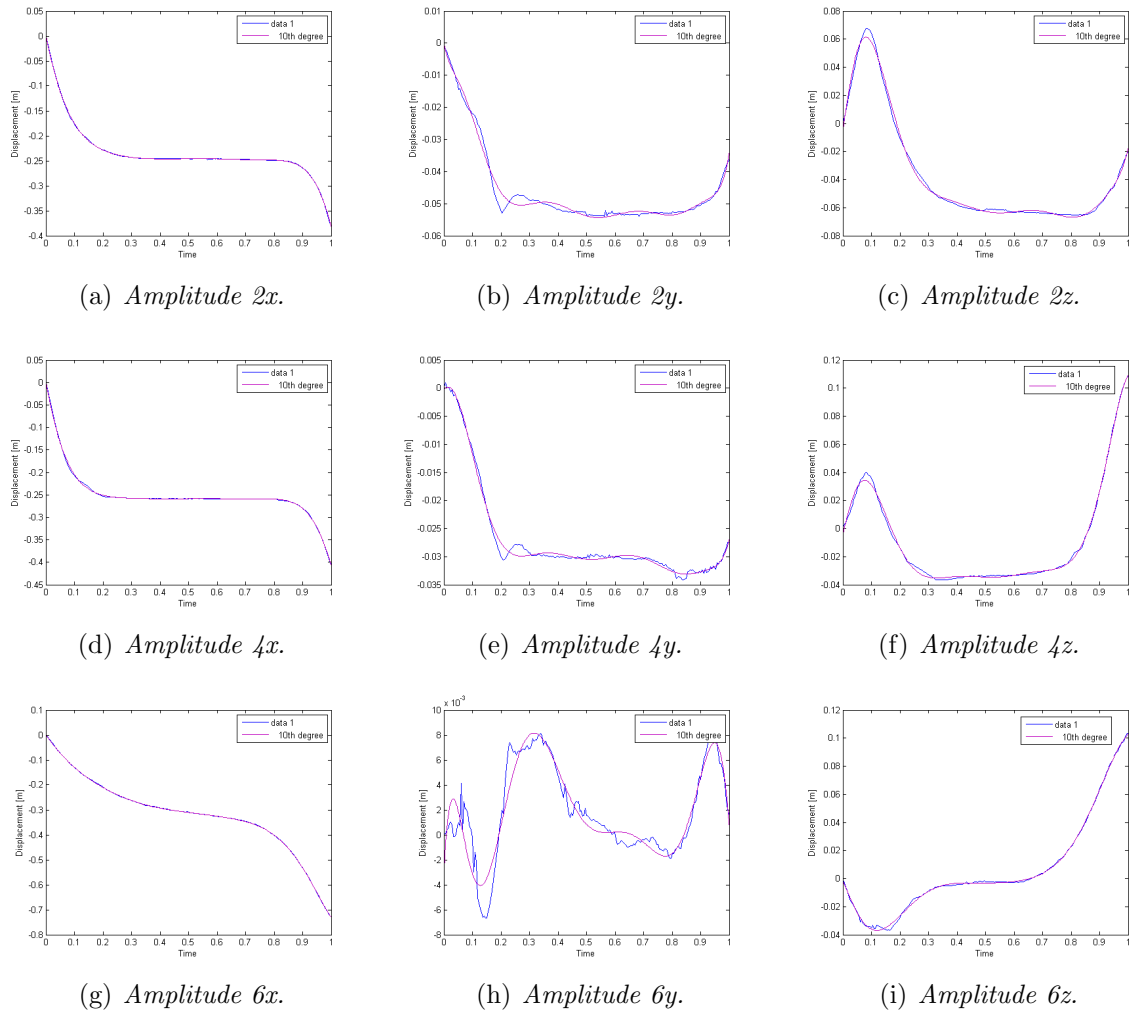


Figure C.1: Original amplitudes plotted together with curve-fitted amplitudes.

## D Python Script

```
"""
odbMaxTsaiWu.py
Code to determine the location and value of the maximum
Tsai-Wu value in an output database.
Usage: abaqus python odbMaxTsaiWu.py -odb odbName
       -elset(optional) elsetName
Requirements:
1. -odb    : Name of the output database.
2. -elset  : Name of the assembly level element set.
               Search will be done only for element belonging
               to this set. If this parameter is not provided,
               search will be performed over the entire model.
3. -help   : Print usage
"""

#~~~~~
from odbAccess import *
from sys import argv,exit
#~~~~~

def rightTrim(input,suffix):
    if (input.find(suffix) == -1):
        input = input + suffix
    return input
#~~~~~

def getMaxTsaiWu(odbName,elsetName):
    """ Print max TsaiWu location and value given odbName
        and elset(optional)
    """
    elset = elemset = None
    region = "over the entire model"
    """ Open the output database """
    odb = openOdb(odbName)
    assembly = odb.rootAssembly

    """ Check to see if the element set exists
        in the assembly
    """
    if elsetName:
        try:
            elemset = assembly.elementSets[elsetName]
            region = " in the element set : " + elsetName;
        except KeyError:
            print 'An assembly level elset named %s does' \
                  'not exist in the output database %s' \
                  % (elsetName, odbName)
    odb.close()
```

```

        exit(0)

    """ Initialize maximum values """
    maxTsaiWu = -0.1
    maxElem = 0
    maxStep = "_None_"
    maxFrame = -1
    TsaiWu = 'TSAIW'
    isTsaiWuPresent = 0
    for step in odb.steps.values():
        print 'Processing Step:', step.name
        for frame in step.frames:
            FrameNo = frame.frameId
            print 'Searching frame %d'% FrameNo
            allFields = frame.fieldOutputs
            if (allFields.has_key(TsaiWu)):
                isTsaiWuPresent = 1
                TsaiWuSet = allFields[TsaiWu]
                if elemset:
                    TsaiWuSet = TsaiWuSet.getSubset(region=elemset)
laban = -1
                for TsaiWuValue in TsaiWuSet.values:
                    if (TsaiWuValue.data > maxTsaiWu):
maxTsaiWu = TsaiWuValue.data
                        maxElem = TsaiWuValue.elementLabel
                        maxStep = step.name
                        maxFrame = frame.frameId

            if(isTsaiWuPresent):
print 'Maximum Tsai-Wu value %s is in element %d'%(
                maxTsaiWu, maxElem)
print 'Location: frame # %d step: %s '% (maxFrame,maxStep)
            else:
                print 'Tsai-Wu is not available in' \
                    'the output database : %s\n' %(odb.name)

    """ Close the output database before exiting the program """
    odb.close()

#=====
# S T A R T
#
if __name__ == '__main__':

    odbName = None
    elsetName = None
    argList = argv
    argc = len(argList)
    i=0
    while (i < argc):
        if (argList[i][:2] == "-o"):

```

```

        i += 1
        name = argList[i]
        odbName = rightTrim(name, ".odb")
    elif (argList[i][:2] == "-e"):
        i += 1
        elsetName = argList[i]
    elif (argList[i][:2] == "-h"):
        print __doc__
        exit(0)
    i += 1
if not (odbName):
    print ' **ERROR** output database name is not provided'
    print __doc__
    exit(1)
getMaxTsaiWu(odbName, elsetName)

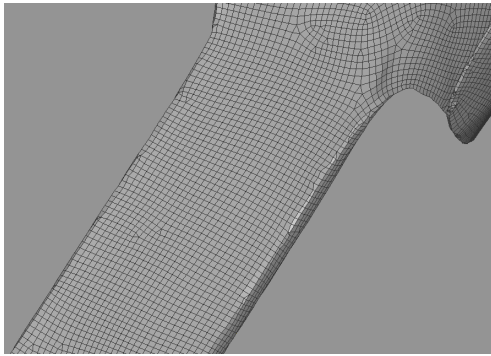
```

## E Geometry clean up

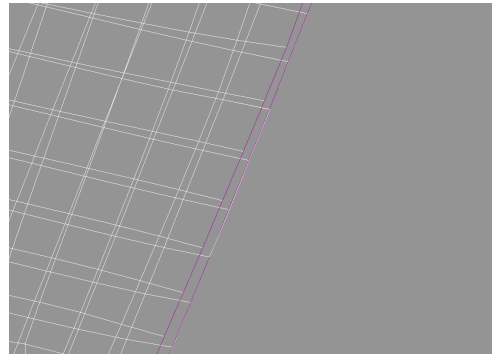
The different steps in the shell extraction and geometry clean up is described below. The steps are related to Figure E.1.

1. Create FEM topology of the triangular stl mesh.
2. Create a mixed mesh that is easier to work with.
3. Split up the model in different sets, one for upper and one for the lower part.
4. Create curves around the model to give smother edges and trim the elements around the curves to fit on the curves (takes away the irregularities at the edges).
5. Create surfaces out of the geometry for both sides of the geometry
6. Close the gap between the sides, which will give the desired geometry that is easier to work with
7. Create the inner, outer or middle surface, by just taking the upper och lower face of the model or by extracting the mid surface.

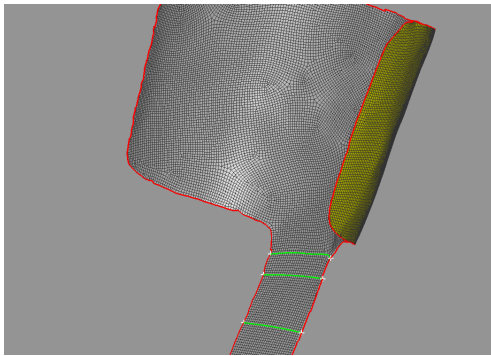




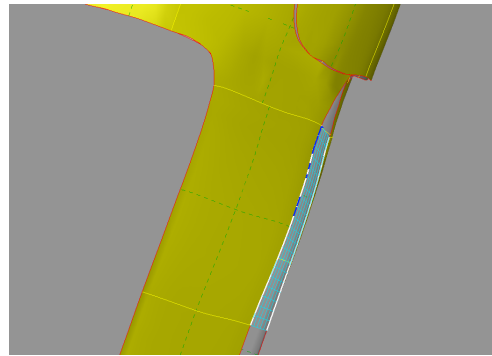
(a) *Step 1 - 2. Showing the new mesh that is easier to work with*



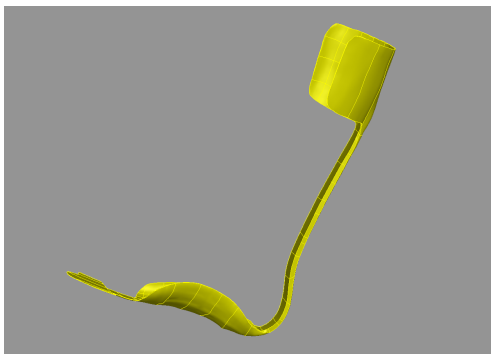
(b) *Step 4. Showing how the curves are smoothing up the edges around the model.*



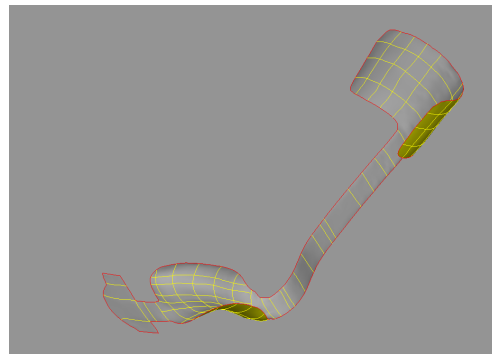
(c) *Step 5. Showing one of the surfaces that were created of the back and front sets.*



(d) *Step 6. Showing the coons that are created to close the gaps.*



(e) *Step 6. Showing the model with the closed gaps.*



(f) *Step 7. Showing the extracted midsurface*

*Figure E.1: The different steps in the shell extraction and geometry clean up.*

## F Stacking sequences

Table F.1 shows the 10 test runs where all plies were substituted from  $45^\circ$  to  $90^\circ$ . Table F.2 shows the 10 test runs where all plies were substituted from  $90^\circ$  to  $45^\circ$ . Results of these tests can be seen in section 6.4.

*Table F.1: Stacking sequence scheme,  $45^\circ$  to  $90^\circ$  .*

Test run	1	2	3	4	5	6	7	8	9	10
Ply 1	$45^\circ$	$90^\circ$	$90^\circ$	$90^\circ$	$90^\circ$	$90^\circ$	$90^\circ$	$90^\circ$	$90^\circ$	$90^\circ$
Ply 2	$45^\circ$	$45^\circ$	$90^\circ$	$90^\circ$	$90^\circ$	$90^\circ$	$90^\circ$	$90^\circ$	$90^\circ$	$90^\circ$
Ply 3	$45^\circ$	$45^\circ$	$45^\circ$	$90^\circ$	$90^\circ$	$90^\circ$	$90^\circ$	$90^\circ$	$90^\circ$	$90^\circ$
Ply 4	$45^\circ$	$45^\circ$	$45^\circ$	$45^\circ$	$90^\circ$	$90^\circ$	$90^\circ$	$90^\circ$	$90^\circ$	$90^\circ$
Ply 5	$45^\circ$	$45^\circ$	$45^\circ$	$45^\circ$	$45^\circ$	$90^\circ$	$90^\circ$	$90^\circ$	$90^\circ$	$90^\circ$
Ply 6	$45^\circ$	$45^\circ$	$45^\circ$	$45^\circ$	$45^\circ$	$45^\circ$	$90^\circ$	$90^\circ$	$90^\circ$	$90^\circ$
Ply 7	$45^\circ$	$45^\circ$	$45^\circ$	$45^\circ$	$45^\circ$	$45^\circ$	$45^\circ$	$90^\circ$	$90^\circ$	$90^\circ$
Ply 8	$45^\circ$	$45^\circ$	$45^\circ$	$45^\circ$	$45^\circ$	$45^\circ$	$45^\circ$	$45^\circ$	$90^\circ$	$90^\circ$
Ply 9	$45^\circ$	$45^\circ$	$45^\circ$	$45^\circ$	$45^\circ$	$45^\circ$	$45^\circ$	$45^\circ$	$45^\circ$	$90^\circ$
Ply 10	$45^\circ$	$45^\circ$	$45^\circ$	$45^\circ$	$45^\circ$	$45^\circ$	$45^\circ$	$45^\circ$	$45^\circ$	$90^\circ$
Ply 11	$45^\circ$	$45^\circ$	$45^\circ$	$45^\circ$	$45^\circ$	$45^\circ$	$45^\circ$	$45^\circ$	$90^\circ$	$90^\circ$
Ply 12	$45^\circ$	$45^\circ$	$45^\circ$	$45^\circ$	$45^\circ$	$45^\circ$	$45^\circ$	$90^\circ$	$90^\circ$	$90^\circ$
Ply 13	$45^\circ$	$45^\circ$	$45^\circ$	$45^\circ$	$45^\circ$	$45^\circ$	$90^\circ$	$90^\circ$	$90^\circ$	$90^\circ$
Ply 14	$45^\circ$	$45^\circ$	$45^\circ$	$45^\circ$	$45^\circ$	$90^\circ$	$90^\circ$	$90^\circ$	$90^\circ$	$90^\circ$
Ply 15	$45^\circ$	$45^\circ$	$45^\circ$	$45^\circ$	$90^\circ$	$90^\circ$	$90^\circ$	$90^\circ$	$90^\circ$	$90^\circ$
Ply 16	$45^\circ$	$45^\circ$	$45^\circ$	$90^\circ$	$90^\circ$	$90^\circ$	$90^\circ$	$90^\circ$	$90^\circ$	$90^\circ$
Ply 17	$45^\circ$	$45^\circ$	$90^\circ$	$90^\circ$	$90^\circ$	$90^\circ$	$90^\circ$	$90^\circ$	$90^\circ$	$90^\circ$
Ply 18	$45^\circ$	$90^\circ$	$90^\circ$	$90^\circ$	$90^\circ$	$90^\circ$	$90^\circ$	$90^\circ$	$90^\circ$	$90^\circ$

*Table F.2: Stacking sequence scheme,  $90^\circ$  to  $45^\circ$  .*

Test run	1	2	3	4	5	6	7	8	9	10
Ply 1	$90^\circ$	$45^\circ$	$45^\circ$	$45^\circ$	$45^\circ$	$45^\circ$	$45^\circ$	$45^\circ$	$45^\circ$	$45^\circ$
Ply 2	$90^\circ$	$90^\circ$	$45^\circ$	$45^\circ$	$45^\circ$	$45^\circ$	$45^\circ$	$45^\circ$	$45^\circ$	$45^\circ$
Ply 3	$90^\circ$	$90^\circ$	$90^\circ$	$45^\circ$	$45^\circ$	$45^\circ$	$45^\circ$	$45^\circ$	$45^\circ$	$45^\circ$
Ply 4	$90^\circ$	$90^\circ$	$90^\circ$	$90^\circ$	$45^\circ$	$45^\circ$	$45^\circ$	$45^\circ$	$45^\circ$	$45^\circ$
Ply 5	$90^\circ$	$90^\circ$	$90^\circ$	$90^\circ$	$90^\circ$	$45^\circ$	$45^\circ$	$45^\circ$	$45^\circ$	$45^\circ$
Ply 6	$90^\circ$	$90^\circ$	$90^\circ$	$90^\circ$	$90^\circ$	$90^\circ$	$45^\circ$	$45^\circ$	$45^\circ$	$45^\circ$
Ply 7	$90^\circ$	$90^\circ$	$90^\circ$	$90^\circ$	$90^\circ$	$90^\circ$	$90^\circ$	$45^\circ$	$45^\circ$	$45^\circ$
Ply 8	$90^\circ$	$90^\circ$	$90^\circ$	$90^\circ$	$90^\circ$	$90^\circ$	$90^\circ$	$90^\circ$	$45^\circ$	$45^\circ$
Ply 9	$90^\circ$	$90^\circ$	$90^\circ$	$90^\circ$	$90^\circ$	$90^\circ$	$90^\circ$	$90^\circ$	$90^\circ$	$45^\circ$
Ply 10	$90^\circ$	$90^\circ$	$90^\circ$	$90^\circ$	$90^\circ$	$90^\circ$	$90^\circ$	$90^\circ$	$90^\circ$	$45^\circ$
Ply 11	$90^\circ$	$90^\circ$	$90^\circ$	$90^\circ$	$90^\circ$	$90^\circ$	$90^\circ$	$90^\circ$	$45^\circ$	$45^\circ$
Ply 12	$90^\circ$	$90^\circ$	$90^\circ$	$90^\circ$	$90^\circ$	$90^\circ$	$90^\circ$	$45^\circ$	$45^\circ$	$45^\circ$
Ply 13	$90^\circ$	$90^\circ$	$90^\circ$	$90^\circ$	$90^\circ$	$90^\circ$	$45^\circ$	$45^\circ$	$45^\circ$	$45^\circ$
Ply 14	$90^\circ$	$90^\circ$	$90^\circ$	$90^\circ$	$90^\circ$	$45^\circ$	$45^\circ$	$45^\circ$	$45^\circ$	$45^\circ$
Ply 15	$90^\circ$	$90^\circ$	$90^\circ$	$90^\circ$	$45^\circ$	$45^\circ$	$45^\circ$	$45^\circ$	$45^\circ$	$45^\circ$
Ply 16	$90^\circ$	$90^\circ$	$90^\circ$	$45^\circ$	$45^\circ$	$45^\circ$	$45^\circ$	$45^\circ$	$45^\circ$	$45^\circ$
Ply 17	$90^\circ$	$90^\circ$	$45^\circ$	$45^\circ$	$45^\circ$	$45^\circ$	$45^\circ$	$45^\circ$	$45^\circ$	$45^\circ$
Ply 18	$90^\circ$	$45^\circ$	$45^\circ$	$45^\circ$	$45^\circ$	$45^\circ$	$45^\circ$	$45^\circ$	$45^\circ$	$45^\circ$

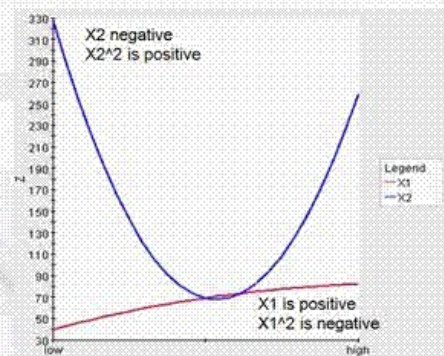
## G Main effect

L3.23

### DOE POST Processing: Main Effects

- **Main Effects** provide information on how a response is influenced, on average, by a factor. Consider the following when reviewing Main Effects in Isight:
  - Magnitude: The larger the magnitude the greater the influence on the response.
  - Direction: Positive main effect as factor increases then response increases. Negative means as factor increases then response decreases
  - Order: Higher 2nd order effect indicates a single parameter's effect on a response is not linear.
  - Interaction: Higher interaction effects indicate that changing two parameters together will greatly influence the response.

Sources	Z
$X1^2$	-2.731578878433136
$X1-X2$	-3.4028200574661436
$X1$	7.049091786687292
$X2^2$	75.21722660169836
$X2$	-11.599282675715047



Introduction to Isight

DS  
SIMULIA

## DOE POST Processing - Theory

- Relationships between inputs and outputs are captured as Main Effects (M).
- Isight uses this fitted polynomial to calculate the relationship between the inputs and the outputs. This relationship is called the main effect (M).
- The derivative of the fitted 2 independent variable polynomial is:

$$dy = c_1 dx_1 + c_2 dx_2 + 2c_3 x_1 dx_1 + 2c_4 x_2 dx_2 + c_5 x_1 dx_2 + c_5 x_2 dx_1$$

**Linear main effects:**

$$Mx_1 = c_1 dx_1$$

$$Mx_2 = c_2 dx_2$$

**Quadratic effects :**

$$Mx_1^2 = 2c_3 x_1 dx_1$$

$$Mx_2^2 = 2c_4 x_2 dx_2$$

**The interaction effect :**  $Mx_1 x_2 = c_5 (x_1 dx_2 + x_2 dx_1)$

**Where:**

$$dx = \text{Max}(x) - \text{Min}(x)$$

X = Baseline value of factor

These effects are then scaled and normalized in Isight.

